Local pulse wave velocity determination : the arterial distension waveform from foot to crest

local pulse wave velocity determination:

the arterial distension waveform

from foot to crest

Illustration cover: The Wave, a sandstone formation on the slopes of the Coyote Buttes, located in Arizona, United States of America.

local pulse wave velocity determination:

the arterial distension waveform from foot to crest

PROEFSCHRIFT

Ter verkrijging van de graad van doctor aan de
Universiteit Maastricht, op gezag van de Rector Magnificus,
Prof. Mr. G.P.M.F. Mols, volgens het besluit van het
College van Decanen, in het openbaar te verdedigen
op woensdag 10 juni 2009 om 16:00 uur.

door

Evelien Hermeling

Geboren op 21 december 1978 te Wijk en Aalburg

Promotores:

Prof. Dr. Ir. A.P.G. Hoeks
Prof. Dr R.S. Reneman

Copromotor:

Dr. Ir. K.D. Reesink

Beoordelingscommissie:

Prof. Dr. P.W. de Leeuw (voorzitter)
Prof. Dr. P. Boutouyrie (Hôpital Européen Georges Pompidou, Parijs, Frankrijk)
Prof. Dr. J.G.R. de Mey
Prof. Dr. Ir. F.N. van de Vosse (Technische Universiteit Eindhoven)
Prof. Dr. J.L. Waltenberger

Financial support by the Netherlands Heart Foundation and Stichting Hartsvrienden RESCAR for the publication of this thesis is gratefully acknowledged.

The scientific work was financially supported by SenterNovem of the Dutch Ministry of Economic Affairs (IS042015).

Financial support by Esaote Europe B.V. for the publication of this thesis is gratefully acknowledged.

Content

Chapter 1

General Introduction

1.1 Introduction

Cardiovascular disease is the number one cause of death in western society. Although some of the patients with cardiovascular events are free of symptoms prior to the event, changes in the arterial tree can be observed at an early stage of the disease process. One of the most important changes in the arterial tree is increased arterial stiffening, which is associated with increased (systolic) blood pressure and, consequently, increased load on the heart (McEniery et al. 2007, Schiffrin 2004). Arterial stiffening does not only occur in such diseases as hypertension (Laurent et al. 2001, Laurent et al. 2003), but also in aging (Reneman et al. 1986). There is increasing evidence that in patients with borderline hypertension arterial stiffening may precede the development of hypertension (Reneman et al. 2005). In a variety of studies it has been shown that arterial stiffening is associated with the risk of coronary artery disease and stroke (Laurent et al. 2003, Mattace-Raso et al. 2006, McLeod et al. 2004, Park et al. 2005). Moreover, local changes in arterial stiffness might be indicative of atherosclerosis (McEniery et al. 2007, McVeigh et al. 2002), a degenerative process of the arterial wall involved in many cardiovascular diseases, like myocardial infarction and stroke. Therefore, arterial stiffness seems to be a good candidate for the assessment of cardiovascular risk. Indeed, recently arterial stiffness has been included in the risk stratification of the guidelines of the European society of hypertension and cardiology (Mancia et al. 2007).

Most of the studies, analyzing the effect of cardiovascular disease and aging on arterial stiffness, are based on the carotid-femoral pulse wave velocity. Carotid-femoral pulse wave velocity provides a measure of the average arterial stiffness over a long trajectory and, hence, does not allow discrimination between arterial segments, e.g. between muscular and elastic arteries, that may respond differently to aging and disease (McEniery et al. 2007). Moreover, atherosclerosis, an inflammation disease affecting the arterial wall locally, might cause local changes in arterial stiffness whereas the stiffness of the unaffected arteries may be unchanged.

To identify local changes in arterial wall dynamics at an early stage a non-invasive easy accessible technique is required. Current measures of local arterial stiffness are the distensibility and compliance coefficient, which are the relative and absolute change in cross-sectional area of an artery for a given change in pressure. The changes in cross-sectional area over the cardiac cycle

can be obtained reliably and accurately with ultrasound (Hoeks et al. 1990). In contrast, local blood pressure recordings are difficult to obtain accurately non-invasively. In stead, blood pressure measurements in the arm are used, which is a poor surrogate as the values obtained may deviate substantially from blood pressure in the carotid arteries, the difference being dependent on cardiovascular condition and age (Waddell et al. 2001).

An alternative is to measure the velocity at which pressure and flow waves travel along the arterial system. This wave velocity is, among others, determined by the elasticity of the arterial wall. In contrast to other methods to determine local stiffness of the arterial wall, local pulse wave velocity assessment does not require measurement of local blood pressure. In the last century different techniques have been proposed to measure wave velocity, but all have one or more potential drawbacks that might hamper accurate and non-invasive assessment or limit interpretation. To fully understand the underlying assumptions and potential drawbacks of these techniques a survey of the characteristics of the arterial system that may influence the measurement of pulse wave velocity locally in an artery is presented.

1.2 Characteristic of the arterial system

Assuming a long wavelength ($\lambda >> d$), a small diameter change ($\Delta d << d$) and a small wall thickness compared with the diameter d ($h << d$), and ignoring viscous effects, the Young's modulus E of a tube wall determines the wave propagation velocity c, according to:

$$c = \sqrt{\frac{E\,h}{\rho\,d}} \qquad 1.1$$

with ρ, the density of the blood. In arteries the assumptions underlining Equation 1.1 are not met and consequently the wave velocity will also be influenced by other factors.

Attenuation of pressure waves

Energy loss, either due to viscosity of the blood or internal damping by the visco-elastic arterial wall, causes attenuation of pressure waves. Indeed, artificially generated pressure pulses with a high frequency (40 - 200 Hz) are attenuated

(Anliker et al. 1968). Attenuation has also been shown at lower frequencies, by applying Fourier analysis of the pressure waves (Luchsinger et al. 1964, Milnor and Bertram 1978, Milnor and Nichols 1975), but without agreement about the attenuation coefficient (Li et al. 1981). This lack of agreement might be caused by the application of Fourier analysis, which is debatable because linearity and periodicity criteria are not met.

The viscosity of blood as exhibited by wall shear stress contributes dominantly to the energy losses in arteries. Blood viscosity might also affect wave velocity, as shown by theoretical analyses (Morgan and Kiely 1954). However, for a high Womersley number ($\alpha > 3$), which is defined by the ratio between the inertial and viscous forces (Womersley 1955), the effect of blood viscosity on wave velocity is small (Taylor 1959a). In the common carotid artery these Womersley numbers ($\alpha > 3$) occur already at a frequency of about 0.5 Hz, consequently the wave velocity will be rather independent of frequency.

Besides blood viscosity, visco-elastic properties of the wall may also cause energy losses (Maxwell and Anliker 1968, Morgan and Kiely 1954). Viscous wall properties will also affect wave velocity (Maxwell and Anliker 1968, Morgan and Kiely 1954, Taylor 1959a), but this effect decreases for higher Womersley numbers and, hence, for higher frequencies (Taylor 1959a). Indeed for artificially generated pulses of 40-200 Hz a frequency independent wave velocity is observed in canine arteries, despite quite large attenuation (Anliker et al. 1968). Using the apparent phase velocity technique and artificially generating pulse waves by fast injection of saline into the aorta in dogs, it has been confirmed that wave velocity is constant for frequencies above 20 Hz (Newman et al. 1986). At lower frequencies the apparent phase velocity is frequency dependent (Latham et al. 1985, Newman et al. 1986, Ting et al. 1990). This method may, however, be very sensitive to reflective interference (Bertram et al. 1997). For an aorta occluded at one site, to obtain a single and complete reflection, the measured phase velocity appears to be rather frequency independent over the 2-20 Hz frequency range, (Busse et al. 1979).

Non-linear pressure-area relationship

The pressure-area relation is not linear (Hayashi et al. 1980, Langewouters et al. 1984), resulting in a pressure-dependent, Young's modulus (E), a measure for arterial stiffness, and, hence, a pressure dependent pulse wave velocity (see Equation 1.1). Indeed, the generation of artificially high frequency pulses in the canine aorta reveals that pulse wave velocity is a function of pressure (Histand

and Anliker 1973). These results were confirmed by transit time measurements for reference points with equal pressure increases (in percentage) in the upstroke of the pressure waves, measured 10-30 cm apart (Pruett et al. 1988). This pressure dependency of the wave velocity has also serious consequences for the applicability of Fourier analysis used, for example, to obtain wave velocity, because the linearity criterion is not met.

Blood flow velocity

Theoretical analysis shows that the pressure wave velocity in a tube is affected by the velocity of the fluid (Morgan and Ferrante 1955), which has been confirmed experimentally (Histand and Anliker 1973). The water-hammer equation, derived from the 1-D pressure wave equation for an elastic tube without friction (Parker and Jones 1990), also includes this property of the arterial system. However, many other techniques to assess pressure wave velocity ignore the effect of blood flow velocity, introducing substantial errors, especially for the aorta or other central arteries with high peak blood flow velocities (± 1 m/s, (Segadal and Matre 1987)) and relatively low pressure wave velocities (± 4 m/s, (Ting et al. 1990)).

Arterial wave reflections

Reflections in the arterial tree, as occurring at bifurcations and other sites along the arterial tree with impedance mismatch, alter pressure and flow waves. Multiple techniques exist to separate the reflected from the incident waves in the arterial tree. Assuming a linear arterial system with a characteristic impedance calculated as the average input impedance at higher frequencies, Westerhof et al. obtained a frequency dependent reflection coefficient, allowing separation of the incident and the reflected wave (Westerhof et al. 1972). The results obtained with this method are comparable to those obtained using the water-hammer equation, which assumes a linear interaction of the forward and backward waves (Parker and Jones 1990). Alternatively, a time delayed reflection will induce an inflection point in the upstroke of the pressure wave originating from the onset of the reflected wave, which can also be used for the separation of incident and reflected waves. Often the inflection point is obtained by taking the fourth derivative of the pressure waveform (Takazawa et al. 1995). In some studies, the pressure increase above this inflection point is completely attributed to the reflected wave (Kelly et al. 1989). The separation of incident and reflected wave is still a topic of debate, because multiple reflections from multiple origins exist in

the arterial tree (Khir et al. 2001, O'Rourke 1967, Segers and Verdonck 2000) and tapering of the aorta might disperse wave reflection (Segers and Verdonck 2000). Moreover, at low frequencies the arterial system acts as a windkessel, due to the associated large wavelength, complicating separation of incident and reflected waves (Mohiuddin et al. 2007, Quick et al. 2006). In addition, the characteristic impedance, calculated as average input impedance for higher frequencies, might be inaccurate. Because 80 % of the power of the pressure wave is contained within the first four harmonic components (Nichols and O'Rourke 2005a) and the attenuation for high frequency waves is large (Anliker et al. 1968), the relative contribution of a high frequent reflected wave to the pulse pressure will be small. Although the amplitude of wave reflections is unknown and might be small, the effect of wave reflections on wave velocity estimation can be large (Benthin et al. 1991, Bertram et al. 1997).

1.3 Measurement of wave velocity

In this section we will briefly discuss the main techniques currently available to measure local wave velocity, focusing on those techniques that are (or might potentially be) applicable to non-invasive assessment of wave velocity. Table 1.1 summarizes the techniques to measure wave velocity, but it does not list all studies on *in vivo* wave velocity estimation.

Phase velocity

The phase velocity is the speed at which a wave with a given frequency propagates. Consequently, all phase velocity measurements use Fourier analysis to obtain wave velocity, and are, therefore, sensitive to non-linearities in the arterial system as described above. The most straightforward method is the apparent phase velocity, which is based on pressure measurements at two-points and phase differences obtained for each frequency component. The apparent phase velocity (c_{app}) is then calculated as:

$$c_{app}(f) = 2\pi f \frac{L}{\Delta\varphi(f)} \qquad 1.2$$

with $\Delta\varphi$, phase difference; f, frequency; L, distance between pressure measurements. This method can be very sensitive to wave reflections as the whole cardiac cycle with multiple reflections is used for Fourier analysis (Bertram

et al. 1997). To suppress reflection interference, pressure waveforms are measured at three different locations (Taylor 1959b) and combined to:

$$\cosh(\gamma L) = \frac{p_1 + p_3}{2 p_2} \qquad 1.3$$

with $p_{1,2,3}$ complex pressure amplitudes measured at location 1,2 and 3; *L*, distance between the locations 1-2 and 2-3. From the complex propagation coefficient, γ, the phase velocity (*c*) can be obtained. A third method uses total reflection (Busse et al. 1979), induced by occlusion of the artery and consequently is not suitable for non-invasive applications. All possible four-point combinations to determine wave velocity based on four measurements of either diameter, flow or pressure are described by She et al. (She et al. 1993). The method based on two pressure and two flow waveform has been used to obtain wave velocity in dogs (Milnor and Nichols 1975). The difficulty with the four-points method is that it requires simultaneous measurement of waveforms of either pressure, flow or diameter at exactly the same location (Hoeks et al. 2000).

Artificial pulses

Induced short bursts of artificial pressure pulses with relatively high frequency (40-200 Hz) can be superimposed on the pressure waveform to obtain the transit time at different pressure levels in the aorta of dogs (Anliker et al. 1968, Histand and Anliker 1973), resulting in a pressure-dependent wave velocity. Moreover, modification of the frequency of the artificial bursts provides a frequency dependent wave velocity (Anliker et al. 1968). The induced artificial pulses propagate in two directions, and can be measured both upstream and downstream of the induction site, allowing separation of pressure wave velocity and mean blood flow velocity. Moreover, because the generated waves are of very high frequencies, the interference of reflected waves is probably very small. Recently, a low frequent continuous wave ultrasound burst was proposed to induce an artificial pressure wave (Zhang 2005, Zhang and Greenleaf 2006), which in theory also allows detection of a frequency, pressure and flow dependent wave velocity. An alternative artificial pulse generation is based on fast injection of saline into the aorta to generate a short pressure pulse which allows detection of apparent phase velocities for much higher frequencies (Newman et al. 1986). A non-invasive approach based on artificial pulses and providing apparent phase velocity was introduced by (Zhang 2005).

Table 1.1 Summary of different methods to obtain the wave velocity

method		who	where	invasive	Values
Phase velocity	2-points (c_{app})	Luchsinger et al. 1964	AoA-AoAb	yes	2-16 m/s
		Latham et al. 1985	AoA - Iliac	yes	4.3 m/s AoR – 6.4 m/s Iliac#
		Ting et al. 1990	AoA - Iliac	yes	4.2 m/s AoR – 6.6 m/s Iliac†
	2-poits occl.	Busse et al. 1979	Dogs, CCA	yes	8 m/s, (2-20Hz)
	3-points	Li et al. 1981	Dogs, AoD, Iliac, CCA, CFA	yes	6.6, 7.7, 8.0, 8.8 m/s
		Latham et al. 1985	Phantom	yes	-
	4-points	Milnor et al.1975	Dogs, CFA	yes	6-7 m/s (2-9Hz)
		She et al. 1993	theory	-	-
Artificial pulses	transit-time	Anliker et al. 1968	Dogs	yes	4.3 m/s (40-140Hz)
		Histand et al.1973	Dogs	yes	4-11 m/s (60–140 mmHg)
		Zhang et al. 2006	phantom	no, US	-
	2-points	Newman et al. 1986	Dogs, Ao-Ab	yes	7-10 m/s (20-100Hz)
		Zhang 2005	ex-vivo	no, US	4-6.5 m/s (100-500Hz)‡
water-hammer		Khir et al. 2001	Dogs, AoA	yes	6.2 m/s
		Rakebrandt et al. 2008	CCA	no, US	6.2 ± 3.6 m/s
Gradient		Brands et al. 1998	Phantom	no, US	-
		Meinders et al. 2001	CCA	no, US	5.5 ± 1.5 m/s
dq / dA		Vulliemoz et al. 2002	AoD	no, MRI	4.9 ± 1.1 m/s
		Rabben et al. 2004	CCA	no, US	3-9 m/s
Transit time	foot-to- foot	Latham et al. 1985	AoA-CFA	yes	4.4 AoA – 8.8 m/s Iliac#
		Ting et al. 1990	AoA-Iliac	yes	4.1 m/s AoA – 5.7 m/s Iliac†
		Chiu et al. 1991	AoT, AoAb	yes	6 or 10 m/s *
		Vulliemoz et al. 2002	AoD	no,MRI	4.9 ± 0.9 m/s
	10-50% threshold	Pruett et al. 1988	Dogs	yes	4-12 m/s (60-140mmHg)
	Cross correlation.	Benthin et al. 1991	CCA	no, US	not reported
		Eriksson et al. 2002	CCA	no, US	8.3 m/s (one subject)

An overview of techniques currently available to measure local wave velocity, that are or might potentially be applicable for non-invasive assessment. CCA, common carotid artery, CFA, common femoral artery, AoA ascending-, AoT, thoracic-, AoAb, abdominal, and AoD, descending aorta. US: ultrasound, MRI, magnetic resonance imaging, for explanation of methods see text. # values at control and during Muller, Vasalva maneuver and occlusion of femoral artery, *compared different techniques to determine systolic foot of the wave, ‡ attenuation coefficient to obtain visco-elastic Young's modulus, †obtained values in normotensives and hypertensives.

Water-hammer method

The water-hammer equation relates the time increment in blood flow velocity *dU* to the time increment in pressure *dp* (Parker and Jones 1990):

$$dp_{\pm} = \pm \rho c \, dU_{\pm} \qquad 1.4$$

In early systole, which is assumed to be free of reflections, the wave velocity directly follows from the slope of the linear regression line of blood flow velocity and pressure (Equation 1.4). Initially the reflection free segment was selected manually (Khir et al. 2001), but later expanded to an automatic and non-invasive method (Rakebrandt et al. 2008). Although this approach incorporates blood flow velocity, the method can only be used in the absence of reflections and requires simultaneous measurements of blood flow velocity and pressure at exactly the same location with equipment with the same frequency characteristics (Hoeks et al. 2000).

Gradient method

In a linear medium, without reflections the wave velocity can be calculated by the Fry equation (Fry et al. 1956):

$$c = -\frac{dp}{dt} \Big/ \frac{dp}{dx} \qquad 1.5$$

with *dp*/*dt* the temporal derivative and *dp*/*dx* the spatial derivative of pressure. To illustrate the effect of reflections on the wave velocity obtained with this so-called gradient method, the pressure is decomposed in a number of harmonics using a Fourier transform. Considering one arbitrary harmonic (ω_0) the pressure is a function of time and position (Zamir 2000)

$$\begin{aligned}
&p(\omega_0, x, t) = \hat{p}_x e^{j\omega_0 t} = \hat{p}_f(\omega_0) e^{j\omega_0 (t - \frac{x}{c})} + \hat{p}_b(\omega_0) e^{j\omega_0 (t + \frac{x}{c})} \\
&\frac{\partial \hat{p}_x}{\partial t} = \left(\hat{p}_f(\omega_0) + \hat{p}_b(\omega_0) \right) j\omega_0 \\
&\frac{\partial \hat{p}_x}{\partial x} = -\left(\hat{p}_f(\omega_0) - \hat{p}_b(\omega_0) \right) \frac{j\omega_0}{\hat{c}(\omega_0)} \\
&\hat{c}(\omega_0) = -\frac{\hat{p}_f(\omega_0) - \hat{p}_b(\omega_0)}{\hat{p}_f(\omega_0) + \hat{p}_b(\omega_0)} \frac{\partial \hat{p}_x / \partial t}{\partial \hat{p}_x / \partial x}
\end{aligned} \qquad 1.6$$

$\hat{p}_f$ and $\hat{p}_b$ are the Fourier coefficients of the forward and backward propagating wave, $\hat{p}_x$, the Fourier coefficient of a pressure wave (summation of forward and backward wave) at position *x*, and *t*, time. This illustration shows that, the Fry equation (1.5) holds only in case of no backward propagating (reflected) waves ($\hat{p}_b$ = 0 in Equation 1.6)

The area-flow method

The 1-D flow equation (Raines et al. 1974) allows for an easy derivation of wave velocity:

$$\frac{dq}{dx}+\frac{dA}{dt}=\frac{dq}{dt}\frac{dt}{dx}+\frac{dA}{dt}=0$$
$$c=-\frac{dx}{dt}=\frac{dq}{dt}\Big/\frac{dA}{dt} \qquad 1.7$$

with *q*, blood flow; *A*, cross-sectional area. In a similar way as the illustration in Equation 1.6, it can be shown that this method requires a reflection free time segment. Therefore, the method was applied to the first part of the upstroke of flow and cross-sectional area as obtained *in vivo* with MRI (Vulliemoz et al. 2002) or ultrasound (Rabben et al. 2004).

Transit time methods

The wave velocity is most commonly measured by deriving the transit time between corresponding time-points on two pressure, flow or diameter waveforms obtained preferentially simultaneously at two locations at a known distance. The foot-to-foot technique measures the transit time based on a time-reference point signalling the upstroke (systolic foot) in the waveform, which is often considered to be free from reflections (Nichols and O'Rourke 2005b), which is not necessarily the case. Moreover, the results might depend on the method used to identify the systolic foot (Chiu et al. 1991, Millasseau et al. 2005). The methods based on the maximum of the second derivative or the intersecting tangent appear to perform better than those based on the local minimum or the maximum of the first derivative of the pressure waveform (Chiu et al. 1991). Alternatively, the transit time can be derived from the cross-correlation between the diameter waveforms (Benthin et al. 1991, Eriksson et al. 2002), although this method might be sensitive to wave reflections (Benthin et al. 1991).

Table 1.2. The characteristics of the arterial system and their effect on different wave velocity methods

method		pressure	freq.	blood vel.	reflections
phase velocity	2-points	sensitive	yes	sensitive	sensitive
	2-points occl.	sensitive	yes	sensitive	not sensitive*
	3-points	sensitive	yes	sensitive	not sensitive
	4-points	sensitive	yes	sensitive	not sensitive
artificial pulses	transit time	yes	yes	yes	negligible sensitive
	2-points	sensitive	yes	sensitive	sensitive at low freq.
wave intensity		no †	no	yes	minor sensitive
gradient method		no †	no	sensitive	minor sensitive
dq-dA method		no †	no	sensitive	minor sensitive
transit time	foot-to-foot	no †	no	no‡	minor sensitive
	10-50% thresh	yes	no	no‡	sensitive
	cross corr.	no	no	sensitive	sensitive

The effect of pressure, frequency (freq.) and blood flow velocity (vel.) and the sensitivity of wave reflections on the different methods to determine wave velocity. Yes (or no) indicates that with this method it is (or it is not) possible to analyze the effect of pressure, frequency, or blood flow velocity on the wave velocity. Sensitive means that this method may be biased, because of the pressure and blood flow velocity dependent wave velocity or reflections. *assumes complete occlusion (occl.), † measured at diastolic blood pressure, ‡ biased with mean blood velocity at time-reference point, which is close to zero at the systolic foot. (cross-corr: cross-correlation; thresh: threshold)

Table 1.2 summarizes the effect of frequency, pressure and blood flow velocity dependency and the sensitivity to reflections of the different techniques to determine wave velocity as discussed above. The method based on artificially generated pulses seems to be the best candidate for measuring local wave velocity as it does not require linearity, allows analysis of the effect of pressure and blood flow velocity on wave velocity and is not sensitive to reflective interference. However, in the present state of the art this approach is the most challenging technique to apply non-invasively. The transit time method is probably the second best, because it has only minor sensitivity to reflections and is relatively easy to apply non-invasively.

1.4 Objective

The main objective of this study is to develop an accurate and reliable non-invasive method to assess local arterial stiffness by means of non-invasive pulse wave velocity measurements. Local pulse wave velocity will be determined by measuring in a short stretch of an artery (less then 2 cm in length) arterial diameter waveform velocity by means of high resolution ultrasound. The study focuses on the assessment of stiffness in elastic arteries, because there is evidence that in contrast to muscular arteries the dynamic properties of these arteries change strongly during aging (Reneman et al. 1986) and disease processes (McEniery et al. 2007). The windkessel-effect, which is the cushioning function of large arteries, is most important in the proximal aorta, being the elastic part of this artery. Because the elastic properties of the common carotid artery are similar to that of the aorta (Studinger et al. 2000) the local pulse wave velocity method developed is applied to the common carotid artery because of easy access to ultrasound.

1.5 Content of the thesis

The mechanical characteristics of the arterial wall can be obtained from the diameter and pressure waveforms. The mechanical characteristics include diameter change, the distensibility and compliance coefficients, and the Young's modulus. Chapter 2 gives a survey of the methods in use to describe these characteristics as well as the mathematical and physical interrelationships between those parameters and the limitations of these methods.

We propose a non-invasive method, based on high resolution multiple M-line ultrasound, to obtain local pulse wave velocity in the common carotid artery using the transit time technique. Chapter 3 specifies this method and demonstrates in a phantom set-up, scaled to physiological conditions, that local pulse wave velocity can be obtained with a precision of better than 1 %. We will show that when strict filtering is applied the second derivative outperforms the intersecting tangent and threshold method to identify the systolic foot. However, when less strict filtering is applied the performance of the second derivative method deteriorates strongly.

In Chapter 4 we will show that *in vivo* the systolic foot in the distension waveform is no good time-reference point to measure local pulse wave velocity in the common carotid artery, because this time-reference point is influenced by an

early reflected wave. It is shown that an inflection point in the upstroke following the systolic foot might induce an apparent non-linear propagation of the systolic foot along the arterial segment of interest, which introduces an error in the estimated pulse wave velocity.

If the distance to the reflection site is known, reflections themselves might be used for the assessment of global pulse wave velocity, this method is discussed in Chapter 5. It is shown that care should be taken when an inflection point, signalling the arrival of a reflected wave is used to estimate transit time and especially pulse wave velocity without knowing the site of reflection, as it may lead to erroneous conclusions.

In Chapter 6 we consider the dicrotic notch in the distension waveform as an alternative time-reference point to measure local pulse wave velocity. The proposed method is tested in young and older subjects and the results obtained are compared with stiffness measurements based on the distensibility coefficient. It is shown that local pulse wave velocity measurements when using the dicrotic notch as time-reference point are reliable and allow discrimination between young and older subjects.

The validity of the exponential pressure-area relationship, as assumed in Chapter 2, is investigated in a group of 21 subjects undergoing coronary angiography involving intra-arterial pressure recordings (Chapter 7). In this Chapter we will also investigate the consequences of a pressure-dependent arterial stiffness for the assessment of pulse wave velocity.

In the general discussion (Chapter 8) we will briefly review the technical aspects of the pulse wave velocity measurement by means of multiple M-mode ultrasound. Moreover, we will consider the local pulse wave velocity as a method to determine an intrinsic arterial stiffness parameter. In addition, we will explore pulse wave velocity measurements to derive local (central) pulse pressure by assuming an exponential pressure-area relation and using only diastolic blood pressure as additional input. Furthermore, we will address whether other reflected waves may interfere with the identification of the systolic foot or the dicrotic notch. Finally, we will discuss the relevance of the dicrotic notch method for carotid-femoral pulse wave velocity measurements.

References

Anliker M, Histand MB, and Ogden E. Dispersion and attenuation of small artificial pressure waves in the canine aorta. Circ Res 23: 539-551, 1968.

Benthin M, Dahl P, Ruzicka R, and Lindstrom K. Calculation of pulse-wave velocity using cross correlation--effects of reflexes in the arterial tree. Ultrasound Med Biol 17: 461-469, 1991.

Bertram CD, Gow BS, and Greenwald SE. Comparison of different methods for the determination of the true wave propagation coefficient, in rubber tubes and the canine thoracic aorta. Med Eng Phys 19: 212-222, 1997.

Brands PJ, Willigers JM, Ledoux LA, Reneman RS, and Hoeks AP. A noninvasive method to estimate pulse wave velocity in arteries locally by means of ultrasound. Ultrasound Med Biol 24: 1325-1335, 1998.

Busse R, Bauer RD, Schabert A, Summa Y, and Wetterer E. An improved method for the determination of the pulse transmission characteristics of arteries in vivo. Circ Res 44: 630-636, 1979.

Chiu YC, Arand PW, Shroff SG, Feldman T, and Carroll JD. Determination of pulse wave velocities with computerized algorithms. Am Heart J 121: 1460-1470, 1991.

Eriksson A, Greiff E, Loupas T, Persson M, and Pesque P. Arterial pulse wave velocity with tissue Doppler imaging. Ultrasound Med Biol 28: 571-580, 2002.

Fry DL, Casper AG, and Mallos AJ. A catheter tip method for measurement of the instantaneous aortic blood velocity. Circ Res 4: 627-632, 1956.

Hayashi K, Handa H, Nagasawa S, Okumura A, and Moritake K. Stiffness and elastic behavior of human intracranial and extracranial arteries. J Biomechanics 13: 175-184, 1980.

Histand MB and Anliker M. Influence of flow and pressure on wave propagation in the canine aorta. Circ Res 32: 524-529, 1973.

Hoeks AP, Brands PJ, Smeets FA, and Reneman RS. Assessment of the distensibility of superficial arteries. Ultrasound Med Biol 16: 121-128, 1990.

Hoeks AP, Willigers JM, and Reneman RS. Effects of assessment and processing techniques on the shape of arterial pressure-distension loops. J Vasc Res 37: 494-500, 2000.

Kelly R, Hayward C, Avolio A, and O'Rourke M. Noninvasive determination of age-related changes in the human arterial pulse. Circulation 80: 1652-1659, 1989.

Khir AW, O'Brien A, Gibbs JS, and Parker KH. Determination of wave speed and wave separation in the arteries. J Biomech 34: 1145-1155, 2001.

Langewouters GJ, Wesseling KH, and Goedhard WJA. The static elastic properties of 45 human thoracic and 20 abdominal aortas in vitro and the parameters of a new model. J Biomech 17: 425-435, 1984.

Latham RD, Westerhof N, Sipkema P, Rubal BJ, Reuderink P, and Murgo JP. Regional wave travel and reflections along the human aorta: a study with six simultaneous micromanometric pressures. Circulation 72: 1257-1269, 1985.

Laurent S, Boutouyrie P, Asmar R, Gautier I, Laloux B, Guize L, Ducimetiere P, et al. Aortic stiffness is an independent predictor of all-cause and cardiovascular mortality in hypertensive patients. Hypertension 37: 1236-1241., 2001.

Laurent S, Katsahian S, Fassot C, Tropeano AI, Gautier I, Laloux B, and Boutouyrie P. Aortic stiffness is an independent predictor of fatal stroke in essential hypertension. Stroke 34: 1203-1206, 2003.

Li JK, Melbin J, Riffle RA, and Noordergraaf A. Pulse wave propagation. Circ Res 49: 442-452, 1981.

Luchsinger PC, Snell RE, Patel DJ, and Fry DL. Instanteous Pressure Distribution Along the Human Aorta. Circ Res 15: 503-510, 1964.

Mancia G, De Backer G, Dominiczak A, Cifkova R, Fagard R, Germano G, Grassi G, et al. 2007 Guidelines for the Management of Arterial Hypertension: The Task Force for the Management of Arterial Hypertension of the European Society of Hypertension (ESH) and of the European Society of Cardiology (ESC). J Hypertens 25: 1105-1187, 2007.

Mattace-Raso FU, van der Cammen TJ, Hofman A, van Popele NM, Bos ML, Schalekamp MA, Asmar R, et al. Arterial stiffness and risk of coronary heart disease and stroke: the Rotterdam Study. Circulation 113: 657-663, 2006.

Maxwell JA and Anliker M. The dissipation and dispersion of small waves in arteries and veins with viscoelastic wall properties. Biophys J 8: 920-950, 1968.

McEniery CM, Wilkinson IB, and Avolio AP. Age, hypertension and arterial function. Clin Exp Pharmacol Physiol 34: 665-671, 2007.

McLeod AL, Uren NG, Wilkinson IB, Webb DJ, Maxwell SR, Northridge DB, and Newby DE. Non-invasive measures of pulse wave velocity correlate with coronary arterial plaque load in humans. J Hypertens 22: 363-368, 2004.

McVeigh GE, Hamilton PK, and Morgan DR. Evaluation of mechanical arterial properties: clinical, experimental and therapeutic aspects. Clin Sci (Lond) 102: 51-67, 2002.

Meinders JM, Kornet L, Brands PJ, and Hoeks AP. Assessment of local pulse wave velocity in arteries using 2D distension waveforms. Ultrason Imaging 23: 199-215, 2001.

Millasseau SC, Stewart AD, Patel SJ, Redwood SR, and Chowienczyk PJ. Evaluation of carotid-femoral pulse wave velocity: influence of timing algorithm and heart rate. Hypertension 45: 222-226, 2005.

Milnor WR and Bertram CD. The relation between arterial viscoelasticity and wave propagation in the canine femoral artery in vivo. Circ Res 43: 870-879, 1978.

Milnor WR and Nichols WW. A new method of measuring propagation coefficients and characteristic impedance in blood vessels. Circ Res 36: 631-639, 1975.

Mohiuddin MW, Laine GA, and Quick CM. Increase in pulse wavelength causes the systemic arterial tree to degenerate into a classical windkessel. Am J Physiol Heart Circ Physiol 293: H1164-1171, 2007.

Morgan GW and Ferrante WR. Wave propagation in elastic tubes filled with streaming liquid. J Acoust Soc Am 27: 715-725, 1955.

Morgan GW and Kiely JP. Wave propgation in a viscous fluid contained in a flexible tube. J Acoust Soc Am 26: 323-328, 1954.

Newman DL, Sipkema P, Greenwald SE, and Westerhof N. High frequency characteristics of the arterial system. J Biomechanics 19: 817-824, 1986.

Nichols WW and O'Rourke MF. Principles of recording and analysis of arterial waveforms. In: McDonald's blood flow in arteries (5th edition ed.). London: Edward Arnold, 2005a.

Nichols WW and O'Rourke MF. Properties of the arterial wall: theory. In: McDonald's blood flow in arteries (5th edition ed.). London: Edward Arnold, 2005b, p. 59.

O'Rourke MF. Pressure and flow waves in systemic arteries and the anatomical design of the arterial system. J Appl Physiol 23: 139-149, 1967.

Park SM, Seo HS, Lim HE, Shin SH, Park CG, Oh DJ, and Ro YM. Assessment of arterial stiffness index as a clinical parameter for atherosclerotic coronary artery disease. Circ J 69: 1218-1222, 2005.

Parker KH and Jones CJ. Forward and backward running waves in the arteries: analysis using the method of characteristics. J Biomech Eng 112: 322-326, 1990.

Pruett JD, Bourland JD, and Geddes LA. Measurement of pulse-wave velocity using a beat-sampling technique. Ann Biomed Eng 16: 341-347, 1988.

Quick CM, Berger DS, Stewart RH, Laine GA, Hartley CJ, and Noordergraaf A. Resolving the hemodynamic inverse problem. IEEE Trans Biomed Eng 53: 361-368, 2006.

Rabben SI, Stergiopulos N, Hellevik LR, Smiseth OA, Slordahl S, Urheim S, and Angelsen B. An ultrasound-based method for determining pulse wave velocity in superficial arteries. J Biomech 37: 1615-1622, 2004.

Raines JK, Jaffrin MY, and Shapiro AH. A computer simulation of arterial dynamics in the human leg. J Biomech 7: 77-91, 1974.

Rakebrandt F, Palombo C, Swampillai J, Schon F, Donald A, Kozakova M, Kato K, et al. Arterial Wave Intensity and Ventricular-Arterial Coupling by Vascular Ultrasound: Rationale and Methods for the Automated Analysis of Forwards and Backwards Running Waves. Ultrasound Med Biol, 2008.

Reneman RS, Meinders JM, and Hoeks AP. Non-invasive ultrasound in arterial wall dynamics in humans: what have we learned and what remains to be solved. Eur Heart J 26: 960-966, 2005.

Reneman RS, van Merode T, Hick P, Muytjens AM, and Hoeks AP. Age-related changes in carotid artery wall properties in men. Ultrasound Med Biol 12: 465-471, 1986.

Schiffrin EL. Vascular stiffening and arterial compliance: implications for systolic blood pressure. Am J Hypertens 17: 39S-48S, 2004.

Segadal L and Matre K. Blood velocity distribution in the human ascending aorta. Circulation 76: 90-100, 1987.

Segers P and Verdonck P. Role of tapering in aortic wave reflection: hydraulic and mathematical model study. J Biomech 33: 299-306, 2000.

She J, Bertram CD, and Gow BS. Analysis of all possible combinations of four measurements determining true propagation in arteries. J Biomed Eng 15: 379-386, 1993.

Studinger P, Lenard Z, Reneman R, and Kollai M. Measurement of aortic arch distension wave with the echo-track technique. Ultrasound Med Biol 26: 1285-1291, 2000.

Takazawa K, Tanaka N, Takeda K, Kurosu F, and Ibukiyama C. Underestimation of vasodilator effects of nitroglycerin by upper limb blood pressure. Hypertension 26: 520-523, 1995.

Taylor MG. An experimental determination of the propagation of fluid oscillations in a tube with a visco-elastic wall; together with an analysis of the characteristics required in an electrical analogue. Phys Med Biol 4: 63-82, 1959a.

Taylor MG. Wave travel in arteries: University of London, 1959b.

Ting CT, Chang MS, Wang SP, Chiang BN, and Yin FC. Regional pulse wave velocities in hypertensive and normotensive humans. Cardiovasc Res 24: 865-872, 1990.

Vulliemoz S, Stergiopulos N, and Meuli R. Estimation of local aortic elastic properties with MRI. Magn Reson Med 47: 649-654, 2002.

Waddell TK, Dart AM, Medley TL, Cameron JD, and Kingwell BA. Carotid pressure is a better predictor of coronary artery disease severity than brachial pressure. Hypertension 38: 927-931, 2001.

Westerhof N, Sipkema P, van den Bos GC, and Elzinga G. Forward and backward waves in the arterial system. Cardiovasc Res 6: 648-656, 1972.

Womersley JR. Method for the calculation of velocity, rate of flow and viscous drag in arteries when the pressure gradient is known. J Physiol 127: 553-563, 1955.

Zamir M. The Physics of Pulsatile Flow. New York: Springer-Verlag, 2000.

Zhang X. Noninvasive method for estimation of complex elastic modulus of arterial vessels. IEEE Trans Ultrason Ferroelectr Freq Control 52: 642-652, 2005.

Zhang X and Greenleaf JF. Measurement of wave velocity in arterial walls with ultrasound transducers. Ultrasound Med Biol 32: 1655-1660, 2006.

Chapter 2

Artery wall mechanics determined by means of ultrasound

Published as book chapter:

Arnold P.G. Hoeks, Evelien Hermeling, Robert S. Reneman. Artery wall mechanics determined by means of ultrasound. Vascular hemodynamics: bioengineering and clinical perspectives. Ed. Peter J. Yim, New York, John Whiley & Sons 2008: 133-156

Abstract

The mechanical properties of the arterial wall play an important role in reducing the heart load and conveying blood pressure and blood volume to the periphery. Because aging and cardiovascular disorders strongly impact the conduit function of the arterial system, the relevant parameters, such as lumen size, wall thickness, local blood pressure, distensibility, compliance, elasticity coefficient, and pulse wave velocity have been measured. In this Chapter we will address the relevant non-invasive techniques, mostly based on ultrasound, to acquire the parameters in the normal population as well as in specific subject groups, e.g. hypertensives and diabetics. Moreover, we will discuss the mathematical and physical interrelationships between those parameters. It will be shown that the assumptions, applied to derive these relationships, inherently lead to approximations. Some characteristics are difficult to measure directly, e.g. local pulse pressure, prompting suggestions for alternatives to assess the mechanical properties of arterial walls.

2.1 Introduction

Many decades ago Strandness and colleagues (Strandness et al. 1966) realized that Doppler techniques could be used to non-invasively identify atherosclerotic lesions in arteries accessible to ultrasound. Since then non-invasive vascular ultrasound, generally combining anatomic and flow information, has gradually been developed and is now routinely used to diagnose these lesions clinically (Polak 1995). Non-invasive vascular ultrasound is also used to measure intima-media thickness (IMT), a parameter commonly employed in epidemiological (Bots et al. 1997; O'Leary et al. 1999) and intervention studies (Boutouyrie et al. 2000) as a possible indicator of atherosclerotic disease (Simon et al. 2002; Bots et al. 2005; Lorenz et al. 2006; Staub et al. 2006).

Recently, the focus of non-invasive vascular ultrasound has been extended to the assessment of artery wall properties, in terms of distension, circumferential strain, distensibility, compliance and Young's modulus (Hoeks et al. 1990; Tardy et al. 1991; Riley et al. 1992; Hoeks et al. 1999). Understanding these mainly dynamic parameters is of utmost importance in patient management, because loss of elastic properties of elastic arteries, as in aging (Reneman et al. 1985;

Reneman et al. 1986), and in borderline (Van Merode et al. 1988; Van Merode et al. 1993) and essential hypertension (Laurent et al. 1994a; Laurent 1995), contributes substantially to the increase in systolic arterial and pulse pressure, which are known independent risk factors (Menotti et al. 1989; Safar et al. 2003). Ultrasonic techniques are now available to non-invasively determine lumen diameter, distension (pulsatile changes in diameter due to changes in blood pressure during the cardiac cycle), circumferential strain, and intima media thickness with great detail. Because these parameters can be determined with one and the same ultrasound system (Brands et al. 1999), their interrelation at a particular site along the arterial tree can be investigated. Moreover, these parameters in combination with blood pressure can be used to quantify the storage capacity of arteries and the stress-strain relation of arterial walls.

This Chapter will address the most important achievements in the non-invasive assessment of artery wall dynamics in humans. The focus will be on the interrelationship between parameters describing the mechanical characteristics of the arterial wall. These relationships are subsequently used to derive parameters which are generally difficult to measure non-invasively (e.g., local pulse pressure and local pulse wave velocity). A special point of concern will be the non-invasive determination of the elasticity coefficient (Young's modulus) of wall material. This leads automatically to a discussion of techniques currently used to measure the relevant parameters, i.e., local blood pressure, lumen diameter and wall thickness. In the last decade specific age and patients groups were subjected to a detailed examination of vascular condition. Here we will discuss the changes observed in aging and in essential and borderline hypertension. The changes in artery wall properties in atherosclerosis and diabetes will be discussed as well. Although most of the data presented are derived from clinical studies; observations made in epidemiological and pharmacological studies are included where relevant.

2.2 Properties of vascular dynamics

Lumen diameter and wall thickness

Let us consider a circular cross-section of an artery with an initial lumen diameter d and wall thickness *h*. Let us assume that the wall material is incompressible (conservation of volume) but can deform. The change in lumen diameter Δd due

to a change in transmural pressure requires a change in wall thickness Δh to maintain the wall volume $\pi\, d\, h$:

$$\pi d\, h = \pi(d + \Delta d)(h + \Delta h) \Rightarrow\ \varepsilon_h = \frac{\Delta h}{h} = \frac{-\Delta d}{d} \qquad 2.1$$

To arrive at the expression for the relative change in wall thickness ε_h (radial wall strain) second order effects are ignored ($\Delta d << d$, $\Delta h << h$, $h << d$). The relative change in wall thickness is the inverse of the relative change in diameter. Now let us consider the displacement Δx of the outside wall as function of wall thickness for an imposed change in lumen diameter:

$$\Delta x = \Delta d / 2 + \Delta h = 0.5\, \Delta d(1 - 2h / d) \qquad 2.2$$

Because of the assumed conservation of volume, a gradient in radial displacement occurs over the artery wall which increases with relative wall thickness (h / d). The displacement of the outside wall will be 20 % down with respect to that of the wall-lumen interface for an h/d of 10 %. Consequently at the outer wall the circumferential strain, i.e., the relative change in circumference, will be down by 40 % for an h / d = 10 %:

$$strain = \frac{\pi(\Delta d + 2\Delta h)}{\pi(d + 2h)} = \frac{\Delta d(1 - 2h / d)}{d(1 + 2h / d)} \qquad 2.3$$

This equation leads to a first order estimate for the average circumferential wall strain ε_c

$$\varepsilon_c = \frac{\Delta \mathrm{d}(1 - \mathrm{h} / \mathrm{d})}{\mathrm{d}(1 + \mathrm{h} / \mathrm{d})} \qquad 2.4$$

It can be concluded from the above expressions that a change in lumen diameter primarily affects the inner layers of the wall while the outer layer, e.g. the tunica adventitia, will be exposed to a lower radial strain and a considerably lower circumferential strain.

Distensibility and compliance

Parameters to characterize the elastic behavior of arteries are distensibility and compliance, defined as the observed relative (ΔV / V) and absolute (ΔV) change

in arterial lumen volume (V) for an imposed change in pressure (Δp), respectively. The distensibility reflects the mechanical load of the artery wall, while the compliance reflects the ability to store temporarily blood volume, thereby reducing blood pressure increase during ventricular ejection.

Distensibility and compliance are generally expressed as changes in lumen cross-sectional area A during the cardiac cycle rather than changes in lumen volume. This is allowed, because artery length hardly changes during the cardiac cycle due to longitudinally tethering of arteries at their *in vivo* length (Patel and Fry 1966; L'Italien et al. 1994). Moreover, if the volume of wall material is indeed constant, then theoretically the wall strain in the longitudinal direction of a rotation symmetric artery will be zero and there will be no change in length regardless of whether the artery is tethered. The expression for distensibility coefficient (DC), i.e. the distensibility per unit of artery length, in terms of a reference lumen diameter d (usually the end-diastolic diameter) and the change in diameter Δd (distension) due to a change in pressure Δp, assuming a circular lumen cross-section is

$$DC = \frac{\Delta A / A}{\Delta p} = \frac{((d+\Delta d)^2 - d^2)/d^2}{\Delta p} \approx \frac{2\Delta d}{d\,\Delta p} \quad [1/\text{Pa}] \qquad 2.5$$

The approximation induces an error of 5 % in DC for a relative change in lumen diameter of 10 % which is quite a normal value for the common carotid artery of a young healthy subject. Small animals may exhibit a considerably larger strain (Van Gorp et al. 1996) and the approximation should then be avoided. The compliance coefficient (CC) can be rewritten as

$$CC = \frac{\Delta A}{\Delta p} = \frac{\pi((d+\Delta d)^2 - d^2)}{4\Delta p} \approx \frac{\pi d\,\Delta d}{2\Delta p} \quad [\text{m2/Pa}] \qquad 2.6$$

Elasticity

The elasticity coefficient E, also known as Young's modulus, is defined as the change in circumferential stress S_c (force divided by area) divided by the circumferential strain (relative change in circumference). This definition may be confusing since a high value indicates a stiff (less elastic) artery. Assuming that the stress gradient over the wall is negligible (thin walled tube), the circumferential wall stress follows from the Lamé equation, which can easily be obtained by considering a plane through the axis of an arterial segment with

length *L*. In equilibrium the forces in the wall counterbalance the downward force *p L d* on the plane caused by the transmural blood pressure *p*:

$$2S_c\,h\,L = p\,L\,d \Rightarrow 2S_c\,h = p\,d \qquad 2.7$$

Using a first order Taylor series expansion the change in stress $\sigma_c = \Delta S_c$ due to a change in pressure Δp can be approximated with:

$$2\Delta S_c = 2\sigma_c = \frac{d}{h}\Delta p + p\frac{\Delta d}{h} - p\frac{d\,\Delta h}{h^2} = \frac{d\,p}{h}\left(\frac{\Delta p}{p} + \frac{2\Delta d}{d}\right) \qquad 2.8$$

In this approximation the relative change in wall thickness is approximated by the relative change in diameter (Equation 2.1). Let Δp be the pulse pressure (systolic minus diastolic blood pressure), then the fractional change in blood pressure will be about 0.3, while the corresponding fractional change in artery diameter is generally less than 0.1. To neglect the latter with respect to the fractional change in blood pressure, it should even be less than 0.01, which would presume very stiff arteries. For a small *h* / *d* the relative change in circumference at the lumen-wall interface (Equation. 2.3) can be approximated by Δd/d and the ratio of wall stress and circumferential strain (elasticity coefficient) transfers into:

$$E = \frac{\sigma_c}{\Delta d / d} = \frac{\Delta p\,d}{2h\,\Delta d / d} = \frac{d}{h\,DC} \qquad 2.9$$

$$E = \frac{\Delta p\,d}{2h\,\Delta d / d} = \frac{\Delta p\,d^2 d}{2h\,d\,\Delta d} = \frac{2\Delta p\,R_i^2}{(R_o^2 - R_i^2)}\frac{R_i}{\Delta R_i} \quad \text{[Pa]} \qquad 2.10$$

Expression 2.10 with R_i and R_o denoting the inner and outer radius of the artery, respectively, is a conversion from Equation 2.9 to reveal the similarity with the expressions as they appear in textbooks.

The non-linear variation in strains with radial position complicates a theoretical derivation of wall properties based on observed transmural blood pressure and diameter values, even if the situation is simplified (see below) to rotation symmetry and a homogeneously incompressible wall (Taylor and Gerrard 1977a; Taylor and Gerrard 1977b; Demiray 1983; Fung 1984; Nichols and O'Rourke 1998; Zamir 2000). In its most simple form the expression for a minor perturbation σ_c around S_c for an imposed change in blood pressure corresponds to the Lamé equation (Equation 2.7). However, the simplification discards the

pressure dependent term (last term Equation 2.8) which would otherwise render the result non-linear. If we maintain this term and rearrange the expression for the elasticity coefficient (Equation 2.10), we obtain:

$$E = \frac{d^2 p}{2h\Delta d}\left(\frac{\Delta p}{p} + \frac{2\Delta d}{d}\right) = \frac{d^2 \Delta p}{2h\Delta d} + \frac{d\,p}{h} \quad \text{[Pa]} \qquad 2.11$$

Clearly the elasticity coefficient E increases with transmural pressure due to the contribution of the last term.

In the derivation of the Young's modulus *E* (Equation 2.9), the contribution of wall thickness is only partly accounted for. Moreover, the mutual interaction between radial, circumferential and longitudinal (incremental) strains is ignored. Let us denote the strains in axial, circumferential and radial direction by ε_z, ε_c, and ε_h respectively, while the corresponding incremental stresses are given by σ_z, σ_c and σ_h. Then, the stress-strain relations in either direction due to a pressure increase Δp are given by:

$$\begin{aligned} \varepsilon_z E &= \sigma_z - \mu(\sigma_h + \sigma_c) \\ \varepsilon_h E &= \sigma_h - \mu(\sigma_z + \sigma_c) \\ \varepsilon_c E &= \sigma_c - \mu(\sigma_h + \sigma_z) \end{aligned} \qquad 2.12$$

In concordance with the assumed material property of volume incompressibility, the Poisson ratio μ = 0.5, while the longitudinal strain ε_z will be zero. Isolating σ_z gives:

$$\varepsilon_c E = \frac{3}{4}(\sigma_c - \sigma_z) \qquad 2.13$$

Expression 2.13 indicates that the circumferential strain not only depends on the circumferential stress but also on the transmural stress. The circumferential strain ε_c follows from Equation 2.4, the incremental circumferential stress σ_c is provided by Equation 2.8, while the incremental radial stress σ_h equals the change in transmural pressure Δp.

$$E = \frac{3d(d+h)}{4\Delta d(d-h)}\left(\frac{d\,p}{2h}\left(\frac{\Delta p}{p}+\frac{2\Delta d}{d}\right)-\Delta p\right)$$
$$E = \frac{3d(d+h)}{4\Delta d(d-h)}\left(\Delta p\left(\frac{d}{2h}-1\right)+\frac{\Delta d\,p}{h}\right) \qquad 2.14$$
$$E = \frac{3d(d+h)\Delta p}{4\Delta d(d-h)}\left(\frac{d}{2h}-1+\frac{\Delta d\,p}{\Delta p\,h}\right)$$

For a small wall thickness with respect to the diameter ($h << d$) and stiff arteries (Δd small for a given Δp) the first term between parentheses will dominate and Equation 2.14 can be simplified to:

$$E = \frac{3d^2\Delta p}{8h\Delta d} = \frac{1.5\Delta p R_i^2}{(R_o^2 - R_i^2)}\frac{R_i}{\Delta R_i} = \frac{3d}{4hDC} \qquad 2.15$$

Comparing Equations 2.13 and 2.9 shows the effect of the mutual interaction of the orthogonal stresses; it lowers the estimate for E by 25 %. To appreciate the effect of the assumptions made to convert Equation 2.14 to Equation 2.15 (estimated elasticity coefficient), let us consider an artery with a lumen diameter of 6 mm and a mean transmural pressure of 100 mmHg (13 kPa), subjected to a change in transmural pressure (pulse pressure) of 40 mmHg (= 5 kPa). Then, the relative error in the estimated E will only be 4.8 % for an $h / d = 0.01$ and a relative diameter change of $\Delta d / d = 0.01$, but will increase dramatically to 37 % if both quantities assume realistic values ($h / d = 0.1$; Δd / d = 0.1) and to 41 % for an increase in mean pressure to 120 mmHg. Equation 2.14, instead of Equation 2.15, does not solve all the problems, because its derivation assumes that the stresses within the wall do not depend on the radial position. However, the most serious limitation of the above derivation is the implicit assumption about a finite wall thickness: it seems like the artery is isolated from its environment. In reality it is embedded in tissue which can be considered as part of the wall, causing stiffer wall behaviour (Zhang and Greenleaf 2006).

Pulse wave velocity

The derivation for the pulse wave velocity is based on Newton's law, applied to a thin cross-sectional slice of an artery, bounded by planes I and II with an area A, an incremental thickness δz and a specific mass ρ, and the law of conservation

of mass (Figure 2.1). The blood velocity is v_z with a velocity gradient δv_z while the pressure is p_z with a pressure gradient δp_z, both along the axis of the artery.

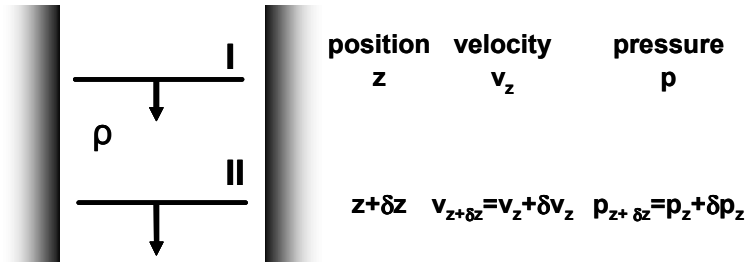

Figure 2.1 Definition of basic parameters for the derivation of the pressure wave velocity.

In the incremental time interval δt mass $\rho A\, v_z\, \delta t$ and $\rho A(v_z + \delta v_z)\, \delta t$ enters and leaves the slice, respectively, resulting in an increase of the mass of the slice of $\delta m = \rho A\, \delta v_z\, \delta t$. Let us assume that blood is incompressible and the contribution of a possible longitudinal gradient in diameter is negligible since the slice thickness is very small with respect to the wavelength. Using the relationship $\rho A = m / \delta z$ (specific mass is mass divided by volume) results in:

$$\frac{\delta m}{m \delta t} = -\frac{\delta v_z}{\delta z} \qquad 2.16$$

The force exerted by the pressure on plane I is $p_z A$ while on plane II it is $(p_z + \delta p_z)\, A$. Assuming that the contribution of a possible gradient of the velocity is negligible the pressure gradient $-\delta p_z A$ causes an acceleration $\delta v_z / \delta t$ of the mass $\rho A\, \delta z$:

$$\frac{\delta p_z}{\delta z} = -\rho \frac{\delta v_z}{\delta t} \qquad 2.17$$

The final step is to link the change in volume to the change in pressure based on the material properties. For an elastic artery the distensibility D of a segment with initial volume V is defined as (cf. Equation 2.5):

$$D = \frac{\delta V}{V \delta p_z} = \frac{\delta (m / \rho)}{(m / \rho) \delta p_z} = \frac{\delta m}{m \delta p_z} \qquad 2.18$$

Substitution of Equation 2.18 in Equation 2.16 results in:

$$\frac{D\,\delta p_z}{\delta t} = -\frac{\delta v_z}{\delta z} \qquad 2.19$$

Differentiation of Equation 2.19 and Equation 2.17 with respect to *t* and *z*, respectively, and elimination of v results in the familiar wave equation:

$$\frac{\delta^2 p_z}{\delta t^2} = \frac{1}{\rho D}\frac{\delta^2 p_z}{\delta z^2} \qquad 2.20$$

Substitution of a general harmonic solution $p_z = \hat{p}\cos(2\pi ft - 2\pi z/\lambda)$ with $c_p = \lambda f$, λ the wavelength, *f* frequency and c_p the propagation speed of the wave results in the Bramwell-Hill equation:

$$-\hat{p}4\pi^2 f^2 \cos(2\pi f t - 2\pi z/\lambda) = \frac{-\hat{p}4\pi^2}{\rho D \lambda^2}\cos(2\pi f t - 2\pi z/\lambda)$$
$$c_p = \sqrt{\frac{1}{\rho D}} = \sqrt{\frac{1}{\rho DC}} \qquad 2.21$$

Equation 2.21 offers also the opportunity to express the pulse wave velocity c_p as function of pressure *p* and flow *q* by using the notion of characteristic impedance *Z* (Westerhof 1993). In the absence of wave reflections, *Z* can be expressed either by a pressure-flow relationship or by the mean cross-sectional area $\bar{A}$ and distensibility (Rabben et al. 2004):

$$Z = \sqrt{\frac{\rho}{\bar{A}^2 \cdot DC}} = \frac{dp}{dq} = \frac{dp}{dA}\frac{dA}{dq} = \frac{1}{A\,DC}\frac{dA}{dq} \qquad 2.22$$

In the above conversion use is made of Equation 2.18. Solving Equation 2.22 for *dq* / *dA* and using Equation 2.21 result in:

$$\frac{dq}{dA} = \sqrt{\frac{1}{\rho DC}} = c_p \qquad 2.23$$

2.3 Measurement and processing of key parameters

To calculate the key parameters describing the dynamic mechanical characteristics of arterial segments (Reneman et al. 2005; Laurent et al. 2006), i.e. the distensibility and compliance coefficients and the Young's modulus, we need wall thickness and local diameter and blood pressure waveforms. Since the local blood pressure waveform in, e.g., the carotid artery is difficult to acquire, the pulse pressure (difference between systolic and diastolic pressure) measured elsewhere (brachial artery) is substituted for the pressure increment Δp. However, tapering and peripheral pressure wave reflections cause the systolic blood pressure in the brachial artery, but not the diastolic pressure, to be substantially higher than that in the carotid artery. Consequently the pulse pressure is overestimated and the mechanical parameters are underestimated. The difference in pulse pressure on both locations depends on the age of the subject and the cardiovascular condition (Waddell et al. 2001; Laurent et al. 2006).

An alternative to acquire pulse pressure is provided by a tonometer (Kelly et al. 1989), a pencil-like probe, containing a high-fidelity micromanometer. It is used to flatten an artery transcutaneously against a bony structure, thereby balancing the circumferential stresses in the artery wall. If the probe can be maintained in a steady position the time-dependent change in blood pressure is truthfully recorded. However, the recording requires calibration of the diastolic blood pressure. Because in diastole the pressure drop over the central arteries is negligible if measured at heart level, any accessible location can be selected for the calibration procedure, e.g., the brachial artery. Under steady state conditions the diastolic blood pressure exhibits only minor fluctuations, allowing for an incidental reference measurement, for example, with a conventional sphygmomanometer or an oscillometric blood pressure meter. Likewise, assuming that mean arterial pressure (*MAP*) is also the same in the major arteries, the average of the tonometer waveform over a cardiac cycle can be equated to the *MAP* derived in another way. Unfortunately, there is no physically sound algorithm to estimate *MAP* from oscillometric blood pressure readings. The reported values for *MAP*, but also for the recorded systolic and diastolic blood pressures, may vary considerably (Amoore et al. 1997). Since diastolic pressure and *MAP* are used to calibrate the tonometer readings any error in the reference values will equally emerge in the tonometer blood pressure values.

The approach as outlined above assumes that the tonometer is held firmly in position, meaning that the applied force should vary in accordance with the blood

pressure to be measured. This requirement is difficult to comply with, resulting in distorted pressure registrations especially in late systole. The other pre-requisite is that a solid background supports the artery of interest. This is true for the radial, brachial and femoral arteries, but not for the carotid artery. That is why blood pressure results for this artery are subject to dispute, especially since for ethical reasons verification measurements are scarce and virtually absent for the normal population.

Diastolic diameter and its pulsatile change over the cardiac cycle can be measured accurately and reliably with modern echo tracking systems (Kool et al. 1994), using a two-dimensional B-mode imager attached to a vessel wall moving detector system (Hoeks et al. 1990). The displacement detection algorithm is based upon radiofrequency (RF) correlation tracking rather than narrow-band Doppler processing (Hoeks et al. 1993). Processing in the RF domain has the advantage that the high depth resolution offered by the echo-mode (wide-band RF signals) is maintained. A fine depth resolution is essential since the displacement gradient over the wall can be substantial (cf. Equation 2.2). On the other hand, for a wide-band RF signal the frequency dependent attenuation causes a significant downward shift in the mean RF frequency depending on depth location and intervening tissues. That is why displacement detection based on echo-mode RF processing involves the estimation of both the phase shift over subsequent observations and the underlying mean RF frequency. This is readily achieved for RF signals with a specific spectral shape, e.g. a Gaussian distribution (or at least a symmetric distribution). Then, the shape of the cross-correlation function of the RF signals, converted to a complex representation using the Hilbert transform, is well defined (Brands et al. 1997; Brands et al. 1999; Meinders et al. 2001a; Hoeks and Reneman 2005). Only three complex coefficients are required (autocorrelation, correlation at depth and time lag 1, respectively) to estimate the local carrier frequency (phase at depth lag 1), displacement (phase at time lag 1), signal level (autocorrelation), and the RF bandwidth and signal-to-noise ratio (amplitude of the coefficients).

Displacement detection using echo-mode RF signals has a good precision (Bennett et al. 2007), even when extremely short (few ms) temporal estimation windows are used. This is because the random appearance of reflections, i.e. its random phase, is maintained while processing the signal (Hoeks et al. 1993). Moreover, the signal segment considered for displacement detection (Meinders et al. 2001a), as set at the onset of the registration, is automatically repositioned based on the observed displacement, ensuring that throughout the cardiac cycle the same wall segment is tracked despite wall displacements of more than 2

times the resolution of the echo system. The same procedure is followed for both the anterior and posterior wall; the difference between both gives the change in lumen diameter over time (distension waveform), while the initial distance between the selected segments is used as an estimate for the end-diastolic lumen diameter. In recent systems, artery wall-lumen transitions at end-diastole are identified automatically, allowing beat-to-beat acquisition and presentation of the end-diastolic diameter and distension waveform. The end-diastolic diameter is not the true lumen diameter since the identification algorithm locks onto the large ultrasound echo-transient of the media-adventitia interface. Hence, the estimated diameter is the adventitia-to-adventitia distance minus one resolution of the echo system (trailing edge of anterior wall echo).

To get the true lumen diameter, algorithms have been developed that, starting from an arbitrary position within the lumen, looks for transients in echo level. If they are consistent in time or in position and the change in echo level is substantial, then it is quite likely that the transient is caused by the lumen-intima boundary. Again an error is made because the distance between the trailing echo edge of the anterior intima-lumen interface and the leading edge of the posterior interface is considered.

Once the positions of the adventitia-media and intima-lumen boundaries are established it is a small step to derive the intima-media thickness. However, at the anterior artery wall, large trailing echoes from the adventitia extend into the media and may even partially cover the media-intima transition, especially for young subjects or for echo systems with an inadequate resolution (Touboul et al. 2006). That is why generally only the intima media thickness measured at the posterior wall is considered (Willekes et al. 1999b). The intima media thickness should not be confused with wall thickness because the latter also includes the adventitia layer whose outer boundary cannot reliably be distinguished with present ultrasound techniques.

The use of the intima media thickness rather than whole wall thickness in assessing artery wall dynamics is acceptable, because the media is the most important determinant of these dynamics, at least under normal circumstances and in hypertension. In atherosclerosis, however, the intima is the layer most affected. Ever since the first intima media thickness measurements by Pignoli et al. (Pignoli et al. 1986) a variety of automated techniques has been developed (Selzer et al. 1994; Graf et al. 1999). All these techniques provide a mean intima media thickness extracted from B-mode images over a length of 10-20 mm, thereby reducing the obscuring effect of ultrasound speckle. In the past, the end-

diastolic images were selected from video-recordings according to a standard TV format with only 25 frames per second and thus a limited temporal resolution. Nowadays real-time B-mode display is decoupled from the TV-standard, allowing a considerable increase in image quality and image update rate. However, the B-mode image stream, and thus the image threshold level, remains susceptible to the settings for gain and amplitude compression (Bots et al. 1994; Touboul et al. 2006).

The local relative dynamic amplitude characteristics of RF signals are inherently insensitive to gain settings and are not modified by non-linear processing techniques, e.g., amplitude thresholding and dynamic range compression. That is why it is logical to extend the RF system for the measurement of end-diastolic diameter d and relative change in diameter $\Delta d / d$ with an automated method to derive the local intima media thickness from the recorded RF signals. If the RF signals have been recorded in M-mode, then the final intima media thickness estimate will be the mean of subsequent observations (Hoeks et al. 1997; Willekes et al. 1999b). For RF signals recorded in B-mode the spatial mean over a short image segment length provides an instantaneous estimate of wall thickness (Meinders et al. 2003).

2.4 Pressure and diameter waveforms

As stated before the estimation of mechanical parameters requires that both pressure and diameter waveforms are obtained at the same location and preferable simultaneously. For the carotid artery, a predilection site for atherosclerotic disease and, hence, a site of clinical interest, local pressure measurements are quite difficult. Substitution of the carotid pulse pressure by the pulse pressure obtained from the nearby brachial artery is not an option because of an unpredictable difference between both pulse pressures (Waddell et al. 2001).

In paragraph 2.2 attempts were made to develop a theoretical expression for the pressure-diameter relationship of an artery. Because of the interrelation between pressure, diameter, wall thickness and stresses only an approximation could be obtained under quite rigid constraints (stiff artery). For the physiological pressure range, experimental measurements confirmed an exponential relationship between the time-dependent pressure $p(t)$ and cross-sectional area $A(t) = \pi d^2 / 4$ (Hayashi et al. 1980; Stettler et al. 1981; Langewouters et al. 1984; Powalowski and Pensko 1988):

$$p(t) = p_o e^{\gamma A(t)} \qquad 2.24$$

The unknown constant γ can be derived if the local blood pressure and lumen area are known. This is the case for the diastolic pressure p_d and area A_d; and for the systolic pressure p_s and area A_s. Solving the resulting set of two equations gives:

$$p(t) = p_d e^{\alpha\left(\frac{A(t)}{A_d}-1\right)} \qquad 2.25$$

with:

$$\alpha = \frac{A_d \ln(p_s / p_d)}{A_s - A_d} \qquad 2.26$$

Since the wall rigidity index α (dimensionless) is pressure independent, Equation 2.26 is valid over a large physiological pressure range (Hayashi et al. 1980; Stettler et al. 1981; Langewouters et al. 1984; Powalowski and Pensko 1988). The rigidity index as used here is the reciprocal of the stiffness parameter defined earlier (Hayashi et al. 1980).

Equation 2.26 requires that the local diastolic and systolic blood pressures are known, but generally this is not the case. However, Equation 2.25 offers the opportunity to derive the local pressure waveform, in conjunction with the local diameter waveform, using blood pressures recorded elsewhere. It is based on the assumption that for the major arteries diastolic blood pressures and *MAP* do not vary with location. This assumption is reasonable since in the brachial artery mean wall shear stress, and hence friction loss, is low: the mean pressure drop over the major arteries is about 1 mmHg. Suppose that the area (diameter) waveform were recorded in the common carotid artery and the blood pressure waveform with a tonometer in the radial artery. Starting with an initial guess for α, based on the diastolic and systolic blood pressures observed elsewhere (Equation 2.26), provides a first estimate of the local pressure waveform. The observed difference between its time average and the peripheral *MAP* initiates subsequently an iterative adaptation procedure for α until the carotid and peripheral *MAP* are equal (Meinders and Hoeks 2004). For the final value of α, Equation 2.26 describes the pressure waveform in the carotid artery, linked to the local area (diameter) waveform.

Given Equation 2.25 it is now possible to estimate the distensibility and compliance coefficients and pulse wave velocity at any pressure, e.g. at 100 mmHg (Hayashi 1993):

$$DC = \left.\frac{\delta A}{A\delta p}\right|_{p=100} = \left.\frac{A_d}{\alpha A(p)p}\right|_{p=100} = \frac{A_d}{100\alpha A_{100}}$$
$$PWV = \sqrt{\frac{1}{\rho DC}} = \sqrt{\frac{100\alpha A_{100}}{\rho A_d}} \qquad 2.27$$
$$CC = \left.\frac{\delta A}{\delta p}\right|_{p=100} = \frac{A_d}{100\alpha}$$

The value A_{100} follows from Equation 2.25 by substituting p = 100 mmHg (= 13.3 kPa) and solving the equation. Indeed, for an exponential relationship between lumen area and pressure, the mechanical parameters turn out to be pressure dependent, complicating direct comparison of subject groups with different blood pressures. Equation 2.27 in combination with Equation 2.25 offer convenient ways to circumvent the problems associated with local blood pressure measurements. The diastolic pulse wave velocity provides a direct estimate for the rigidity index α. Then, the local pressure waveform is known without the iteration procedure or assumption about a possible drop in *MAP*. Its combination with the diameter waveform provides isobaric estimates for distensibility and compliance. Because the latter are now based on derivatives rather than large increments (pulse pressure and associated pulsatile change in lumen diameter) the effect of non-linear relationship is inherently suppressed.

For elastic arteries, e.g. the common carotid artery, the above approach can be simplified by assuming for the physiological pressure range a linear relationship between pressure and area (Van Bortel et al. 2001). Again the mean of the pulsatile pressure waveform $(MAP - p_d)$ is now directly related to the mean of the pulsatile area waveform $(\bar{A} - A_d)$:

$$MAP - p_d = \zeta(\bar{A} - A_d)$$
$$\zeta = \frac{MAP - p_d}{\bar{A} - A_d} \qquad 2.28$$
$$p(t) = \frac{MAP - p_d}{\bar{A} - A_d} A(t)$$

2.5 What we have learned?

Across mammals the blood pressure is of the same order (West et al. 1997; Greve et al. 2006), although the orthostatic contribution to transmural pressure will vary with size. Hence, the arteries are subjected to the same load, which has to be born primarily by the vascular smooth muscular fibers. Then the Young's modulus, the circumferential wall stress and the relative change in diameter, and thus the distensibility, will be of the same order across species. This consideration does not apply for the compliance, which increases with mammal size (absolute change in vessel cross-section).

The general statement above is not intended to stimulate generalization and extrapolation. Within species individual and inter-arterial variations of a factor of 5 are quite likely. That dynamic wall behavior of elastic arteries (ascending and descending aorta, carotid artery) differs from that of muscular arteries (coronary artery, femoral and brachial artery) is not surprising, but that their properties adapt differently to, for example, aging and hypertension was unknown till the introduction of dynamic vascular ultrasound (Cheng et al. 2002; Reneman et al. 2005; Laurent et al. 2006). The carotid intima media thickness also increases substantially as function of age at an estimated rate of 7 to 10 μm / year (Dinenno et al. 2000; Kornet et al. 2000; Homma et al. 2001; Tanaka et al. 2001; Yanase et al. 2006), or varies within a relatively short arterial segment (Willekes et al. 1999a).

Proper interpretation of the data is hampered by the various methods in use to acquire and process the basic data (diameter, wall thickness, blood pressure). In a large number of studies the adventitia-adventitia diameter is used as a substitute for the lumen diameter. Because the carotid artery intima media thickness increases considerably with age, the involved error is confounding the statistical analysis. There is still no consensus about the expression to use for the Young's modulus and it is quite unlikely that a universal solution will be found (see paragraph 2.2). Lastly the discussion about artery properties is clouded by the indiscriminate use of distensibility and compliance. Especially the English literature uses compliance where distensibility is intended (Lehmann et al. 1996; Gosling and Budge 2003).

Aging

Under normal circumstances distensibility and compliance of the elastic carotid artery decrease linearly with age from the third age decade onwards, the

reduction of compliance being less steep than the reduction of distensibility (Reneman et al. 1986; Cheng et al. 2002). The latter can be explained by the increase in diameter with increasing age (Reneman et al. 1985; Reneman et al. 1986; Riley et al. 1992) (Table 2.1). In this way elastic arteries counteract the reduction of their ability to store volume and, hence, the increase in systolic arterial and pulse pressure, with increase in age. In our analysis end-diastolic diameter is considered. When mean diameters were considered the difference in reduction between distensibility and compliance would have been quantitatively different, but qualitatively similar. Distension and circumferential strain also decrease with age (Figure 2.2; Table 2.1).

Table 2.1. Diameter and strain as function of age in the common carotid artery

		females			**males**	
Age (y)	**n**	**d [mm]**	**Δd / d [%]**	**n**	**d [mm]**	**Δd / d [%]**
10-19	10	5.9 ± 0.3	13 ± 2	8	6.0 ± 0.3	14 ± 3
20-29	12	6.0 ± 0.3	10 ± 1	12	6.5 ± 0.6	10 ± 2
30-39	15	6.2 ± 0.5	8 ± 2	18	6.5 ± 0.5	9 ± 2
40-49	10	6.4 ± 0.6	7 ± 2	10	6.5 ± 0.4	6 ± 2
50-59	8	6.3 ± 0.31)	6 ± 21)	7	6.4 ± 0.51)	5 ± 21)

Diameter (d) and percentage systolic circumferential strain (Δd / d*100%) as function of age per decade in the right common carotid artery in females (n = 55) and in males (n = 56). mean ± standard deviation

1) Significantly different from second age decade. After Samijo et al, 1998 (Samijo et al. 1998)

The loss of dynamic properties along the arterial tree is inhomogeneous. At older age distensibility of the muscular common femoral artery is reduced, but the distensibility of the deep and superficial muscular femoral arteries (Van Merode et al. 1996) and the compliance of the muscular brachial artery are not (Benetos et al. 1993; Van der Heijden-Spek et al. 2000). Similarly in the elastic carotid artery bifurcation, distensibility of the bulb, where predominantly the baroreceptors are located, is more severely affected by age than the distensibility of the common carotid artery (Reneman et al. 1985; Van Merode et al. 1993).

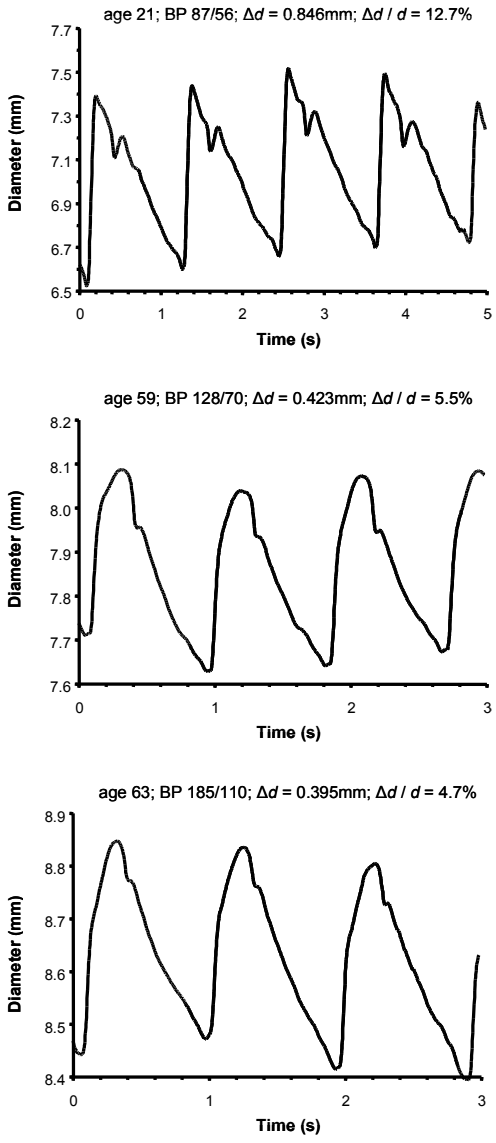

Figure 2.2 Distension waveforms as recorded in the common carotid artery of a young (top) and an older normotensive volunteer (middle), and an older hypertensive patient (bottom). During the recordings the volunteers and the patient were fully relaxed. Note the reduced distension (Δd) and circumferential strain (Δd / d; d = diameter), at even a higher blood pressure, in normotensive volunteer at older age, reflecting increased arterial stiffness. In hypertension arterial stiffness is further increased as indicated by the slightly reduced distension and the substantially reduced circumferential strain at a significantly higher blood pressure. After Reneman et al. 2005.

Hypertension

In patients with essential hypertension arterial stiffening (Green et al. 1966; Gribbin et al. 1979; Cheng et al. 2002) is not a generalized phenomenon along the arterial tree. In untreated hypertensive patients, at ambient mean arterial pressure, distensibility and compliance of the elastic carotid artery, but not of the radial artery (Hayoz et al. 1992), are significantly reduced (Laurent et al. 1994a). In the latter the Young's modulus was found to be similar in essential hypertensive patients and in age-matched control subjects (Laurent et al. 1994b).

Table 2.2. Carotid artery diameter and distensibility and compliance in subject with and without hypertension.

parameters	HT (n = 15)	NT (n = 14)
- at mean arterial pressure		
diameter (mm)	7.3 ± 0.3	6.9 ± 0.2
distensibility (MPa^{-1})	7.8 ± 0.7[1)]	11.7 ± 1.7
compliance (mm^2/kPa)	0.6 ± 0.1[1)]	0.9 ± 0.1
- at 100 mmHg		
diameter (mm)	7.5 ± 0.3	7.3 ± 0.2
distensibility (MPa^{-1})	10.0 ± 1.0	9.0 ± 1.1
compliance (mm^2/kPa)	0.8 ± 0.1	0.7 ± 0.1

Carotid artery diameter, distensibility and compliance in patients with essential hypertension (HT; 54 ± 15 years) and in age-matched normotensives (NT; 48 ± 15 years). Data in the table are mean ± standard error of the mean.
1) Significantly different from NT. After Laurent et al, 1994c

It is still incompletely understood whether in essential hypertension the reduction of artery wall distensibility and compliance of the elastic arteries (Table 2.2) is caused by the increase in blood pressure or that intrinsic changes in the wall contribute to this process (Cheng et al. 2002). The observation of Laurent et al (Laurent et al. 1994c) is in favor of a dominant role of increased arterial pressure, but our observations in borderline hypertensives (Van Merode et al. 1993; Reneman and Hoeks 2000) indicate that the reduction of dynamic artery wall properties cannot be fully explained by increased blood pressure (Table 2.3). This is in line with the observation that blood pressure reduction in hypertensive patients by nitroglycerine does not normalize artery stiffness (Stewart et al. 2006). In young spontaneously hypertensive rats the reduced

dynamic artery wall properties are independent of elevated blood pressures (Van Gorp et al. 2000), which agrees with the more recent finding that in younger essential hypertensives, intrinsic changes in the artery wall contribute to increased stiffness of the arteries (Bussy et al. 2000). Therefore, in the treatment of patients with essential and borderline hypertension not only reduction of blood pressure, but also enhancement of compliance of elastic arteries has to be considered, especially because the loss of compliance and distensibility strongly correlates with left ventricular hypertrophy (Boutouyrie et al. 1995). Compliance and distensibility of elastic arteries can be increased substantially by pharmacological intervention (increases up to 16 %), but one should bear in mind that not all anti-hypertensive drugs improve artery wall compliance, despite their blood pressure lowering effect (Van Bortel et al. 1995; Giannattasio and Mancia 2002).

Table 2.3. Systolic circumferential strain in the common carotid artery and the carotid artery bulb

Subject	n	CCA	B_p	B_{max}	B_d
BHT	16	6.3 ± 1.3	3.8 ± 1.4 [1)]	5.1 ± 1.4 [1) 2)]	5.4 ± 1.6 [1) 2)]
NTO	15	7.5 ± 1.9	5.7 ± 2.3 [1)]	7.0 ± 1.9	5.4 ± 2.3 [1)]
NTY	18	9.5 ± 2.2	9.2 ± 2.4	9.9 ± 2.3	8.7 ± 2.6

Percentage peak systolic circumferential strain ($\Delta d / d * 100$ %; mean ± standard deviation) in the common carotid artery (CCA), and in the proximal (B_p) and distal (B_d) parts of the carotid artery bulb as well as at the level of its maximum diameter (B_{max}) in normotensive young (NTY; 24 ± 3 years) and older (NTO; 38 ± 5 years) volunteers, and in borderline hypertensives (BHT; 38 ± 3 years). mean ± standard deviation

1) Significantly different from CCA; 2) Significantly different from *Bp*. After Van Merode et al, 1993

Diabetes

In cross-sectional studies, elastic and muscular arteries are generally found to be stiffer in diabetic patients than in age matched control subjects (Cheng et al. 2002), although the findings in insulin dependent diabetes mellitus (IDDM; type I diabetes) are inconsistent. For example, in patients with uncomplicated IDDM Kool et al. (Kool et al. 1995) did not find an obvious reduction of wall properties of elastic and muscular arteries in young patients, while Hu et al. (Hu et al. 1996) observed increased stiffness of the descending aorta in children and adolescents. The observations in non-insulin dependent diabetes mellitus (NIDDM; type II diabetes) are far more consistent in the studies published so far.

In cross-sectional (Emoto et al. 1998) and population based studies (Henry et al. 2003; van Popele et al. 2006) NIDDM was shown to be associated with loss of distensibility and compliance of both elastic and muscular arteries. Distensibility of the carotid artery is even reduced in healthy, non-diabetic subjects with an insulin resistance syndrome (Van Popele et al. 2000; Henry et al. 2003), indicating that artery stiffening is an early marker of pathology in this disorder.

Atherosclerosis

Relatively little is known about arterial dynamic properties in atherosclerosis (Cheng et al. 2002). In hypertensive patients arterial stiffness is associated with the presence and extent of atherosclerosis (Blacher et al. 1999). Population-based studies demonstrate that both aortic and common carotid artery stiffness have a strong positive association with carotid intima media thickness and severity of plaque in these vessels (Van Popele et al. 2001). The carotid-femoral pulse wave velocity, but not the carotid distensibility, provides additional predictive value for coronary events (Mattace-Raso et al. 2006).

2.6 Conclusions

An important shortcoming in the non-invasive assessment of dynamic vascular properties is the lack of a direct method to reliably determine pulse pressure non-invasively at the site of measurement. Using brachial pulse pressure as a substitute for carotid pulse pressure is not ideal because disease processes affect brachial and carotid artery wall properties, and, hence, pulse pressure, differently (Waddell et al. 2001). There is no pulse pressure substitute for the femoral artery. Reliable non-invasive acquisition of the pulse pressure waveform is also necessary to adequately compare normotensives and hypertensives at isobaric pressures, requiring the construction and comparison of full pressure-diameter relations. A direct approach is only feasible for radial and brachial arteries (Laurent et al. 1994b) because these arteries allow (simultaneous) acquisition of pressure and diameter waveforms. For the carotid artery a simple approach allows the derivation of the local pressure waveform from the diameter waveform assuming a linear relationship (Van Bortel et al. 2001). This can be extended to an exponential pressure-area relationship (Hayashi et al. 1980), with the rigidity coefficient as a single parameter (Meinders and Hoeks 2004), allowing a more general approach for the characterization of the mechanical behavior of arteries. However, its implementation requires knowledge about the

mean arterial pressure, which is quite susceptible for measurement artifacts. This problem can be avoided if techniques become available to acquire the local pulse wave velocity (Meinders et al. 2001b). Then, it will be possible to fully explore the effect of age and risk factors on the mechanical properties of both elastic and muscular arteries locally. This may eventually settle the current dispute about possible associations between central (carotid-femoral pathway) or carotid arterial stiffness on the one hand and coronary or cerebral vascular disease on the other hand (Mattace-Raso et al. 2006).

References

Amoore JN, Geake WB, Scott DHT. Oscillometric non-invasive blood pressure measurements: the influence of the make of instruments on readings? Med Biol Eng Comput 1997;35:131-134

Benetos A, Laurent S, Hoeks AP, Boutouyrie PH, Safar ME. Arterial alterations with aging and high blood pressure. Arterioscler Thromb 1993;13:90-97

Bennett MJ, McLaughlin S, Anderson T, McDicken WN. Error analysis of ultrasonic tissue Doppler velocity estimation techniques for quantification of velocity and strain. Ultrasound Med Biol 2007;33:74-81

Blacher J, Asmar R, Djane S, London GM, Safar ME. Aortic pulse wave velocity as a marker of cardiovascular risk in hypertensive patients. Hypertension 1999;33:1111-1117.

Bots ML, Grobbee DE, Hofman A, Witteman JC. Common carotid intima-media thickness and risk of acute myocardial infarction: the role of lumen diameter. Stroke 2005;36:762-7

Bots ML, Hofman A, Grobbee DE. Increased common carotid intima-media thickness. Adaptive response or a reflection of atherosclerosis? Findings from the Rotterdam study. Stroke 1997;28:2442-2447

Bots ML, Mulder PG, Hofman A, van Es GA, Grobbee DE. Reproducibility of carotid vessel wall thickness measurements. The Rotterdam study. J Clin Epidemiol 1994;47:921-930

Boutouyrie P, Bussy C, Hayoz D, Hengstler J, Dartois N, Laloux B, Brunner H, Laurent S. Local pulse pressure and regression of arterial wall hypertrophy during long-term antihypertensive treatment. Circulation 2000;101:2601-2606

Boutouyrie P, Laurent S, Girerd X, Benetos A, Lacolley P, Abergel E, Safar M. Common carotid artery stiffness and patterns of left ventricular hypertrophy in hypertensive patients. Hypertension 1995;25(Part1):651-659

Brands PJ, Hoeks APG, Ledoux LAF, Reneman RS. A radio frequency domain complex cross-correlation model to estimate blood flow velocity and tissue motion by means of ultrasound. Ultrasound Med Biol 1997;23:911-920

Brands PJ, Hoeks APG, Willigers J, Willekes C, Reneman RS. An integrated system for the non-invasive assessment of vessel wall and hemodynamic properties of large arteries by means of ultrasound. Eur J Ultrasound 1999;9:257-266

Bussy C, Boutouyrie P, Lacolley P, Challande P, Laurent S. Intrinsic stiffness of the carotid arterial wall material in essential hypertensives. Hypertension 2000;35:1049-54

Cheng KS, Baker CR, Hamilton G, Hoeks AP, Seifalian AM. Arterial elastic properties and cardiovascular risk/event. Eur J Vasc Endovasc Surg 2002;24:383-97

Demiray H. Incremental elastic modulus for isotropic elastic bodies with application to arteries. J Biomech Eng 1983;105:308-9

Dinenno FA, Jones PP, Seals DR, Tanaka H. Age-associated arterial wall thickening is related to elevations in sympathetic activity in healthy humans. Am J Physiol Heart Circ Physiol 2000;278:H1205-H1210

Emoto M, Nishizawa Y, Kawagishi T, Maekawa K, Hiura Y, Kanda H, Izumotani K, Shoji T, Ishimura E, Inaba M, Okuno Y, Morii H. Stiffness indexes beta of the common carotid and femoral arteries are associated with insulin resistance in NIDDM. Diabetes Care 1998;21:1178-82

Fung YC. Biodynamics: Circulation. Springer-Verlag: New York, 1984

Giannattasio C, Mancia G. Arterial distensibility in humans. Modulating mechanisms, alterations in diseases and effects of treatment. J Hypertens 2002;20:1889-99

Gosling RG, Budge MM. Terminology for describing the elastic behavior of arteries. Hypertension 2003;41:1180-2

Graf S, Gariepy J, Massonneau M, Armentano RL, Mansour S, Barra JG, Simon A, Levenson J. Experimental and clinical validation of arterial diameter waveform and intimal media thickness obtained from B-mode ultrasound image processing. Ultrasound Med Biol 1999;25:1353-63

Green MA, Friedlander R, Boltax AJ, Hadjigeorge CG, Lustig GA. Distensibility of arteries in human hypertension. Proc Soc Exp Biol Med 1966;121:580-585

Greve JM, Les AS, Tang BT, Draney Blomme MT, Wilson NM, Dalman RL, Pelc NJ, Taylor CA. Allometric scaling of wall shear stress from mice to humans: quantification using cine phase-contrast MRI and computational fluid dynamics. Am J Physiol Heart Circ Physiol 2006;291:H1700-8

Gribbin B, Pickering TG, Sleight P. Arterial distensibility in normal and hypertensive man. Clin Sci 1979;56:413-417

Hayashi K. Experimental approaches on measuring the mechanical properties and constitutive laws of arterial walls. J Biomech Eng 1993;115:481-488

Hayashi K, Handa H, Nagasawa S, Okumura A, Moritake K. Stiffness and elastic behavior of human intracranial and extracranial arteries. J Biomechanics 1980;13:175-184

Hayoz D, Rutschmann B, Perret F, Niederberger M, Tardy Y, Mooser V, Nussberger J, Brunner HR. Conduit artery compliance and distensibility are not necessarily reduced in hypertension. Hypertension 1992;20:1-6

Henry RM, Kostense PJ, Spijkerman AM, Dekker JM, Nijpels G, Heine RJ, Kamp O, Westerhof N, Bouter LM, Stehouwer CD. Arterial stiffness increases with deteriorating glucose tolerance status: the Hoorn Study. Circulation 2003;107:2089-95

Hoeks APG, Arts TGJ, Brands PJ, Reneman RS. Comparison of the performance of the cross correlation and Doppler autocorrelation technique to estimate the mean velocity of simulated ultrasound signals. Ultrasound Med Biol 1993;19:727-740

Hoeks APG, Brands PJ, Smeets FAM, Reneman RS. Assessment of the distensibility of superficial arteries. Ultrasound Med Biol 1990;16:121-128

Hoeks APG, Brands PJ, Willigers JM, Reneman RS. Non-invasive assessment of mechanical properties of arteries in health and disease. Proc Insttn Mech Engrs 1999;213:195-202

Hoeks APG, Reneman RS. Do Doppler systems color arteries red? In: Blood flow modelling and diagnostics. TA Kowalewski et al., Eds. Polish Academy of Sciences: Warsaw, 2005:243-271

Hoeks APG, Willekes C, Boutouyrie P, Brands PJ, Willigers JM, Reneman RS. Automated detection of local artery wall thickness based on M-line signal processing. Ultrasound Med Biol 1997;23:1017-1023

Homma S, Hirose N, Ishida H, Ishii T, Araki G. Carotid plaque and intima-media thickness assessed by b-mode ultrasonography in subjects ranging from young adults to centenarians. Stroke 2001;32:830-5.

Hu J, Wallensteen M, Gennser G. Increased stiffness of the aorta in children and adolescents with insulin-dependent diabetes mellitus. Ultrasound Med Biol 1996;22:537-43

Kelly R, Hayward C, Avolio A, O'Rourke M. Noninvasive determination of age-related changes in the human arterial pulse. Circulation 1989;80:1652-1659

Kool MJ, Lambert J, Stehouwer CD, Hoeks AP, Struijker Boudier HA, Van Bortel LM. Vessel wall properties of large arteries in uncomplicated IDDM. Diabetes Care 1995;18:618-624

Kool MJF, Van Merode T, Reneman RS, Hoeks APG, Struijker Boudier HAJ, Van Bortel LMAB. Evaluation of reproducibility of a vessel wall movement detector system for assessment of large artery properties. Cardiovasc Res 1994;28:610-614

Kornet L, Reneman RS, Hoeks APG. Age-related increase in femoral intima-media thickness in healthy humans [Letter]. Arterioscler Thromb Vasc Biol 2000;20:2172

L'Italien GJ, Chandrasekar NR, Lamuraglia GM, Pevec WC, Dhara S, Warnock DF, Abbott WM. Biaxial elastic properties of rat arteries in vivo: influence of vascular wall cells on anisotropy. Am J Physiol 1994;267:H574-H579

Langewouters GJ, Wesseling KH, Goedhard WJA. The static elastic properties of 45 human thoracic and 20 abdominal aortas in vitro and the parameters of a new model. J Biomech 1984;17:425-435

Laurent S. Arterial wall hypertrophy and stiffness in essential hypertensive patients. Hypertension 1995;26:355-362

Laurent S, Caviezel B, Beck L, Girerd X, Billaud E, Boutouyrie P, Hoeks A, Safar M. Carotid artery distensibility and distending pressure in hypertensive humans. Hypertension 1994a;23:878-883

Laurent S, Cockcroft J, Van Bortel L, Boutouyrie P, Giannattasio C, Hayoz D, Pannier B, Vlachopoulos C, Wilkinson I, Struijker-Boudier H. Expert consensus document on arterial stiffness: methodological issues and clinical applications. Eur Heart J 2006;27:2588-605

Laurent S, Girerd X, Mourad JJ, Lacolley P, Beck L, Boutouyrie P, Mignot JP, Safar M. Elastic modulus of the radial artery wall material is not increased in patients with essential hypertension. Arterioscler Thromb 1994b;14:1225-1231

Laurent S, Lacolley P, Girerd X, Caviezel B, Beck L, Challande P, Safar M. Isobaric arterial compliance is not reduced in essential hypertensives. Arch Mal Coeur Vaiss 1994c;87:1069-1072

Lehmann ED, Hopkins KD, Gosling RG. Multiple definitions of 'compliance'. Clin Sci (Colch) 1996;90:433-4.

Lorenz MW, von Kegler S, Steinmetz H, Markus HS, Sitzer M. Carotid intima-media thickening indicates a higher vascular risk across a wide age range: prospective data from the Carotid Atherosclerosis Progression Study (CAPS). Stroke 2006;37:87-92

Mattace-Raso FU, van der Cammen TJ, Hofman A, van Popele NM, Bos ML, Schalekamp MA, Asmar R, Reneman RS, Hoeks AP, Breteler MM, Witteman JC. Arterial stiffness and risk of coronary heart disease and stroke: the Rotterdam Study. Circulation 2006;113:657-63

Meinders JM, Brands PJ, Willigers JM, Kornet L, Hoeks AP. Assessment of the spatial homogeneity of artery dimension parameters with high frame rate 2-D B-mode. Ultrasound Med Biol 2001a;27:785-794

Meinders JM, Hoeks AP. Simultaneous assessment of diameter and pressure waveforms in the carotid artery. Ultrasound Med Biol 2004;30:147-54

Meinders JM, Kornet L, Brands PJ, Hoeks AP. Assessment of local pulse wave velocity in arteries using 2D distension waveforms. Ultrason Imaging 2001b;23:199-215

Meinders JM, Kornet L, Hoeks AP. Assessment of spatial inhomogeneities in intima media thickness along an arterial segment using its dynamic behavior. Am J Physiol Heart Circ Physiol 2003;285:H384-91

Menotti A, Seccareccia F, Giampaoij S, Giuli B. The predictive role of systolic, diastolic and mean blood pressure on cardiovascular and all causes of death. J Hypertens 1989;7:595-599

Nichols WW, O'Rourke MF. McDonald's blood flow in arteries. Edward Arnold: London, 1998

O'Leary DH, Polak JF, Kronmal RA, Manolio TA, Burke GL, Wolfson SK. Carotid artery intima and media thickness as a risk factor for myocardial infaction and stroke in older adults. N Engl J Med 1999;340:14-22

Patel DJ, Fry DL. Longitudinal tethering of arteries in dogs. Circ Res 1966;19:1011-1021

Pignoli P, Tremoli E, Poli A, Oreste P, Paoletti R. Intimal plus medial thickness of the arterial wall: a direct measurement with ultrasound imaging. Circulation 1986;74:1399-1406

Polak JF. Peripheral arterial disease. Evaluation with color flow and duplex sonography. Radiol Clin North Am 1995;33:71-90

Powalowski T, Pensko B. A noninvasive ultrasonic method for the elasticity evaluation of the carotid arteries and its application in the diagnosis of the cerebro-vascular system. Arch Acoustics 1988;13:109-126

Rabben SI, Stergiopulos N, Hellevik LR, Smiseth OA, Slordahl S, Urheim S, Angelsen B. An ultrasound-based method for determining pulse wave velocity in superficial arteries. J Biomech 2004;37:1615-22

Reneman RS, Hoeks AP. Noninvasive vascular ultrasound: an asset in vascular medicine. Cardiovasc Res 2000;45:27-35

Reneman RS, Meinders JM, Hoeks AP. Non-invasive ultrasound in arterial wall dynamics in humans: what have we learned and what remains to be solved. Eur Heart J 2005;26:960-6

Reneman RS, Van Merode T, Hick P, Hoeks APG. Flow velocity patterns in and distensibility of the carotid artery bulb in subjects of various ages. Circulation 1985;71:500-509

Reneman RS, Van Merode T, Hick P, Muytjens AMM, Hoeks APG. Age-related changes in carotid artery wall properties in man. Ultrasound Med Biol 1986;12:465-471

Riley WA, Barnes RW, Evans GW, Burke GL. Ultrasonic measurement of the elastic modulus of the common carotid artery. The atherosclerosis risk in communities (ARIC) study. Stroke 1992;23:952-956

Safar ME, Levy BI, Struijker-Boudier H. Current perspectives on arterial stiffness and pulse pressure in hypertension and cardiovascular diseases. Circulation 2003;107:2864-9

Samijo SK, Willigers JM, Barkhuysen R, Kitslaar PJEHM, Reneman RS, Hoeks APG. Wall shear stress in the common carotid artery as function of age and gender. Cardiovasc Res 1998;39:515-522

Selzer RH, Hodis HN, Kwong-Fu H, Mack WJ, Lee PL, Liu CR, Liu CH. Evaluation of computerized edge tracking for quantifying intima-media thickness of the common carotid artery from B-mode ultrasound images. Atherosclerosis 1994;111:1-11

Simon A, Gariepy J, Chironi G, Megnien JL, Levenson J. Intima-media thickness: a new tool for diagnosis and treatment of cardiovascular risk. J Hypertens 2002;20:159-69

Staub D, Meyerhans A, Bundi B, Schmid HP, Frauchiger B. Prediction of cardiovascular morbidity and mortality: comparison of the internal carotid artery resistive index with the common carotid artery intima-media thickness. Stroke 2006;37:800-5

Stettler JC, Niederer P, Anliker M. Theoretical analysis of arterial hemodynamics including the influence of bifurcations. Part I: Mathematical model and prediction of normal pulse patterns. Annals Biom Eng 1981;9:145-164

Stewart AD, Jiang B, Millasseau SC, Ritter JM, Chowienczyk PJ. Acute reduction of blood pressure by nitroglycerin does not normalize large artery stiffness in essential hypertension. Hypertension 2006;48:404-10

Strandness DE, Jr., McCutcheon EP, Rushmer RF. Application of a transcutaneous Doppler flowmeter in evaluation of occlusive arterial disease. Surg Gynecol Obstet 1966;122:1039-45

Tanaka H, Dinenno FA, Monahan KD, DeSouza CA, Seals DR. Carotid artery wall hypertrophy with age is related to local systolic blood pressure in healthy men. Arterioscler Thromb Vasc Biol 2001;21:82-87.

Tardy Y, Meister JJ, Brunner HR, Arditi M. Non-invasive estimate of the mechanical properties of peripheral arteries from ultrasonic and photoplethysmographic measurements. Clin Phys Physiol Meas 1991;12:39

Taylor LA, Gerrard JH. Pressure-radius relationships for elastic tubes and their application to arteries: Part 1--Theoretical relationships. Med Biol Eng Comput 1977a;15:11-7

Taylor LA, Gerrard JH. Pressure-radius relationships for elastic tubes and their applications to arteries: Part 2--A comparison of theory and experiment for a rubber tube. Med Biol Eng Comput 1977b;15:18-21

Touboul PJ, Hennerici MG, Meairs S, Adams H, Amarenco P, Bornstein N, Csiba L, Desvarieux M, Ebrahim S, Fatar M, Hernandez Hernandez R, Jaff M, Kownator S, Prati P, Rundek T, Sitzer M, Schminke U, Tardif JC, Taylor A, Vicaut E, Woo KS, Zannad F, Zureik M. Mannheim Carotid Intima-Media Thickness Consensus (2004-2006). An Update on Behalf of the Advisory Board of the 3rd and 4th Watching the Risk Symposium 13th and 15th European Stroke Conferences, Mannheim, Germany, 2004, and Brussels, Belgium, 2006. Cerebrovasc Dis 2006;23:75-80

Van Bortel LM, Balkestein EJ, van der Heijden-Spek JJ, Vanmolkot FH, Staessen JA, Kragten JA, Vredeveld JW, Safar ME, Struijker Boudier HA, Hoeks AP. Non-invasive assessment of local arterial pulse pressure: comparison of applanation tonometry and echo-tracking. J Hypertens 2001;19:1037-44.

Van Bortel LMAB, Kool MJF, Spek JJ. Disparate effects of antihypertensive drugs on large artery distensibility and compliance in hypertension. Am J Cardiol 1995;76:46E-49E

Van der Heijden-Spek JJ, Staessen JA, Fagard RH, Hoeks AP, Boudier HA, Van Bortel LM. Effect of age on brachial artery wall properties differs from the aorta and is gender dependent: a population study. Hypertension 2000;35:637-642

Van Gorp A, Van Ingen Schenau DS, Willigers J, Hoeks AP, De Mey JG, Struyker Boudier HA, Reneman RS. A technique to assess aortic distensibility and compliance in anesthetized and awake rats. Am J Physiol 1996;270:H780-6

Van Gorp AW, Schenau DS, Hoeks AP, Boudier HA, de Mey JG, Reneman RS. In spontaneously hypertensive rats alterations in aortic wall properties precede development of hypertension. Am J Physiol Heart Circ Physiol 2000;278:H1241-H1247

Van Merode T, Brands PJ, Hoeks APG, Reneman RS. Faster ageing of the carotid artery bifurcation in borderline hypertensive subjects. J Hypertens 1993;11:171-176

Van Merode T, Brands PJ, Hoeks APG, Reneman RS. Different effects of ageing on elastic and muscular arterial bifurcations in men. J Vasc Res 1996;33:47-52

Van Merode T, Hick PJJ, Hoeks APG, Rahn KH, Reneman RS. Carotid artery wall properties in normotensive and borderline hypertensive subjects of various ages. Ultrasound Med Biol 1988;14:563-569

van Popele NM, Elizabeth Hak A, Mattace-Raso FU, Bots ML, van der Kuip DA, Reneman RS, Hoeks AP, Hofman A, Grobbee DE, Witteman JC. Impaired fasting glucose is associated with increased

arterial stiffness in elderly people without diabetes mellitus: the Rotterdam study. J Am Geriatr Soc 2006;54:397-404

Van Popele NM, Grobbee DE, Bots ML, Asmar R, Topouchian J, Reneman RS, Hoeks AP, van Der Kuip DAM, Hofman A, Witteman JCM. Association between arterial stiffness and atherosclerosis: The Rotterdam study. Stroke 2001;32:454-460.

Van Popele NM, Westendorp ICD, Bots ML, Reneman RS, Hoeks APG, Hofman A, Grobbee DE, Witteman JCM. Variables of the insulin resistance syndrome are associated with reduced arterial distensibility in healthy non-diabetic middle-aged women. Diabetologia 2000;43:665-672

Waddell TK, Dart AM, Medley TL, Cameron JD, Kingwell BA. Carotid pressure is a better predictor of coronary artery disease severity than brachial pressure. Hypertension 2001;38:927-931

West GB, Brown JH, Enquist BJ. A general model for the origin of allometric scaling laws in biology. Science 1997;276:122-6

Westerhof N. Arterial haemodynamics. In: The physics of circulation. J Strackee and N Westerhof, Eds. Inst Physics Publ: Bristol, 1993

Willekes C, Brands PJ, Willigers JM, Hoeks APG, Reneman RS. Assessment of local differences in intima-media thickness in the human carotid artery. J Vasc Res 1999a;36:222-228

Willekes C, Hoeks AP, Bots ML, Brands PJ, Willigers JM, Reneman RS. Evaluation of off-line automated intima-media thickness detection of the common carotid artery based on M-line signal processing. Ultrasound Med Biol 1999b;25:57-64

Yanase T, Nasu S, Mukuta Y, Shimizu Y, Nishihara T, Okabe T, Nomura M, Inoguchi T, Nawata H. Evaluation of a new carotid intima-media thickness measurement by B-mode ultrasonography using an innovative measurement software, intimascope. Am J Hypertens 2006;19:1206-12

Zamir M. The physics of blood flow. Springer Verlag: New York, 2000

Zhang X, Greenleaf JF. The stiffening of arteries by the tissue-mimicking gelatin. IEEE Trans Ultrason Ferroelectr Freq Control 2006;53:1534-9

Chapter 3

Measurement of local pulse wave velocity: effect of signal processing on precision

Published as:

Evelien Hermeling, Koen D. Reesink, Robert S. Reneman, Arnold P.G. Hoeks. Measurements of local pulse wave velocity: effect of signal processing on precision. Ultrasound in Med. & Biol. 2007; 33: 774-781

Abstract

Pulse wave velocity provides information about the mechanical properties of the vessel: the stiffer the artery is, the higher the pulse wave velocity will be. Pulse wave velocity measured over a short arterial segment facilitates direct characterization of local wall properties corrected for prevailing pressure without the necessity of measuring pulse pressure locally. Current methods for local pulse wave velocity assessment have a poor precision, but it can be improved by applying linear regression to a characteristic time-point in distension waveforms as recorded simultaneously by multiple M-line ultrasound. We investigated the precision of this method in a phantom scaled according to realistic *in vivo* conditions. Special attention was paid to the identification of the systolic foot of the wave, being the maximum of the second derivative, the intersecting tangent and the 20 % threshold method. Prior to systolic foot detection, the distension waveforms were subjected to pre-processing with various filters. The precision of the maximum of the second derivative had a coefficient of variation of 0.45 % and 10.45 % for an eighth and second order low pass filter, respectively. The intersecting tangent and the threshold method were less sensitive to filtering; the coefficients of variation were 0.66 % and 0.68 % for the high order filter and 2.36 % and 1.43 % for the low order filter, respectively. We conclude that foot detection by a threshold of 20 % or by the tangent method are more suitable as an identification point for the foot of the wave to measure local pulse wave velocity. Both methods are less sensitive to (phase) noise than the maximum of the second derivative method and exhibit good precision with a coefficient of variation of less than 1 %.

3.1 Introduction

Stiffening of the elastic arteries, like the aorta and the carotid arteries, is associated with an increase in systolic blood pressure. Two mechanisms contribute to this association. First, stiffer arteries have a reduced compliance and can therefore not adequately accommodate the volume ejected by the left ventricle. For the same stroke volume, this will result in a higher pulse and systolic pressure. Second, higher aortic stiffness augments the velocity of the pulse wave along the arterial segment, causing wave reflections to return towards the aortic valve earlier in the cardiac cycle, arriving during the ejection phase. This early arrival of the reflected pressure wave contributes to the rise in systolic pressure (Schiffrin 2004). By the foregoing mechanisms, stiffening of the

elastic arteries leads to increased wall stress of the left ventricle causing left ventricular hypertrophy (Boutouyrie et al. 1995). Moreover, increased arterial stiffness may lead to decreased diastolic pressure, thereby jeopardizing coronary perfusion. Increased arterial stiffness is a predictor of cardiovascular morbidity and mortality (Laurent et al. 2001; Laurent et al. 2003; Mattace-Raso et al. 2006).

Pulse wave velocity is used as a measure for arterial stiffness; the stiffer the artery is, the higher the pulse wave velocity will be. The Moens-Korteweg equation gives the relation between the pulse wave velocity (*PWV*), the elastic modulus (*E*), the thickness of the wall (*h*), the lumen diameter (*d*) and the density of the blood (ρ) in a thin walled tube (*h* << *d*).

$$PWV = \sqrt{\frac{E\,h}{\rho\,d}} \qquad 3.1$$

Similarly, the Bramwell-Hill equation (Bramwell and Hill 1922) relates the pulse wave velocity to the distensibility (*D*). The distensibility coefficient is defined by the ratio between the volume change (ΔV) and the pressure change (Δp) relative to the diastolic volume (V_d).

$$PWV = \sqrt{\frac{1}{\rho D}} = \sqrt{\frac{V_d \Delta p}{\rho \Delta V}} \qquad 3.2$$

The change in volume can be obtained from the diameter waveform as function of time, as recorded non-invasively with ultrasound techniques, under the condition of circular cross-section and negligible elongation of the artery during the cardiac cycle (Hoeks et al. 1999; Reneman et al. 2005).

Two approaches can be distinguished to measure the pulse wave velocity *in vivo*. Global pulse wave velocity based on the transit time over a long trajectory of the arterial tree, results in an average pulse wave velocity over a longer arterial segment often composed of both elastic and muscular arteries. When determined locally, pulse wave velocity provides information about stiffness and changes thereof in one type of artery without the necessity of measuring pulse pressure locally. The latter has to be known when assessing local stiffness by means of the distensibility coefficient (Equation 3.2) or compliance. However, pulse pressure in the common carotid artery (CCA) can not accurately be measured non-invasively in all patients (Van Bortel et al. 2001; Meinders and Hoeks 2004) The use of brachial pulse pressure instead of local pulse pressure

underestimates carotid distensibility and compliance (Hoeks et al. 1999; Waddell et al. 2001; Reneman et al. 2005). Being informed of local mechanical properties of arteries is of utmost importance, because their mechanical characteristics vary along the arterial tree and are differently affected by aging and disease (Hoeks et al. 1999; Reneman et al. 2005). Moreover, pulse wave velocity as determined locally in combination with the Bramwell-Hill equation (Equation 3.2) provides a direct estimate of local pulse pressure, a parameter of great importance to obtain information about local hemodynamics and artery wall characteristics.

Global pulse wave velocity

The method most commonly used is the pulse wave velocity measured over a long arterial trajectory, often the carotid–femoral arterial trajectory. The global pulse wave velocity is defined by the distance between the measurement sites and the transit time delay between these two sites. The carotid–femoral pulse wave velocity is an average pulse wave velocity over a long segment composed of arteries with different mechanical characteristics (elasticity, wall thickness to lumen diameter ratio). Although population studies have shown that an increased carotid–femoral pulse wave velocity, indicating enhanced arterial stiffness, is a predictor of coronary heart disease (Mattace-Raso et al. 2006) and stroke (Laurent et al. 2003; Mattace-Raso et al. 2006). The assessment of carotid–femoral pulse wave velocity is subject to error, because of lack of standardization of the method (Xu 2003; Van Bortel 2006). The commercially available devices that measure carotid–femoral pulse wave velocity use different timing algorithms to assess the transfer time, i.e. different characteristic time-points of the waveform, which cannot be used interchangeably (Millasseau et al. 2005). Moreover, as the wave travels along the arterial system its shape is modified, due to differences in arterial wall properties along the trajectory. Therefore, the characteristic time-point used to identify the onset of the wave is shifted to a different position within the waveform, which results in inaccurate estimation of the transit time. An additional major source of error is the distance measurement (normally done with a tape measure), assuming a straight arterial segment. Since the carotid and femoral pulse waves travel in opposite directions, the use of the distance between the carotid and femoral artery will cause overestimation of the pulse wave velocity.

Local pulse wave velocity

Recently, methods have been developed that measure the pulse wave velocity over a short segment of an artery. These local pulse wave velocity methods can be distinguished according to the technique used.

The pulse wave velocity can be calculated from the linear relation between the change in pressure on the one hand and the change in volume flow on the other (Khir et al. 2001). This method requires simultaneous measurement of both pressure and blood flow velocity at the same location. With this method pulse wave velocity could be measured invasively with a coefficient of variation of about 20 %

An alternative is to use the ratio of the temporal gradient and the spatial gradient of the arterial diameter waveform as a measure of the local pulse wave velocity. Brands et al. used two ultrasound probes, spaced at 9 mm, to calculate these gradients, resulting in a coefficient of variation of 3.5 % in a phantom (Brands et al. 1998). This method requires visual feedback via a real-time B-mode image to position the probes with respect to the artery and it is not suitable for *in vivo* applications because of the interfering effects on pressure wave propagation and reflection. Meinders et al. (2001b) introduced a multiple M-line system with 16 lines to obtain the diameter waveform simultaneously at 16 positions. A major advantage of this approach is that the segment length is set by the characteristics of the ultrasound probe and does not vary over measurements. The temporal and spatial gradients were calculated from the time derivative of the diameter waveform. i.e., diameter velocity, instead of the diameter waveform itself. In a phantom with a pulse wave velocity of 3 m/s, pulse wave velocity could be determined with a coefficient of variation of about 0.5 %. However, the precision in young healthy volunteers was found to be poor (coefficient of variation is 30 %).

Cross-correlation between diameter velocities obtained at different measurement sites can be used to determine the time-shift between these sites. In this way, local pulse wave velocity was estimated in the fetal descending aorta, by tracking the wall position at two different measurement sites (Struijk et al. 1992). The derivative of the diameter waveform was used for cross-correlation between the measurement sites. Struijk et al. measured the pulse wave velocity over 30 mm of the aorta with a coefficient of variation of 18 %. Eriksson (Eriksson et al. 2002) used tissue Doppler imaging to get velocity traces of multiple M-lines (number of M-lines is 8, 12 or 16). The velocity trace of each line was correlated with the next one, providing the time-shift between subsequent lines. The

regression analysis of the observed time-shift and the position of the M-lines provided a direct estimate of local pulse wave velocity with a coefficient of variation of 10 % in a phantom. *In vivo* this method was tested only on one single subject with a coefficient of variation of 7.7 %.

The local pulse wave velocity measurement techniques presently in use have some limitations. They have a poor precision in a phantom or *in vivo* and/or are unsuitable for non-invasive application in humans. The discrepancy between phantom and *in vivo* results may be explained by improper scaling of the experiments. The aim of the present study was to quantify the effect of recording and signal processing steps on the quality of the pulse wave velocity estimation based on regression analysis. The regression analysis is applied to the recording position and the time-shift between the feet of the distension waveforms, i.e. the change in diameter over time. The foot of the distension waveform is used, because it is hardly affected by reflections. Reflections may change the shape of the distension waveform, obscuring the time-shift between distension waveforms. Besides the commonly used methods to determine the foot of the distension waveform, i.e. the maximum of the second derivative of the distension waveform or the intersecting tangent method, a third characteristic time-point is considered that uses 20 % of the maximal distension as the foot of the distension waveform.

3.2 Methods

The phantom set-up

To evaluate the precision and the accuracy of pulse wave velocity measurements, experiments were performed in a phantom set-up (see Figure 3.1), consisting of a pneumatic pulse generator, a water tank and a water bath. The pulse generator produced a rectangular-shaped pressure pulse (amplitude of 150 kPa) by opening a valve for 150 ms. The pulse generator is connected to a water tank partly filled with water and acting as a windkessel. The air-pulse is transformed to a water pressure wave that ends in an elongated water bath (3.5 m long and 5 cm wide). The ultrasound probe was placed facing upwards at a small opening filled with silicone in the middle of the water bath. The water-air reflection was located at a distance of 4 cm from the probe. The probe was positioned horizontally by visual inspection ensuring that the ultrasound beam

direction was perpendicular to the water-air reflection and thus to pressure wave propagation.

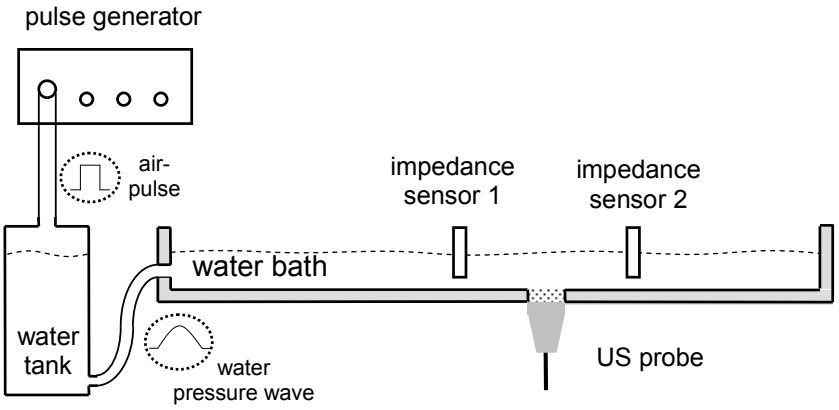

Figure 3.1. The phantom set-up consists of a pulse generator producing a rectangular air pulse, a water tank that transforms the air-pulse into a wave, and a water bath (length 3.5m) in which the wave propagates. The wave is measured by the ultrasound system placed at the opening in the bottom of the water bath filled with silicone and two impedance sensors located at either side of the ultrasound (US) probe.

Two impedance sensors were placed at 0.5 m upstream and 0.5 m downstream of the probe. Each sensor consisted of two parallel plates, separated by 2 mm, with the plates partly placed inside the conductive water and partly in the non-conductive air. The impedance across the plates will change accordingly with a change in water height, resulting in a measure of the water height as function of time. The impedance sensors and the ultrasound probe measured the wave simultaneously. The impedance sensors were not calibrated and therefore did not provide information about the absolute changes in water height. Instead the time-shift between the feet of the waves at each impedance sensor was used to calculate pulse wave velocity over a distance of 1 m (PWV_{imp}), acting as a reference value for the local pulse wave velocity measured by the ultrasound system (PWV_{US}). Before each wave was generated a two minute period was allowed to reduce interference of residual waves.

Data acquisition

The radio frequency (RF) data were collected with a Picus ultrasound system (Esaote Europe, Maastricht, the Netherlands). The system was equipped with a 7.5 MHz linear array transducer with a length of 40 mm. The RF data had an effective center frequency of approximately 6 MHz and a bandwidth of 4 MHz and was sampled at 33.3 MHz. For the pulse wave velocity measurements, the scanner was operating in fast B-mode (also called multiple M-line mode), producing fourteen M-mode lines spaced over a segment of about 16.4 mm (pitch 1.26 mm). The RF data matrix obtained from the system is a 3-D function of depth, time and position along the probe. The fast B-mode has a high temporal resolution, but a crude B-mode. The maximal frame rate is 800 Hz, determined by the number of M-lines (14) and the pulse repetition frequency. The latter depends on the maximal depth range of the ultrasound measurement (for superficial arteries the pulse repetition is 11 kHz). The RF data was stored on a hard disk and was analyzed off-line.

Data processing

The RF data were processed on a PC and computations were performed with Matlab (The MathWorks, Natick, MA). First the DC component of the RF signals was removed and a band pass filter was applied (second order Butterworth band pass with cut-off frequencies of 4 and 8 MHz). The distension wave, reflecting the motion of the water surface, was calculated for each M-line separately using a wall track system (Hoeks et al. 1999; Meinders et al. 2001a). In the wall track system, the surface motion was calculated by applying the complex cross correlation model (Brands et al. 1997). The position of the correlation window was selected manually at the first time-point for each position along the probe. The distension waveform was calculated by integrating the surface motion over time. For each time-point the position of the correlation window was updated using the previous position and the observed surface motion.

Scaling

Using the Bramwell-Hill equation (Equation 3.2), $V_d = h\,A$, $\Delta V \Delta h\,A$ and $\Delta P = \rho\, g\, \Delta h$, and by assuming a water bath with infinite width, it can be shown that the water height inside the water bath determines the velocity of the propagating wave (h is height of water bath, dh is change in water height, g is gravitation constant and A is surface area).

$$PWV = \sqrt{gh} \qquad 3.3$$

Because the water surface should be within the field of focus, the water height was only small (25 mm), and the anticipated pulse wave velocity (0.52 m/s) low compared to *in vivo* conditions. To make the precision of the signal processing steps comparable, the set-up and processing was scaled to *in vivo* conditions. In the set-up the dimension of the probe remained the same, but time was scaled with a factor of 10. The frame rate of the ultrasound system was set at 100 Hz to scale the observation frequency to the expected pulse wave velocity. To scale the pressure waveform to the distension waveform *in vivo*, the propagating wave had an amplitude of 1 mm with a rise time of 350 ms. The dimensions of the data window for the cross-correlation model had a temporal size of 50 ms with a maximal overlap of 40 ms and size in depth of 890 µm. The cut-off frequencies of the filters applied to the distension waveform (sample rate 20 Hz) were all scaled according to the same criteria.

Distension Wave Processing

To reduce the effect of wave perturbations, caused by building vibrations, the observed distension waveform was filtered with a zero-phase Butterworth low-pass filter with different characteristics. The systolic feet were calculated from the distension waveforms after applying A) an eighth order filter with cut-off frequency of 2 Hz, B) a second order filter with cut-off frequency of 2 Hz and C) an eighth order filter with cut-off frequency of 4 Hz. A 2 Hz (4 Hz) cut-off frequency corresponds to a 20 Hz (40 Hz) cut-off frequency *in vivo* which is well beyond the maximum frequency of the pressure wave (Newman et al. 1986). After the filtering process the distension waveform was interpolated to a sample frequency of 10 kHz. The interpolated distension waveform was used to calculate the characteristic time-points of the foot of the distension waveform.

Three approaches were used to identify the systolic foot, i.e. the start of the distension waveform. First, the time-point with maximal acceleration was used by determining the second derivative (see Figure 3.2). This derivative was obtained by applying a first order derivative filter with a relatively high cut-off frequency of 1.5 Hz in a forward and reverse direction on the interpolated distension waveform (zero phase second order high-pass filter). Because a derivative filter was applied, the second derivative is expressed in arbitrary units. The maximum of the second derivative before the peak of the distension waveform is indicated

by $T_{sf,2nd}$. Second, the intersection of the tangent through the steepest part of the slope with the absolute minimum value of the distension wave ($T_{sf,tang}$). The first zero-crossing point of the second derivative after $T_{sf,2nd}$ is the time-point with maximum slope. At this time-point we calculated the incremental slope and extrapolated it to the minimum of the distension waveform. Third, the time-point ($T_{sf,20\%}$) at 20 % of the upslope of the distension waveform.

Because of the scanning nature of the ultrasound system, the adjacent distension waveforms were shifted in phase by a time lag of 1 divided by the pulse repetition frequency; accordingly the systolic feet were corrected for this time lag before the pulse wave velocity was calculated.

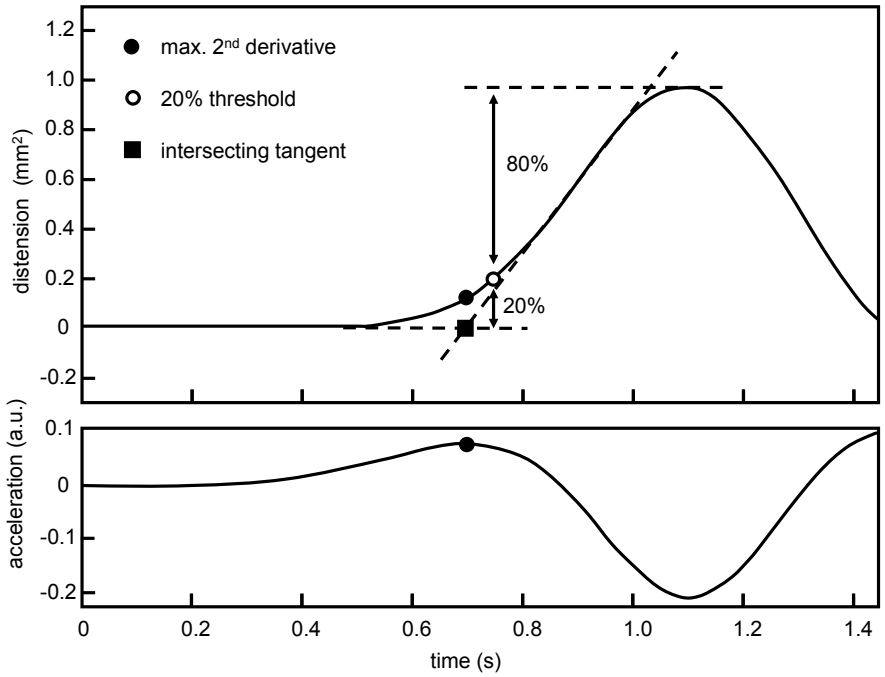

Figure 3.2 The foot of the distension waveform is identified in three ways: 1) the maximum of the second derivative or acceleration, $T_{sf,2nd}$ (bottom), 2) the 20% threshold $T_{sf,20\%}$ (top), and 3) the intersection of the tangent through the point with maximal slope with the absolute minimal value of the distension wave $T_{sf,tang}$ (top)

Statistical analysis

The RF data processing resulted in fourteen systolic feet originating from fourteen distension waveforms distributed over 16.4 mm. A regression line was

calculated with the systolic foot (T_{sf}) as dependent variable and the position (x) as independent variable, which was a fixed value determined by the probe (pitch):

$$T_{sf} = \beta_0 + \beta_1 x + \varepsilon \qquad 3.4$$

In this linear regression model the parameters β_0 and β_1 are the regression coefficients and ε is the residual. The PWV_{US} can be calculated from the regression coefficient ($PWV_{US} = 1 / \beta_1$); the regression coefficient is calculated for each of the three methods to determine the systolic foot (T_{sf}).

The measurements were repeated ten times to obtain the precision of PWV_{US}, expressed by the standard deviation of the estimate and by the coefficient of variation, which is defined as the standard deviation divided by the mean. The relative error of the pulse wave velocity estimate by ultrasound was determined by statistical comparison with the reference (PWV_{imp})

$$relative\,error = \left(PWV_{imp} - PWV_{US}\right) \Big/ PWV_{imp} \qquad 3.5$$

3.3 Results

Table 3.1 presents PWV_{US} and PWV_{imp} as obtained with three different methods, based on 10 repeated measurements. The wave perturbations were best filtered out by applying an 8th order filter with a cut-off frequency of 2 Hz (Filter A). Using Filter A all three foot detection methods had a high precision and a coefficient of variation of less than 0.7%. The coefficient of variation of the $PWV_{US,2nd}$ is 0.45 % and is better than that of $PWV_{US,20\%}$ and $PWV_{US,tang}$ (coefficient of variation is 0.68 % and 0.66 %, respectively).

The precision of $PWV_{US,2nd}$ decreased strongly, when applying a less steep (Filter B) or a wider filter (Filter C): the coefficient of variation increased from 0.45 % (Filter A) to 10.45 % (Filter B) or to 2.2 % (Filter C). In contrast to the 20-fold increase in coefficient of variation of $PWV_{US,2nd}$, the $PWV_{US,20\%}$ remained relatively stable with a coefficient of variation of 0.68 % for Filter A, 1.43 % for Filter B and 0.93 % for Filter C. The $PWV_{US,tang}$ showed the same pattern as the $PWV_{US,20\%}$ with a coefficient of variation of 0.66 % (Filter A), 2.36 % (Filter B) and 1.18 % (Filter C).

Table 3.1. Statistics of pulse wave velocity measurements

	Second derivative	Intersecting tangent	20% threshold	Impedance
	Filter A: 8th order LP with cut-off frequency of 2 Hz			
mean (m/s)	0.5070	0.5139	0.5135	0.5225
SD (m/s)	0.0023	0.0034	0.0035	0.0009
CV	0.45%	0.66%	0.68%	0.17%
rel. error	2.96%	1.65%	1.73%	-
	Filter B: 2nd order LP with cut-off frequency of 2 Hz			
mean (m/s)	0.5094	0.5199	0.5180	
SD (m/s)	0.0532	0.0123	0.0074	
CV	10.45%	2.36%	1.43%	
rel. error	2.52%	0.50%	0.86%	
	Filter C: 8th order LP with cut-off frequency of 4 Hz			
mean (m/s)	0.5159	0.5212	0.5165	
SD (m/s)	0.0113	0.0061	0.0048	
CV	2.20%	1.18%	0.93%	
rel. error	1.27%	0.25%	1.15%	

The mean, standard deviation (SD) and the coefficient of variation (CV) as well as the relative (rel.) error of the ultrasound measurement compared to the impedance measurement, are shown for each of the three low pass filters (LP) applied. The different methods to calculate the local pulse wave velocity are 1) the maximum of the second derivative, 2) the intersecting tangent method and 3) the 20 % threshold method

With Filter A, the relative error for $PWV_{US,2nd}$ (2.96 %) was high compared to the precision of the measurement (coefficient of variation is 0.45 %). This is a consequence of the non-random distribution of the residual of the ultrasound measurements, as shown in Figure 3. Because the residual has a peculiar pattern that is similar for each measurement, it is possible to correct for the residual pattern. The correction for each M-line is the difference between the time-points expected according to PWV_{imp} and the mean $T_{sf,2nd}$ for each M-line. The time-points according to PWV_{imp} are calculated by dividing the position of each M-line on the probe by the PWV_{imp}. Correction for the systematic error led to an unbiased estimation of the PWV_{US}. However, the correction procedure did not change the precision. The specific distribution of the residual showed the same trend in all measurements of PWV_{US}, but was more apparent when the

precision was better. The relative error seems to be inversely related to the precision of the measurement.

3.4 Discussion

The findings in the present study show that in a phantom set-up all methods to calculate the local pulse wave velocity have a very good precision if a highly selective filter is used, i.e. a high order filter (eighth) with a low cut-off frequency (2 Hz), to suppress small wave perturbations in the distension waveform. However, if a second order filter instead of an eighth order filter is used, the precision of $PWV_{US,2nd}$ decreases strongly. This decrease in precision is less pronounced in the $PWV_{US,tang}$, while the $PWV_{US,20\%}$ has the best precision under these conditions. Contrary to the second derivative pulse wave velocity, which is sensitive to wave perturbations, the 20 % threshold and intersecting tangent pulse wave velocity are only little affected by the wave perturbations.

The method proposed in this study is based on regression analysis of echo position as the independent variable and the characteristic time-points at the start of the distension waveform as the dependent variable. The influence of signal processing steps on the quality of the pulse wave velocity estimation was analyzed in a phantom set-up. Because phase velocity, i.e. the speed of propagation of a frequency component, is frequency independent (Li et al. 1981) the systolic foot of the distension waveform is a good measure for the characteristic velocity of all the frequency components of the pulse wave. Moreover, the foot of the systolic phase is little affected by reflections. Reflections, that occur *in vivo*, can change the shape of the distension waveform, obscuring the time-shift between waveforms.

The precision of the pulse wave velocity measurement is determined by the frame rate of the system, i.e. the sample frequency for any echo line position, relative to the rise time of the distension waveform. *In vivo*, the pulse wave velocity is high (5 m/s) compared to the pulse wave velocity measured in the phantom (0.5 m/s), necessitating scaling of the frame rate and the time scale by a factor of 10. Because measurements in the phantom are performed under realistic conditions, the observed precision of the pulse wave velocity measurement is likely to be similar to the precision under physiological conditions. *In vivo*, however, besides reflections and other disturbances, an incidentally high pulse wave velocity (~ 10 m/s) and decreased rise time of the distension waveform may reduce the precision of the pulse wave velocity. On the

other hand, the distension waveform of arteries exhibits a pronounced foot. To make the transition from phantom to *in vivo* measurements, it may be of interest to consider the effect of an increase in frame rate at the expense of the number of echo-lines.

Other methods to measure the local pulse wave velocity over a short range of 10-20 mm, are either invasive or lack precision in a phantom or *in vivo*. Our group (Meinders et al. 2001b) has measured local pulse wave velocity by calculating the temporal and spatial gradient of the diameter velocity. In a phantom the precision was high (coefficient of variation of 0.5 %) and comparable to the precision obtained in the present study (coefficient of variation of $PWV_{US,2nd}$ is 0.45 %). *In vivo*, however the performance of the gradient method deteriorated considerably (coefficient of variation of 30 %). The discrepancy between phantom and *in vivo* findings can be explained as follows. First, in the present study we showed that the second derivative, which is equal to the temporal gradient of the diameter velocity used by Meinders et al., has a high precision in the phantom, but this precision highly depends on signal processing. Second, changes in speckle pattern, as observed *in vivo*, cause random phase shifts in the spatial gradient which lead to a poor coefficient of variation of the spatial gradient (Meinders et al. 2001b). By using the feet of the distension waveforms and their corresponding acquisition position instead of the spatial gradient this problem is circumvented. Third, the spatial gradient of the diameter velocity is sensitive to differences in distension amplitude related to the initialization of the correlation windows and to an inhomogeneous distensibility (Meinders et al. 2001a). Both the second derivative and the threshold method used here are independent of the absolute distension amplitude and may therefore be more suitable for application *in vivo*.

Carotid-femoral pulse wave velocity has the disadvantage that the pulse waves travel in opposite directions and the distance between the sites can not be measured accurately, which hampers the applicability in the clinic. Our method can be used on a small arterial segment. The approach provides the possibility to obtain information on local stiffness over a short stretch of artery with the same structural and functional properties. Moreover, the distance between the measurement sites is dictated by the distance between the piezo-electrical elements of the ultrasound probe and the angle of measurement. It is rather simple to keep the angle (by visual inspection of the B-mode image) within a five degree limit, which translates into a bias of maximally 0.4 %.

As follows from the adjusted Bramwell-Hill equation (Equation 3.3), the height of the water level determines the pulse wave velocity, but this relationship is not used to calculate the pulse wave velocity. Precise measurement of the water height is not possible due to cohesion forces: an error of 1 mm for a water level of 25 mm leads to 2 % error for the pulse wave velocity estimate. Instead the pulse wave velocity was measured over a distance of 1 meter by two impedance sensors. This method has a high precision due to the large transit time compared to the local pulse wave velocity measurements. The impedance sensors are placed at 0.5 m on either site of the ultrasound probe, which reduces possible difference in pulse wave velocity due to differences in water height. Because of the length of the water bath (3.5 m), possible reflections will not interfere with the transit time measurements. As the PWV_{imp} has a good accuracy and precision, it is used as a reference method to evaluate the proposed pulse wave velocity measurement.

The residual of the regression analysis shows a peculiar pattern which explains the relatively large bias in the PWV_{US} measurement compared to PWV_{imp}. Although the origin of the residual pattern is not exactly known, it is unlikely that the pattern is originating from the phantom set-up, because changes in water level and distension waveform did not change the pattern of the residual. Also, the residual pattern is persistent if the measurements are performed at a different frame rate. This indicates that the error is originating from the hardware of the ultrasound system. A possible explanation for the error could be that beams at different positions are not parallel. An angle between two adjacent beams of 0.2° and the reflection-site at a distance of 4 cm lead to an additional delay between the distension waveforms of 0.2 ms. Because the pattern is similar for each measurement it is possible to correct for it. The result is an unbiased estimate of the pulse wave velocity with a high precision; a variation coefficient of 0.45 %.

The systematic distribution of the residual does not only cause a bias, but it also demonstrates the precision of the method: even extremely small erroneous delays caused by the hardware are revealed. In other words the bottleneck of these measurements is not determined by the systolic foot measurement or the reproducibility of the wave in the phantom, but by the hardware of the ultrasound system. For *in vivo* measurements, inspection of the residual is also informative; a systematic distribution of the residual (after correction for the hardware residual) may indicate that, besides time-shifts due to the propagation of the wave, other factors influence the time-points of the systolic feet. For example, reflected waves from a bifurcation point alter the systolic foot, which may lead to

a non-linear relation between the systolic foot and the recording position. The systematic distribution of the residual reveals this non-linear relation and may therefore identify the interference of the reflection.

The bias caused by the systematic error mentioned above decreases when a less precise method is used. Random noise has a positive effect on the bias of the pulse wave velocity estimates. The asynchronous timing of the pressure wave with respect to frame acquisition causes random phase noise. A higher frame rate with respect to the frequency content of the pressure wave will suppress this phase noise and will favor selective filtering. Although the rise time of the distension waveform is scaled to the *in vivo* situation, *in vivo* the distension waveforms may exhibit higher harmonics, and disturbances (like phase noise), which cannot be filtered out completely. Because of this limitation the maximum of the second derivative, which has a poor precision applying less selective filtering, is not the method of choice for *in vivo* use: it is less robust.

To apply the proposed method *in vivo* caution should be taken. The pressure wave generated in the phantom is very constant throughout the measurements and only minimal changes in distension waveform occur along the path in the water bath. *In vivo*, a bifurcation distal to the measurement site leads to reflections, which modify the shape of the distension waveforms dependent on the recording position relative to the bifurcation. The positive reflection of a bifurcation, for example, can increase the slope of the intersecting tangent, which causes the relevant time-point to occur later. Because the reflection arrives earlier in the echo-lines located closer to the bifurcation, it may lead to a non-linear relationship between the recording line position and the systolic foot and/or an overestimation of the pulse wave velocity. A similar effect is seen when using the 20 % threshold or the maximum of the second derivative to obtain the regression line.

3.5 Conclusion

We have shown that local pulse wave velocity over a range of 16.4 mm can be measured with good precision, by determining the regression line through echo line position and the time-points of the foot of the distension waveform of a multiple M-line recording. The 20 % threshold method is suitable to determine the systolic foot of the distension waveform, as an alternative to the maximum of the second derivative and the intersection tangent methods commonly used to detect this foot. Especially the maximum of the second derivative was shown to

be sensitive to noise in contrast to the 20 % threshold method. The proposed method allows evaluation of the pulse wave velocity assessment by analysis of the residual of the regression line. A systematic distribution of the residual may find its origin in the hardware (as shown here) and may be used to identify the influence of reflections on the systolic foot detection. The applicability of this method *in vivo* needs further examination, as the effect of reflections on the systolic foot has not been accounted for in the phantom measurements.

References

Boutouyrie P, Laurent S, Girerd X, Benetos A, Lacolley P, Abergel E, Safar M. Common carotid artery stiffness and patterns of left ventricular hypertrophy in hypertensive patients. Hypertension 1995;25:651-659

Bramwell J and Hill A. The velocity of the pulse wave in man. Proc Roy Soc London Ser B 93: 298-306, 1922.

Brands PJ, Hoeks APG, Ledoux LAF, Reneman RS. A radio frequency domain complex cross-correlation model to estimate blood flow velocity and tissue motion by means of ultrasound. Ultrasound Med Biol 1997;23:911-920

Brands PJ, Willigers JM, Ledoux LA, Reneman RS, Hoeks AP. A noninvasive method to estimate pulse wave velocity in arteries locally by means of ultrasound. Ultrasound Med Biol 1998;24:1325-35

Eriksson A, Greiff E, Loupas T, Persson M, Pesque P. Arterial pulse wave velocity with tissue Doppler imaging. Ultrasound Med Biol 2002;28:571-80

Hoeks APG, Brands PJ, Willigers JM, Reneman RS. Non-invasive assessment of mechanical properties of arteries in health and disease. Proc Insttn Mech Engrs 1999;213:195-202

Khir AW, O'Brien A, Gibbs JS, Parker KH. Determination of wave speed and wave separation in the arteries. J Biomech 2001;34:1145-55

Laurent S, Boutouyrie P, Asmar R, Gautier I, Laloux B, Guize L, Ducimetiere P, Benetos A. Aortic stiffness is an independent predictor of all-cause and cardiovascular mortality in hypertensive patients. Hypertension 2001;37:1236-1241.

Laurent S, Katsahian S, Fassot C, Tropeano AI, Gautier I, Laloux B, Boutouyrie P. Aortic stiffness is an independent predictor of fatal stroke in essential hypertension. Stroke 2003;34:1203-6

Li JK, Melbin J, Riffle RA, Noordergraaf A. Pulse wave propagation. Circ Res 1981;49:442-452

Mattace-Raso FU, van der Cammen TJ, Hofman A, van Popele NM, Bos ML, Schalekamp MA, Asmar R, Reneman RS, Hoeks AP, Breteler MMet al. Arterial stiffness and risk of coronary heart disease and stroke: the Rotterdam Study. Circulation 2006;113:657-63

Meinders JM, Brands PJ, Willigers JM, Kornet L, Hoeks AP. Assessment of the spatial homogeneity of artery dimension parameters with high frame rate 2-D B-mode. Ultrasound Med Biol 2001a;27:785-94

Meinders JM, Hoeks AP. Simultaneous assessment of diameter and pressure waveforms in the carotid artery. Ultrasound Med Biol 2004;30:147-54

Meinders JM, Kornet L, Brands PJ, Hoeks AP. Assessment of local pulse wave velocity in arteries using 2D distension waveforms. Ultrason Imaging 2001b;23:199-215

Millasseau SC, Stewart AD, Patel SJ, Redwood SR, Chowienczyk PJ. Evaluation of carotid-femoral pulse wave velocity: influence of timing algorithm and heart rate. Hypertension 2005;45:222-6

Newman DL, Sipkema P, Greenwald SE, Westerhof N. High frequency characteristics of the arterial system. J Biomechanics 1986;19:817-824

Reneman RS, Meinders JM, Hoeks AP. Non-invasive ultrasound in arterial wall dynamics in humans: what have we learned and what remains to be solved. Eur Heart J 2005;26:960-6

Schiffrin EL. Vascular stiffening and arterial compliance: implications for systolic blood pressure. Am J Hypertens 2004;17:39S-48S

Struijk PC, Wladimiroff JW, Hop WCJ, Simonazzi E. Pulse pressure assessment in the human fetal descending aorta. Ultrasound Med Biol 1992;18:39

Van Bortel LM. Is arterial stiffness ready for daily clinical practice? J Hypertens 2006;24:281-3

Van Bortel LM, Balkestein EJ, van der Heijden-Spek JJ, Vanmolkot FH, Staessen JA, Kragten JA, Vredeveld JW, Safar ME, Struijker Boudier HA, Hoeks AP. Non-invasive assessment of local arterial pulse pressure: comparison of applanation tonometry and echo-tracking. J Hypertens 2001;19:1037-44.

Waddell TK, Dart AM, Medley TL, Cameron JD, Kingwell BA. Carotid pressure is a better predictor of coronary artery disease severity than brachial pressure. Hypertension 2001;38:927-31

Xu J. Do we need a better approach for measuring pulse-wave velocity? Ultrasound Med Biol 2003;29:1373

Chapter 4

Confluence of incident and reflected waves interferes with systolic foot detection

Published as

Evelien Hermeling, Koen D. Reesink, Robert S. Reneman, Arnold P.G. Hoeks. Confluence of incident and reflected waves interferes with systolic foot detection in the carotid artery distension waveform. Journal of Hypertension. 2008; 26: 2374-2380

Abstract

Local pulse wave velocity, a direct measure of arterial stiffness, can be measured using the systolic foot of the pressure waveform as time-reference point. The accuracy and precision of the systolic foot identification, which may be disturbed by early wave reflections, heavily affects pulse wave transit time measurements. We investigated within subjects the existence of early wave reflections and their interference with the systolic foot identification. Fourteen ultrasound derived distension waveforms, spaced over 16.4 mm, were simultaneously recorded in the common carotid artery 3 cm proximal of the bifurcation of twelve young subjects. The second derivatives of the distension waveforms were calculated to identify the systolic foot and an inflection point preceding systolic peak distension. Pulse wave transit time (*TT*) was calculated as the time difference between the most proximal and most distal time-point, using either the systolic foot or the inflection point. The time to reflection (ΔT_{SF_IP}) was defined as the time difference between the systolic foot (SF) and the inflection point (IP). Both TT_{SF} and TT_{IP} could be determined with good intra-subject precision: 0.7 and 1.4 ms, respectively. The systolic foot is running forward, TT_{SF} = 3.1 $\pm$ 0.9 ms, while the inflection point appears to run backwards, TT_{IP} = -3.9 $\pm$ 1.4 ms. ΔT_{SF_IP} was 44.3 $\pm$ 8.8 ms. Despite the good intra-subject reproducibility, confluence of incident and reflected waves disturbs identification and discrimination of the systolic foot and the inflection point, resulting in biased estimates. Therefore both points are unsuitable for local pulse transit time measurements in the common carotid artery.

4.1 Introduction

Aging and cardiovascular diseases are associated with stiffening of the arteries (Laurent et al. 2001, Laurent et al. 2003, Mattace-Raso et al. 2006). Pulse wave velocity is a direct measure of arterial stiffness and is currently measured along the carotid-femoral trajectory, providing an indication of regional stiffness. However, the carotid-femoral trajectory comprises both elastic and muscular arteries that respond differently to aging and cardiovascular disease. Methods to measure stiffness locally, e.g. by distensibility, require estimation of local pulse pressure (Hoeks et al. 1990) which may be a major source of error as it is difficult to accurately assess non-invasively (Van Bortel et al. 2002). Recently, it

has been proposed to non-invasively derive artery stiffness locally from pulse wave velocities (Brands et al. 1998, Eriksson et al. 2002, Meinders et al. 2001), thereby eliminating the need for local pulse pressure measurements. Normally, the pulse wave velocity is calculated as the distance between two measurement sites divided by the transit time of a reference point in the pressure or distension waveform (which is the diameter change over time). The systolic foot of the waveform is often suggested as reference point for measuring the pulse wave velocity as it is thought to be free from reflections (Nichols and O'Rourke 2005b). Moreover, local blood flow velocity, which modulates the pulse wave velocity independently of arterial stiffness (Histand and Anliker 1973), is close to zero at the systolic foot.

Besides the incident wave, initiated by ejection of the stroke volume by the left ventricle and signalled by the systolic foot, secondary waves contribute to the arterial pressure waveform. These waves are reflected waves, caused by impedance mismatches in the arterial tree, as present at bifurcations and arterial segments with non-uniform stiffness or with tapering. A wave reflected somewhere in the lower body periphery will appear as a forward running wave in the brachial and carotid arteries, with a time delay with respect to the incident wave that depends on the distance of the reflection site to the heart and the average pulse wave velocity (Nichols 2005). The onset of a wave reflection is signalled by an inflection in the pressure waveform and can be extracted by considering time derivatives of the waveform (Kelly et al. 1989, Murgo et al. 1980). Current methods to analyze direction of propagation of both incident and reflected waves require either simultaneously measured local blood pressure and flow (Khir and Parker 2005, Parker and Jones 1990, Westerhof et al. 1972), or a relatively long and homogeneous arterial trajectory (Hope et al. 2005), which are both difficult to accomplish *in vivo*.

Recently, we showed that in a phantom set-up, by means of multiple M-line ultrasound, using the systolic foot as reference point, local pulse wave velocity can be measured with good precision and accuracy (Hermeling et al. 2007). Pulse wave velocity as measured in this way is completely determined by the transit time because the distance between the piezo-electrical elements of the ultrasound probe dictates the distance between the measurement sites. The accuracy and precision of the transit time measurements *in vivo* is affected by reflections, either from within the selected arterial segment or from other regions. In local pulse wave velocity measurements, it is easy to select an arterial segment without reflection sites within the measurement segment, so that only backward and forward propagating waves have to be considered. Unlike forward

reflection waves, backward propagating waves may change the shape of the pressure waveform and consequently its derivatives over the measured segment, possibly interfering with the systolic foot and affecting the pulse wave velocity estimation.

The aim of the present study is to determine *in vivo* the intra-subject precision of local pulse transit time, and hence pulse wave velocity measurements, using the systolic foot of distension waveforms as reference. Distension waveforms are recorded simultaneously at fourteen locations over a 16.4 mm segment of the common carotid artery (CCA) by means of an ultrasound scanner with high temporal and spatial resolution. We analyze the propagation direction of wave reflections in early systole. The repercussion of these reflected waves on systolic foot detection and the consequences for local pulse wave velocity measurement are considered as well.

4.2 Methods

Subjects

Twelve young male volunteers aged 26 ± 4 years (mean $\pm$ standard deviation) were recruited and gave written informed consent prior to enrolment. The joint medical ethical committee of the University of Maastricht and the Academic Hospital Maastricht, Netherlands approved the study. After 10 minutes rest in supine position, a straight arterial segment of the left CCA was identified with the ultrasound probe at least 3 cm proximally of the carotid artery bulb. Seven echo-recordings of seven seconds each were obtained with the ultrasound probe positioned parallel to the artery. Subsequently, the right CCA was measured according to the same protocol. ECG and blood pressure recordings (Finapres 2300, Ohmeda, Englewood, Colorado, USA) were obtained simultaneously to facilitate automatic processing.

Data recording

A PICUS ultrasound scanner (Esaote Europe, Maastricht, Netherlands) with a 7.5 MHz linear array probe was used. The scanner was operating in multiple M-mode, producing fourteen M-mode recordings simultaneously at a frame rate of 800 Hz (Meinders et al. 2001). The pitch between the M-lines was 1.26 mm, thus

in total, a segment of 16.4 mm of the CCA was covered. The RF-data, sampled at 33.3 MHz, were stored on a hard disk for off-line analysis. Before determining wall movement, linear interpolation in time was performed on the RF-data to remove the time skew between M-lines (Meinders et al. 2001). After manually selecting the wall-lumen interfaces at both the posterior and anterior walls for all fourteen M-lines, a wall track system (Brands et al. 1997, Hoeks et al. 1999) was used to obtain the distension waveforms. The wall track system uses a modelled complex cross correlation function (Brands et al. 1997) to derive wall movement as function of time. A relatively small temporal correlation window (5 ms, 4 sample points) and a large spatial correlation window (0.79 mm, 34 sample points) were used to obtain distension waveforms with high temporal resolution and good precision. The distension waveforms were low pass filtered to reduce high frequency noise, using a first order low pass filter with a cut-off frequency of 60 Hz subsequently applied in a forward and reverse direction, to cancel out filter-related phase shifts. After 10-fold interpolation, the second time derivative of the distension waveform, i.e., the acceleration waveform, was calculated using a first order high pass derivative filter with a cut-off frequency of 80 Hz, again applied in both the forward and the reverse direction.

Distension waveforms analysis

To determine the transit time of the incident wave, caused by left ventricle ejection, and transit time of the wave reflection, causing the inflection point in the upstroke, the systolic foot and the inflection point were identified in each of the distension waveforms as the first maximum of the acceleration waveform before the systolic peak and the local maximum of the acceleration waveform between the systolic foot and the systolic peak, respectively.

The transit time required for the pressure waves to pass the considered CCA segment TT_{SF} or TT_{IP} was calculated as the time difference between the time-point of the systolic foot or the inflection point in the most distal waveform minus the time-point of the systolic foot or the inflection point in the most proximal waveform. Time to reflection, i.e. the time delay (ΔT_{SF_IP}) between the systolic foot and the dicrotic notch was determined for the most proximal waveform.

Statistics

Average values (of either TT_{SF}, TT_{IP} or ΔT_{SF_IP}) for each subject and both arteries (subject means) were calculated by taking the mean over seven median values

calculated for each measurement containing 4-7 beats. The subject standard deviations were also obtained from these median values. The intra-subject variation (precision) was defined as the standard deviation of the error, i.e., the difference between subject mean and median values, over all subjects. Statistical differences between TT_{IP} and TT_{SF} (or left and right) were analyzed by Student paired t-test. Values are reported as mean ± standard deviation (SD).

Table 4.1 Subject characteristics

	mean (range)
age (years)	26 (22-37)
weight (kg)	75 (63-88)
height (cm)	186 (177-195)
BMI (kg / m2)	22 (18 -25)
DBP (mmHg)	71 (58-92)
SBP (mmHg)	122 (109-141)
HR (1/min)	60 (40-74)

Characteristics of the subjects, data expressed as mean (range). DBP, diastolic blood pressure; SBP, systolic blood pressure; HR, heart rate; BMI, body mass index.

4.3 Results

Subject characteristics are shown in Table 4.1. An example of a multiple M-mode recording is shown in Figure 4.1, with in Figure 4.1a and c the fourteen distension and acceleration waveforms, respectively. To aid detailed visualization, the waveforms are displayed with an offset, gradually increasing with the line number. Figure 4.1b and Figure 4.1d show the same waveforms, but focused on the upstroke only. The systolic foot appeared earlier in the cardiac cycle in the proximal than in the distal waveforms. In contrast, the inflection point arrived earlier in the distal waveforms than in the proximal waveforms, indicating that the direction of propagation of the inflection point is opposite to that of the systolic foot.

In Figure 4.2a, the transit times of the systolic foot and the inflection point for all subjects are summarized. All subjects exhibit a positive TT_{SF} (3.1 ± 0.9 ms), which is in accordance with the observation in Figure 4.1 that the systolic foot arrives earlier in the proximal than in the distal waveforms. TT_{SF} had an intra-

subject variation (precision) of 0.7 ms. The inflection point had a negative transit time, TT_{IP} = -3.9 ± 1.5 ms (intra-subject variation 1.4 ms), that is, the inflection point appeared first in distal waveform. Figure 4.2b shows the time delay between the systolic foot and the inflection point, (ΔT_{SF_IP} = 44.3 ± 8.8 ms). The intra-subject variation of ΔT_{SF_IP} was small (1.3 ms) compared to the relatively large inter-subject variation (8.8 ms) within the subject group.

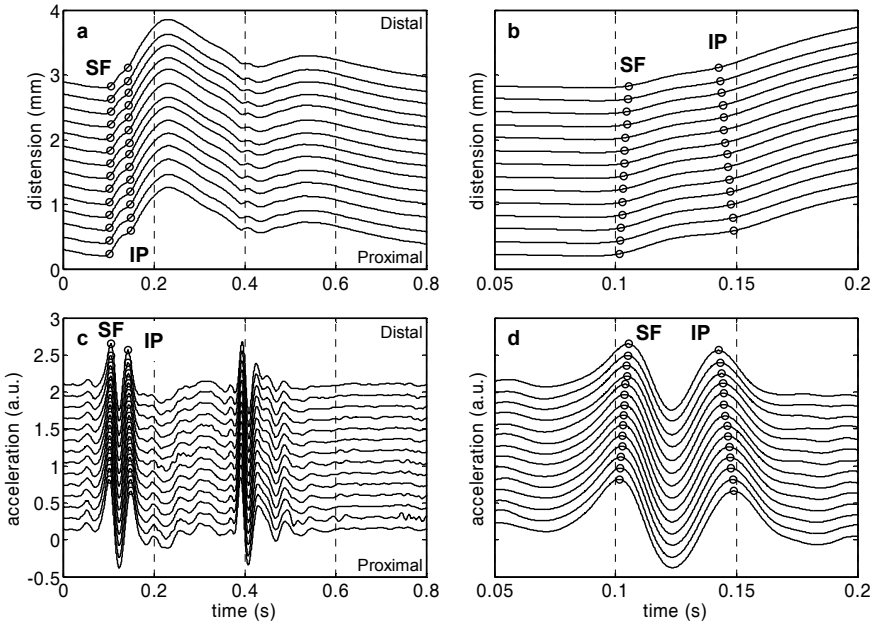

Figure 4.1. a) Fourteen simultaneously recorded distension waveforms, displayed with an offset (bottom trace is proximal registration). The circles indicate the characteristic time-points of the distension waveforms, the first circles designate the systolic foot (SF) followed by the inflection point (IP). b) Same fourteen distension waveforms (as Figure 4.1a), but over a shorter time-interval. c) The second derivative (acceleration) of the fourteen distension waveforms of Figure 4.1a. d) Same acceleration waveforms as in Figure 4.1c, but over a shorter time-interval.

A preliminary estimate of the local pulse wave velocity can be derived from the transit time (TT_{SF}) over the 16.4 mm long arterial segment (x). Assuming a constant pulse wave velocity (PWV) and using the time to reflection (ΔT_{SF_IP}), which is the round trip time, the distance (D) to the reflection site can be estimated by:

$$D = \frac{PWV\,\Delta T_{SF\_IP}}{2} = \frac{x\,\Delta T_{SF\_IP}}{2TT_{SF}} \qquad 4.1$$

The estimated distance to the reflection site was 13 ± 5 cm. Because the probe was positioned at about 3 cm proximal of the carotid artery bulb, the reflection site is distal to the carotid artery bifurcation.

Difference between transit times of the systolic foot and the inflection point was significant (3.1 ms versus 3.9 ms, p = 0.01). Comparing left and right CCA, a significant difference was observed in TT_{IP} (p = 0.02) and ΔT_{SF_IP} (p = 0.01), but not in TT_{SF} (p = 0.13), see Table 4.2.

Table 4.2 Timing difference as observed between left and right CCA.

	Left CCA	Right CCA	Paired t-test
TT_{SF} (ms)	3.4 ± 0.9	2.9 ± 1.0	p = 0.13
TT_{IP} (ms)	-4.6 ± 1.5	-3.3 ± 1.0	p = 0.02
ΔT_{SF_IP} (ms)	41.6 ± 7.9	46.5 ± 9.3	p = 0.01
R-R interval (ms)	1017 ± 199	1052 ± 195	p < 0.001
MAP (mmHg)	92 ± 20	89 ± 19	p = 0.03

Difference between left and right CCA measurements as observed in transit times of systolic foot (TT_{SF}) and inflection point (TT_{IP}), delay between the systolic foot and the inflection point, time to reflection, (ΔT_{SF_IP}), R-R interval and mean arterial pressure (*MAP*). Values are mean ± standard deviation.

In two cases (subject 3 left CCA and subject 11 right CCA; Figure 4.2), it was not possible to determine the TT_{IP}, because the inflection point could not be identified in the more distal waveforms. Figure 4.3 shows the acceleration waveforms (like Figure 4.1d) of the left CCA of subject 3. In these cases, it was impossible to establish the inflection point in the more distal waveforms because it was merged with the systolic foot. Visual inspection of the acceleration waveforms suggests that also in these cases the inflection point reflects a backward running wave. Moreover, the propagation of the systolic foot is non-linear, which is the result of interference of the inflection point with the systolic foot (Figure 4.3). This interference of the inflection point with the systolic foot predominantly occurs for those cases where the time between the systolic foot and the inflection point (ΔT_{SF_IP}) is shorter (Figure 4.2b), which may result in a biased TT_{SF}.

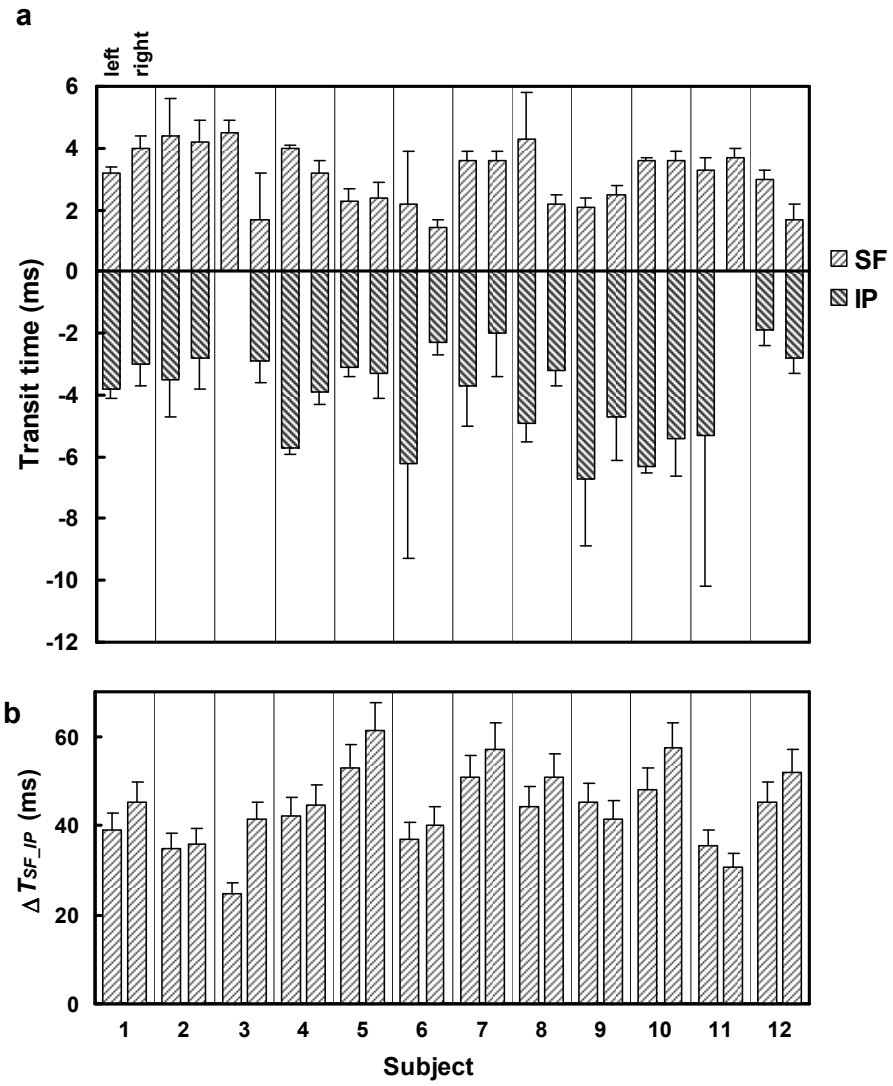

Figure 4.2 a) Transit time of the systolic foot (SF) and the inflection point (IP) of all subjects over a short arterial segment of 16.4 mm (mean ± standard deviation). b) Time delay between the systolic foot and the inflection point (mean + standard deviation).

4.4 Discussion

In the present study, we were able to derive the direction of propagation and the interaction of pressure waves within a short carotid artery segment of 16.4 mm. The precision (intra-subject variation of TT_{SF} is 0.7 ms) of the methods allows analysis of propagation of characteristic time-points of the pressure wave over the short distance (TT_{SF} = 3.1 $\pm$ 0.9 ms). We found that the onset of the systolic wave is rapidly followed by a reflected wave travelling in reverse direction (TT_{IP} = -3.9 $\pm$ 1.5 ms). In some cases the inflection point of the reflected wave and the systolic foot merged, so that the inflection point could not be identified. In a larger number of cases an apparent non-linear propagation of the systolic foot (Figure 4.3) was seen, affecting the accuracy of local transit time measurements.

Our results indicate that a wave reflection observed in early systole, signalled by the inflection point, stems from a site distal from the measurement site. This finding corroborates earlier observations using wave intensity analysis (Bleasdale et al. 2003, Niki et al. 2002, Zambanini et al. 2005).

Because the systolic foot is considered to be free of reflections and to maintain its identity in the propagating wave, it has been proposed as reference point in pulse wave velocity measurements (Nichols and O'Rourke 2005b). Figure 4.3 shows an apparent non-linear propagation of the systolic foot over the considered segment, indicating that even in young volunteers, with a relatively low pulse wave velocity and the probe placed as far as possible from the carotid bifurcation, the systolic foot is affected by reflections. In this study, the transit time is measured using only the most proximal and most distal M-line. Improved precision of transit time and thus pulse wave velocity determination could be obtained by using all fourteen M-lines (Hermeling et al. 2007). The early reflections, however, cause a non-random error that cannot be suppressed by averaging over more M-lines or beats. The interaction of the incident and reflected waves will deteriorate the systolic foot identification, especially if the measurement site is located high in the CCA and the pulse wave velocity is elevated.

The segments of the CCA analyzed in this study were straight and did not contain any branches or tapering. Moreover, because young and healthy volunteers were studied and visual inspection of the B-mode did not show any wall inhomogeneities, the non-linear propagation of the systolic foot and the inflection point cannot be explained by non-uniform stiffness of the CCA.

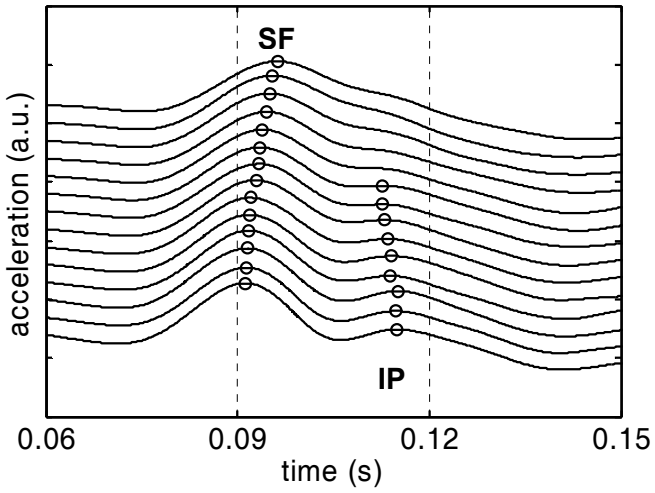

Figure 4.3. Example of how confluence of forward and backward waves precludes identification of the inflection point (IP) in distal waveforms. Note the resultant non-linear propagation of the systolic foot (SF).

Hope et al. (Hope et al. 2005) suggested that dispersion may affect the shape of the pressure waveform. Wave dispersion, i.e., phase distortion caused by a frequency dependent wave speed, will only have a substantial effect for distances greater than the wavelength. The highest frequency component in the distension waveform is 60 Hz. A 60 Hz wave travelling at wave speed of 5 m/s has a wavelength of 8 cm. We considered a CCA segment of only 16.4 mm, which is much smaller than the 60 Hz, i.e. the shortest, wavelength. Therefore, in the present study the effect of wave dispersion on the transit time measurement can be ignored.

To analyze wave reflections in small arterial segments it is crucial to have and maintain good phase characteristics. To avoid phase distortion, the frequency bandwidth of the measurement device should exceed the frequency range of the waveform. Although 99.5 % of the pressure waveform energy is contained in the frequency band below 8 Hz (Nichols and O'Rourke 2005a) a signal frequency content up to 60 Hz is needed to circumvent phase distortion of characteristic time-points of the pressure waveform (Hoeks et al. 2000). Moreover, a sufficiently large bandwidth is needed to distinguish the inflection point from the systolic foot, while the inflection point arrives within 45 ms after the systolic foot. Our study illustrates that by using an ultrasound system operating in multiple M-mode at a high frame rate these phase-related requirements are fulfilled.

Multiple M-line ultrasound measurement provides fourteen distension waveforms with high precision (5 µm) (Hoeks et al. 1990) and good temporal resolution (1.2 ms). In our previous work (Hermeling et al. 2007) it was shown that the second derivative of the distension waveform is sensitive to changes in speckle pattern which might deteriorate the precision of the systolic foot and the inflection point determination. In the present study, a large spatial window of 0.79 mm, which is two to three times the average speckle size, is used to maintain both good precision and high temporal resolution (Hoeks et al. 1993). Changes in speckle pattern may affect precision, but will not cause any bias in TT_{SF}, TT_{IP} or ΔT_{SF_IP}.

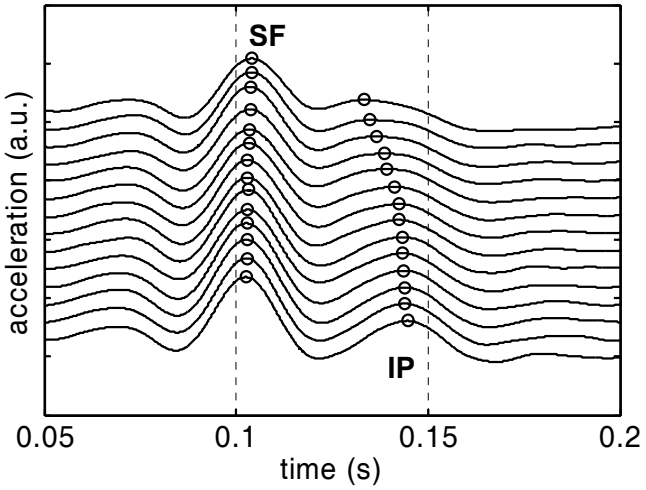

Figure 4.4. Case exhibiting non-linear propagation of inflection point (IP) due to interference with systolic foot (SF).

We found a significant difference between TT_{SF} (3.1 ms) and TT_{IP} (3.9 ms, $p = 0.01$), corresponding to a pulse wave velocity of 5.2 m/s and 4.2 m/s, respectively. The pulse wave velocity (and transit time) is determined by both the stiffness of the artery, determined by the transmural pressure, and local blood flow velocity (Histand and Anliker 1973). At the inflection point, arriving at 45 ms after the systolic foot, a pressure increase of about 20 mmHg will cause an increase in the pulse wave velocity by about 0.9 m/s (Meinders and Hoeks 2004). This is largely counterbalanced by the mean blood flow velocity of approximately 0.7 m/s, which decelerates the pulse wave velocity of the reflected wave. Therefore, the difference in measured transit times cannot be explained by a difference in the pulse wave velocity between the systolic foot and the inflection point. The relatively large wave of the systolic foot modifies the shape

of the acceleration waveform around the inflection point in the more distal waveforms, interfering with detection of the inflection point (Figure 4.4).

Compared to the left CCA, the right CCA recordings show a decreased TT_{IP} ($p = 0.02$) but increased ΔT_{SF_IP} ($p = 0.01$, Table 4.2). Both parameters are measures for pulse transit time and should behave in the same way. The possible interference between the inflection point and the systolic foot is weakest in the proximal waveforms and ΔT_{SF_IP}, which is calculated using the most proximal waveform, is least influenced by this interference. The observed difference in ΔT_{SF_IP} between left (41.6 ms) and right (46.5 ms) is probably correct and can be explained by a lower mean arterial pressure (*MAP*) and heart rate during the right CCA measurement (Table 4.2), resulting in a lower pulse wave velocity (Meinders and Hoeks 2004). Figure 4.5, indeed shows that the left-right difference in *MAP* and ΔT_{SF_IP} are correlated. Because the left CCA of subject 3 showed clear merging of the inflection point with the systolic foot (Figure 4.3) and consequently had biased ΔT_{SF_IP}, it was excluded from the correlation (this subject is marked with a triangle in Figure 4.5). The reduction in *MAP* and RR interval is most likely a consequence of the protocol followed (first left, then right). The decreased *MAP* and heart rate reflect minor hemodynamic adaptations that may still occur after 10 min of rest in supine position (Sala et al. 2006). The increased time to reflection (ΔT_{SF_IP}) during right CCA measurement contrasts with the observed lower right CCA TT_{IP}. An explanation for this is that in the right CCA measurement the inflection point is further away from the systolic foot causing less interference of the inflection point in distal waveforms (observed as non-linear propagation of the inflection point, Figure 4.4). The reduced interference then leads to less overestimation of transit time of the inflection point, i.e. a shorter TT_{IP} compared to left CCA TT_{IP}. The same may hold for TT_{SF}, which is also lower in the right CCA, but the difference in TT_{SF} between both arteries did not reach statistical significance. The differences in incident and reflected wave transit times, as observed between left and right CCA, illustrate that reflected waves do affect the systolic foot detection and that this interference is modulated by even modest changes in arterial hemodynamics.

Clinical implications

The accuracy and precision of local stiffness assessment by means of pulse wave velocity measurements strongly depends on the precision of systolic foot detection. In the case of substantial reflective interference, linear extrapolation of

systolic foot propagation over the first 6 (unaffected) M-lines (Figure 4.3) reveals an overestimation in TT_{SF} of 3 ms. The observed error in transit time corresponds to an error in pulse wave velocity of 50 %. The distensibility coefficient, an alternative local stiffness measure, is subject to an error of 20 % when local pulse pressure deviates by 8 mmHg from the measured value (Waddell et al. 2001). The error in distensibility coefficient converts to an error of 10 % in pulse wave velocity given the Bramwell-Hill relationship (Hermeling et al. 2007), which is substantially smaller than that obtained with systolic foot detection.

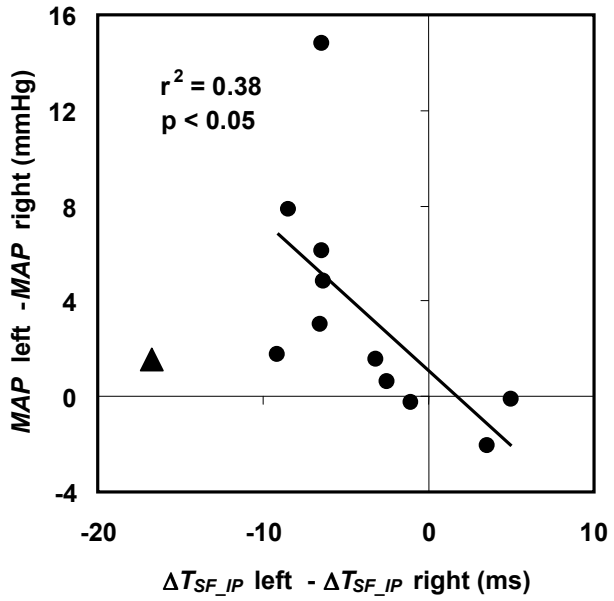

Figure 4.5. Correlation of left-right differences in the time to reflection (ΔT_{SF_IP}) and mean arterial pressure (*MAP*). One subject, indicated with a triangle in the scatter plot, is excluded from the analysis.

In the present study, focus is on local pulse wave velocity measurement, but the reflection-dependent bias observed in TT_{SF} may also affect carotid-femoral pulse wave velocity measurements. The carotid-femoral trajectory is much longer and consequently the transit time between carotid and femoral artery is long (30 to 100 ms) compared to that in local pulse wave velocity measurements. Therefore, a bias in TT_{SF} of 3 ms in the CCA will result in a maximum error of 10 % in carotid-femoral pulse wave velocity for subjects with stiff arteries. In general, the error will be in the order of only 5 %. Millasseau et al. (Millasseau et al. 2005) compared two systolic foot detection methods used to measure carotid-femoral pulse wave velocity. The difference between the two methods was dependent on

the pulse wave velocity, which could be a consequence of the interference of reflected waves with systolic foot detection.

4.5 Conclusion

High resolution ultrasound systems operating in multiple M-mode can be used to analyze the propagation of both systolic foot and reflected waves with relative good precision in arterial segments as short as 16.4 mm. The systolic foot is generally not free of wave reflections, which complicates local pulse wave velocity measurement in the CCA when using the systolic foot as a time-reference point.

References

Bleasdale RA, Mumford CE, Campbell RI, Fraser AG, Jones CJ, and Frenneaux MP. Wave intensity analysis from the common carotid artery: a new noninvasive index of cerebral vasomotor tone. Heart Vessels 18: 202-206, 2003.

Brands PJ, Hoeks APG, Ledoux LAF, and Reneman RS. A radio frequency domain complex cross-correlation model to estimate blood flow velocity and tissue motion by means of ultrasound. Ultrasound Med Biol 23: 911-920, 1997.

Brands PJ, Willigers JM, Ledoux LA, Reneman RS, and Hoeks AP. A noninvasive method to estimate pulse wave velocity in arteries locally by means of ultrasound. Ultrasound Med Biol 24: 1325-1335, 1998.

Eriksson A, Greiff E, Loupas T, Persson M, and Pesque P. Arterial pulse wave velocity with tissue Doppler imaging. Ultrasound Med Biol 28: 571-580, 2002.

Hermeling E, Reesink KD, Reneman RS, and Hoeks AP. Measurement of local pulse wave velocity: effects of signal processing on precision. Ultrasound Med Biol 33: 774-781, 2007.

Histand MB and Anliker M. Influence of flow and pressure on wave propagation in the canine aorta. Circ Res 32: 524-529, 1973.

Hoeks AP, Brands PJ, Smeets FA, and Reneman RS. Assessment of the distensibility of superficial arteries. Ultrasound Med Biol 16: 121-128, 1990.

Hoeks AP, Willigers JM, and Reneman RS. Effects of assessment and processing techniques on the shape of arterial pressure-distension loops. J Vasc Res 37: 494-500, 2000.

Hoeks APG, Arts TGJ, Brands PJ, and Reneman RS. Comparison of the performance of the cross correlation and Doppler autocorrelation technique to estimate the mean velocity of simulated ultrasound signals. Ultrasound Med Biol 19: 727-740, 1993.

Hoeks APG, Brands PJ, Willigers JM, and Reneman RS. Non-invasive assessment of mechanical properties of arteries in health and disease. Proc Insttn Mech Engrs 213: 195-202, 1999.

Hope SA, Tay DB, Meredith IT, and Cameron JD. Waveform dispersion, not reflection, may be the major determinant of aortic pressure wave morphology. Am J Physiol Heart Circ Physiol 289: H2497-2502, 2005.

Kelly R, Hayward C, Avolio A, and O'Rourke M. Noninvasive determination of age-related changes in the human arterial pulse. Circulation 80: 1652-1659, 1989.

Khir AW and Parker KH. Wave intensity in the ascending aorta: effects of arterial occlusion. J Biomech 38: 647-655, 2005.

Laurent S, Boutouyrie P, Asmar R, Gautier I, Laloux B, Guize L, Ducimetiere P, et al. Aortic stiffness is an independent predictor of all-cause and cardiovascular mortality in hypertensive patients. Hypertension 37: 1236-1241., 2001.

Laurent S, Katsahian S, Fassot C, Tropeano AI, Gautier I, Laloux B, and Boutouyrie P. Aortic stiffness is an independent predictor of fatal stroke in essential hypertension. Stroke 34: 1203-1206, 2003.

Mattace-Raso FU, van der Cammen TJ, Hofman A, van Popele NM, Bos ML, Schalekamp MA, Asmar R, et al. Arterial stiffness and risk of coronary heart disease and stroke: the Rotterdam Study. Circulation 113: 657-663, 2006.

Meinders JM and Hoeks AP. Simultaneous assessment of diameter and pressure waveforms in the carotid artery. Ultrasound Med Biol 30: 147-154, 2004.

Meinders JM, Kornet L, Brands PJ, and Hoeks AP. Assessment of local pulse wave velocity in arteries using 2D distension waveforms. Ultrason Imaging 23: 199-215, 2001.

Millasseau SC, Stewart AD, Patel SJ, Redwood SR, and Chowienczyk PJ. Evaluation of carotid-femoral pulse wave velocity: influence of timing algorithm and heart rate. Hypertension 45: 222-226, 2005.

Murgo JP, Westerhof N, Giolma JP, and Altobelli SA. Aortic input impedance in normal man: relationship to pressure wave forms. Circulation 62: 105-116, 1980.

Nichols WW. Clinical measurement of arterial stiffness obtained from noninvasive pressure waveforms. Am J Hypertens 18: 3S-10S, 2005.

Nichols WW and O'Rourke MF. Principles of recording and analysis of arterial waveforms. In: McDonald's blood flow in arteries (5th edition ed.). London: Edward Arnold, 2005a.

Nichols WW and O'Rourke MF. Properties of the arterial wall: theory. In: McDonald's blood flow in arteries (5th edition ed.). London: Edward Arnold, 2005b, p. 59.

Niki K, Sugawara M, Chang D, Harada A, Okada T, Sakai R, Uchida K, et al. A new noninvasive measurement system for wave intensity: evaluation of carotid arterial wave intensity and reproducibility. Heart Vessels 17: 12-21, 2002.

Parker KH and Jones CJ. Forward and backward running waves in the arteries: analysis using the method of characteristics. J Biomech Eng 112: 322-326, 1990.

Sala C, Santin E, Rescaldani M, and Magrini F. How long shall the patient rest before clinic blood pressure measurement? Am J Hypertens 19: 713-717, 2006.

Van Bortel LM, Duprez D, Starmans-Kool MJ, Safar ME, Giannattasio C, Cockcroft J, Kaiser DR, et al. Clinical applications of arterial stiffness, Task Force III: recommendations for user procedures. Am J Hypertens 15: 445-452, 2002.

Waddell TK, Dart AM, Medley TL, Cameron JD, and Kingwell BA. Carotid pressure is a better predictor of coronary artery disease severity than brachial pressure. Hypertension 38: 927-931, 2001.

Westerhof N, Sipkema P, van den Bos GC, and Elzinga G. Forward and backward waves in the arterial system. Cardiovasc Res 6: 648-656, 1972.

Zambanini A, Cunningham SL, Parker KH, Khir AW, Mc GTSA, and Hughes AD. Wave-energy patterns in carotid, brachial, and radial arteries: a noninvasive approach using wave-intensity analysis. Am J Physiol Heart Circ Physiol 289: H270-276, 2005.

Chapter 5

Modeled decomposition of pressure wave does not provide estimates for aortic pulse wave velocity

Published as

Evelien Hermeling, Koen D. Reesink, Arnold P.G. Hoeks, Robert S. Reneman. Modelled decomposition of aortic pressure waveforms does not provide estimates for pulse wave velocity. Hypertension. 2008; 51: e60

Letter to the editor

With great interest we have read the recent article by Qasem and Avolio (Qasem and Avolio 2008, abstract in Appendix), in which they propose a new method to determine aortic pulse wave velocity from waveform decomposition of the central aortic pressure pulse as derived from a single radial artery pulse measurement. The pulse transit time in the aorta is estimated by determining the time difference between the derived forward and backward waves. By using carotid-to-femoral artery pulse wave velocity measurements as an independent method, the validity of the pulse transit time assessment was tested in two groups of subjects. In the first group the relation between measured carotid-femoral artery transit time and pulse transit time was determined, using a regression model, and in the second group the outcome of this relation was tested with presumed independent methods.

Aortic pulse wave velocity is a good indicator of arterial stiffness and an important predictor of cardiovascular risk in diseased and healthy populations. The measurement of aortic pulse wave velocity in man, commonly between the carotid and femoral arteries, however, is not without pitfalls due to the recording of pulse waves moving in opposite directions and the uncertainties in estimating the distance between the two sites of wave recording. Therefore, a method to determine aortic pulse wave velocity, circumventing these disadvantages will be of great clinical importance. The question can be asked, however, whether the method described in the abovementioned article will fulfill this expectation.

We will not argue about the reliability of deriving a central aortic pressure pulse from a peripherally recorded pressure pulse by means of a transfer function; too many letters to editors have been spent on the pros and cons of this derivation already. In expressing our concerns regarding the approach followed by the authors, we assume the central aortic pressure waveform to be derived properly. The central pressure waveform is decomposed into forward and backward components using an artificial triangular flow wave, the peak of which coincides with the first inclination point in the aortic waveform and the end (zero flow) with the dicrotic notch. The authors suggest that the relation between flow and pressure waves is used to determine the pulse transit time. According to the selected wave reflection model, this transit time is equal to the first inclination point (T1), which can directly be obtained from the pressure waveform. It can be argued as to whether positioning of the peak at the moment of the first inclination point is correct, because the peak of measured aortic flow precedes this point (Westerhof et al. 2006). Much to our surprise the forward and backward pressure

waves as assessed in this way are not used in the analysis. The early part of the backward wave up to T1 is set at a constant value of half the end-diastolic blood pressure. The remainder of the systolic phase of the backward and forward waves is reconstructed, the constraints being set by T1 and the ejection duration, with an ambiguous algorithm that does not produce a unique solution. Both moves need clarification, because the arguments given on page 189 can be questioned. Another aspect that needs clarification is the assumption that the site of reflection is in the femoral artery. No arguments are given for this assumption, which is crucial to obtain reliable values of aortic pulse wave velocity calculated from carotid-femoral distance divided by eTR2 / 2 and using carotid-femoral pulse wave velocity as an independent method for evaluation. The approach chosen will fail when the wave is reflected from another site, which is not unlikely considering the observed time delay and the invasively recorded pulse wave velocities (Ting et al. 1990). Even if the reflection site coincides with the measurement site, both approaches should inherently provide different results, because of the contribution of the cardiac-carotid trajectory in the measured carotid-femoral pulse wave velocity. Further, eTR2 is determined by cross-correlation. Before cross-correlation the authors normalize the amplitude of the backward wave to that of the forward wave to avoid inconsistencies. Normalization of the wave, however, does not affect the position of the peak of the cross-correlation. The authors should have been more concerned regarding the reliability of cross-correlating waveforms of different shapes. Unless a uniform, non-tapered, homogenous and straight artery segment with a single reflection point is considered, the shape of the backward wave will be substantially different from that of the forward wave and correlation of these waves will introduce substantial errors in the measurement of the position of maximum correlation. In the approach followed by the authors the outcome is largely determined by the time to the first inflection point (T1).

The clinical evaluation of eTR2 / 2 is not convincing. The correlation between measured transit time and eTR2 / 2 shown in Figure 6 (Appendix) implies that for a change in measured transit time of 1 ms, an error of 0.3 ms in eTR2 / 2 is made, which is rather substantial. Moreover, the Bland-Altman plot in this Figure shows a substantial level-dependent bias, the difference being greater, the higher the transit time is. The comparison of the carotid-femoral pulse wave velocity and carotid-femoral distance divided by eTR2 / 2, as shown in Figure 7 (Appendix), raises additional questions. It is not surprising that the correlation between these parameters is pretty good, because carotid-femoral distance is part of both parameters (Altman 1997). The bias in the Bland-Altman plot, although less pronounced, is also visible in this Figure.

As indicated above, we are very much interested in a well-defined method to measure aortic pulse wave velocity, because of its importance in predicting cardiovascular risk, not only in the clinic, but also in epidemiological studies. The method proposed as well as its evaluation raises many questions. We do get the impression that similar results could have been obtained by measuring directly T1 as delay time. Moreover, it should be realized that a good estimate of aortic pulse transit time, if any, does not solve the problems involved in accurately measuring distance, a parameter required to determine aortic pulse wave velocity.

References

Altman DG. Practical statistics for medical research. London: Chapman & Hall, 1997.

Qasem A and Avolio A. Determination of aortic pulse wave velocity from waveform decomposition of the central aortic pressure pulse. Hypertension 51: 188-195, 2008.

Ting CT, Chang MS, Wang SP, Chiang BN, and Yin FCP. Regional pulse wave velocities in hypertensive and normotensive humans. Cardiovascular Research 24: 865-872, 1990.

Westerhof BE, Guelen I, Westerhof N, Karemaker JM, and Avolio A. Quantification of wave reflection in the human aorta from pressure alone: a proof of principle. Hypertension 48: 595-601, 2006.

Chapter 6

The dicrotic notch as alternative time-reference point to measure local pulse wave velocity.

Submitted as:

Evelien Hermeling, Koen D. Reesink, Liselotte M. Kornmann, Robert S. Reneman, Arnold P.G. Hoeks. The dicrotic notch as alternative time-reference point to measure local pulse wave velocity in the carotid artery by means of ultrasonography.

Abstract

Increased arterial stiffness is associated with cardiovascular disease. Its applicability in individual patient management, however, is limited due to lack of reliable methods. We developed a method to measure arterial stiffness by means of local pulse wave velocity (*PWV*), using multiple M-mode ultrasound and the dicrotic notch (PWV_{DN}) rather than the systolic foot (PWV_{SF}) as time-reference point. Systolic foot and dicrotic notch were determined in fourteen simultaneously recorded distension waveforms obtained in young and older subjects (mean age 26 and 59 years). Linear regression was performed on echo-line position and time-reference point, resulting in a local pulse wave velocity estimate of either PWV_{SF} or PWV_{DN}. PWV_{DN}, at about mean arterial pressure, had a better intra-subject variability (0.6 m/s) than PWV_{SF} (1.1 m/s). The expected difference in stiffness between the two age categories was identified by PWV_{DN} ($p < 0.0001$), but not by PWV_{SF}. Moreover, in contrast to PWV_{SF}, PWV_{DN} showed a significant correlation with age ($r^2 = 0.67$), relative distension (strain, $r^2 = 0.50$) and pulse wave velocity calculated from the distensibility coefficient (PWV_{DC}; $r^2 = 0.54$). PWV_{DN} is a suitable and non-invasive measure of arterial stiffness: it has a good reproducibility and correlates well with age, PWV_{DC} and relative distension. PWV_{DN} does not require additional assessment of distance or local pulse pressure. Furthermore, PWV_{DN} is measured locally, allowing discrimination of age effects between muscular and elastic arteries, at near mean arterial pressure, thereby better reflecting the effective arterial stiffness, which determines the load the left ventricle is subjected to as it ejects blood.

6.1 Introduction

Stiffening of the arterial tree is a major contributor to systolic hypertension (Laurent et al. 2006, McEniery et al. 2007, Schiffrin 2004), and is associated with overall and cardiovascular mortality in hypertensive patients (Laurent et al. 2001), stroke in hypertensive patients (Laurent et al. 2003) and coronary heart disease and stroke in a general population (Mattace-Raso et al. 2006). The degree of arterial stiffness is determined either locally by means of assessment of the distensibility coefficient, the relative increase in diameter for a given increase in pulse pressure, or regionally by means of carotid-femoral pulse wave velocity (Laurent et al. 2006).

The use of these non-invasive techniques in actual clinical patient management, however, is still limited due to potential patient-dependent bias and lack of reproducibility. The main limitation of distensibility coefficient measurement is caused by inaccurate pulse pressure assessment. Local pulse pressure determined by means of applanation tonometry is often underestimated in obese subjects or because of lack of stiff or bony background (Reneman et al. 2005, Van Bortel et al. 2002). As an alternative, pulse pressure is obtained from another location, often the brachial artery, resulting in overestimation of the pulse pressure in for example the carotid artery (Waddell et al. 2001) and, hence, in underestimation of the distensibility coefficient in this artery. Carotid-femoral pulse wave velocity measurements suffer from (1) inaccurate assessment of the distance between the carotid and the femoral arteries, mainly in large belly or breast sized subjects (Laurent et al. 2006, Van Bortel 2006, Van Bortel et al. 2002), (2) the trajectory being composed of both elastic and muscular arteries (McVeigh et al. 2002, Reneman et al. 2005), (3) opposing pulse wave directions (Van Bortel et al. 2002), and (4) lack of a precise and unique definition of time-reference points in pressure or flow waveforms (McVeigh et al. 2002, Millasseau et al. 2005).

Arterial stiffness is recommended for evaluation of cardiovascular risk (Laurent et al. 2006), and, therefore, an accurate and easily applicable measurement technique is required. A possible alternative measure of arterial stiffness is local pulse wave velocity. Multiple methods to measure local pulse wave velocity have been explored, including wave intensity analysis (Khir et al. 2001), the *qA*-method (Rabben et al. 2004), the gradient method (Brands et al. 1998) and the foot-to-foot method (Eriksson et al. 2002). Of special interest is local pulse wave velocity measurement by means of multiple M-line ultrasound (Hermeling et al. 2007, Meinders et al. 2001), because in these methods the distance over which the pulse wave velocity is determined is known a priori, directly related to a fixed echo-line interspacing, and therefore, this method had a good precision in a phantom set-up (coefficient of variation is 0.5%) (Hermeling et al. 2007). Although the principles behind all techniques are different, they all focus on the first part of the upstroke of the pressure or distension waveform, because this region is characterized by a rapid acceleration and is considered to be free from arterial wave reflections (Nichols and O'Rourke 2005). We and others (Hermeling et al. 2008, Rabben et al. 2004), however, observed an early reflection at about 40 ms after the start of the upstroke, interfering with systolic foot detection (Hermeling et al. 2008).

In the present study, we investigated the potential of the dicrotic notch in distension waveforms, as an alternative time-reference point to measure local pulse wave velocity by means of multiple M-line ultrasound. Measurements were performed on the left and right common carotid arteries of subjects in two age categories, a young group (mean age: 26 years) and an older group (mean age: 59 years). Pulse wave velocity estimates obtained by means of the dicrotic notch (PWV_{DN}) were compared with those obtained by means of the systolic foot (PWV_{SF}) as time-reference point in the distension waveform. Local pulse wave velocity as obtained with these methods was compared to the pulse wave velocity calculated from the distensibility coefficient (PWV_{DC}) using the Bramwell-Hill relationship (Bramwell and Hill 1922), and to relative distension (strain). Furthermore, we investigated whether the expected difference between the two age categories could be identified for each of the above mentioned pulse wave velocity methods.

6.2 Methods

Subjects and measurement protocol

Twelve young volunteers aged 26 ± 4 years (mean ± standard deviation) and fourteen older volunteers aged 59 ± 6 years were recruited and gave written informed consent prior to enrolment. The study was approved by the joint medical ethical committee of the Maastricht University and the Academic Hospital Maastricht, the Netherlands.

After 10 min of rest in supine position, three blood pressure recordings were obtained from the left brachial artery using a fully automated Omron 705CP oscillometric device (Omron Healthcare Europe B.V., Hoofddorp, the Netherlands). Subsequently, a straight arterial segment of the left common carotid artery (CCA) was identified by vascular ultrasound. Seven echo-recordings of six seconds each were obtained with the probe positioned longitudinally aligned to the artery, and repositioned after each recording. The right CCA was measured after the left CCA according to the same protocol. Another three brachial blood pressure recordings were obtained directly after the echo-recordings. A three lead ECG was recorded simultaneously to facilitate automatic signal processing.

Ultrasound data recording

A PICUS ultrasound scanner (Esaote Europe, Maastricht, the Netherlands) equipped with a 7.5 MHz linear array was used to obtain multiple M-mode recordings, composed of fourteen simultaneous recordings at a frame rate of 800 Hz (Meinders et al. 2001). The pitch between the M-lines, i.e. the distance between the echo recording positions, was 1.26 mm, thus in total a segment of 16.4 mm of the CCA was covered by the scan plane. The radio frequency ultrasound data, sampled at 33.3 MHz, were stored on hard disk for off-line analysis. The radio frequency data were linearly interpolated in time to eliminate the time skew between M-lines (Meinders et al. 2001). For each recording, the posterior and anterior media-adventitia positions were identified manually for each of the fourteen M-lines. A wall tracking algorithm (Brands et al. 1997, Hoeks et al. 1999) was used to obtain the distension waveforms. The algorithm uses a complex cross-correlation method (Brands et al. 1997) to derive the displacement of the anterior and posterior walls as function of time, the difference between both providing the distension waveform. The diameter waveform is obtained from the distension waveform by adding the initial diameter. A relatively small temporal correlation window (5 ms equivalent to 4 temporal sample points) and a large spatial correlation window (0.79 mm, corresponding to 34 sample points) were used to obtain distension waveforms with high temporal resolution and good precision. The distension waveforms were low pass filtered to reduce high frequency noise, using a first order low pass filter with a cut-off frequency of 80 Hz, subsequently applied in forward and reverse direction to cancel out filter related phase shifts. The second time derivative of the distension waveform, i.e. the acceleration waveform, was calculated using a first order high pass derivative filter with a cut-off frequency of 100 Hz, again applied in both forward and reverse direction.

Calculation of pulse wave velocity

Pulse wave velocity was measured by using either the systolic foot (PWV_{SF}) or the dicrotic notch (PWV_{DN}) in the distension waveforms as time-reference points. The systolic foot and the dicrotic notch were defined as the time-points at which the acceleration waveform reaches a maximum before and after the systolic peak of the distension waveform, respectively, see Figure 6.1. Linear regression was performed on echo line position, as determined by the pitch of the ultrasound probe, and the corresponding time-points (of either the systolic foot or the dicrotic notch) of all fourteen distension waveforms. The reciprocal of the

regression slope is a measure of local pulse wave velocity. The regression coefficient of the linear regression was determined to evaluate the quality of the pulse wave velocity estimate. The pulse wave velocity estimates were accepted for further evaluation if the regression coefficient (r^2) exceeded 0.5. Moreover, because outliers could accidentally have an $r^2 > 0.5$, a minimum of two beats for each measurement and a minimum of two measurements for each CCA were required.

Table 6.1. Subject group characteristics

	young subjects	old subjects	t-test
N	12	14	
age (years)	26 ± 4	59 ± 5	$p < 0.0001$
BMI (kg / m^2)	22 ± 2	26 ± 4	$p = 0.001$
smoking	0	1	$p = 0.37$
diabetes	1	0	$p = 0.29$
hypertension	0	4	$p = 0.05$
DBP (mmHg)	71 ± 8	88 ± 8	$p < 0.0001$
SBP (mmHg)	122 ± 9	145 ± 11	$p < 0.0001$
PP (mmHg)	51 ± 5	57 ± 6	$p = 0.008$
diameter (mm)	6.6 ± 0.5	7.1 ± 0.8	$p = 0.005$
distension (mm)	0.69 ± 0.17	0.34 ± 0.10	$p < 0.0001$

Characteristics of the two age groups. Data expressed as mean ± standard deviation. BMI, body mass index; DBP, diastolic blood pressure; SBP, systolic blood pressure; PP, pulse pressure; diameter (Adventitia-Adventitia diameter); distension, difference between systolic and diastolic adventitia-adventitia diameter.

Intra-subject variability

Analysis of intra-subject variability was performed for both PWV_{SF} and PWV_{DN}. To determine variability for all estimates, having at least two accepted pulse wave velocity estimates, the median was obtained as the measurement mean. Subject means were calculated as the average of all measurement means (2-7) for each subject and each CCA. The intra-subject, inter-registration variability of the method was defined as the standard deviation of differences between subject mean and measurement means of all subjects and all CCAs.

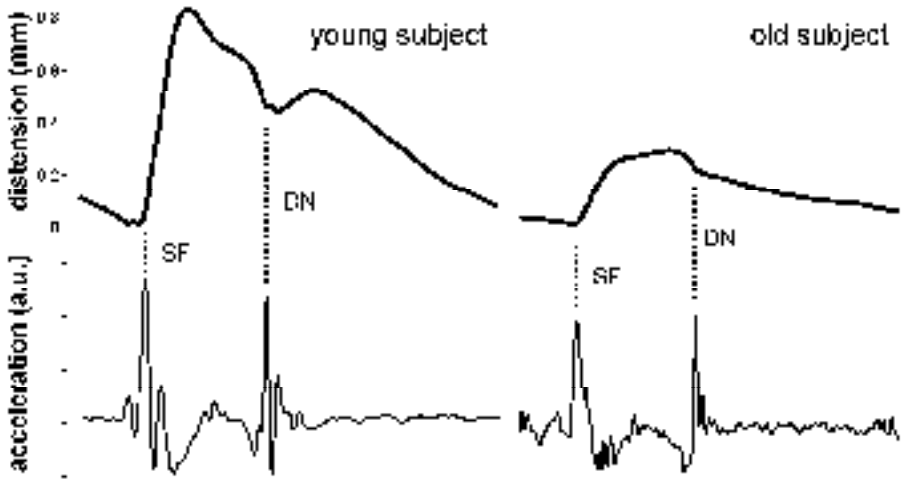

Figure 6.1 Example of a distension and corresponding acceleration waveform of a young and old subject. The systolic foot (SF) and dicrotic notch (DN) are defined as the maximum of the acceleration waveform before and after peak distension.

Analysis of accuracy

Because no gold standard for local stiffness measurement exists, the consistency of the local pulse wave velocity methods were explored by testing whether the expected difference in arterial stiffness, and hence pulse wave velocity, between the age groups could be identified. Furthermore, the local pulse wave velocity was compared to pulse wave velocity calculated from the distensibility coefficient (PWV_{DC}) using the Bramwell-Hill equation (Bramwell and Hill 1922):

$$PWV_{DC} = \sqrt{\frac{1}{\rho DC}} = \sqrt{\frac{A_d \, \Delta p}{\rho \, \Delta A}} \qquad 6.1$$

In which ρ is the density of the blood, (chosen to be 1060 kg / m^2), A_d cross sectional area in diastole, ΔA difference in cross sectional area between systole and diastole and Δp pulse pressure (in Pa). The cross sectional area was obtained from the diameter (d) waveform by assuming a rotationally symmetrical artery ($A = \pi d^2 / 4$).

Agreement between PWV_{DN} and PWV_{DC} was analyzed using scatter and Bland-Altman plots (Bland and Altman 1986). Both local pulse wave velocity methods

(PWV_{SF} and PWV_{DN}) were correlated with relative distension (Δd / d; strain) and age. Statistical differences between the age groups (or left and right CCA) were analyzed with Student's paired t-test. p-values below 0.05 were considered significant. Values are reported as mean ± standard deviation.

6.3 Results

Subjects

Table 6.1 presents the subject characteristics of the two age groups. Diastolic blood pressure, systolic blood pressure and pulse pressure were significantly higher, while CCA diastolic diameter was larger and distension, i.e. systolic peak distension, was lower in the older subjects.

After application of the acceptance criteria of local pulse wave velocity measurements 237 of the 364 measurements and 42 of 52 the CCAs were accepted for the dicrotic notch method. For the systolic foot method 270 of the 364 measurements and 43 of 52 the CCAs were accepted for further analysis.

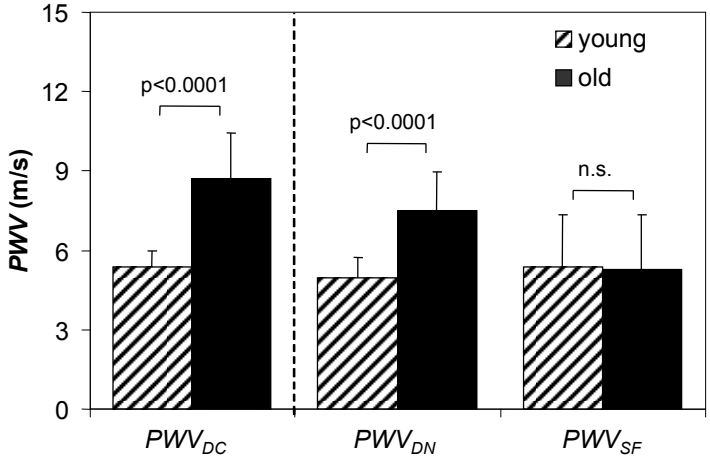

Figure 6.2 Difference in pulse wave velocity in CCA between the young and older subject group, based on distensibility coefficient (PWV_{DC}), and using the dicrotic notch (PWV_{DN}) or the systolic foot (PWV_{SF}) as time-reference point.

Intra-subject variability

The intra-subject variability of PWV_{DN} (0.6 m/s, coefficient of variation is 10 %) was better than that of PWV_{SF} (1.1 m/s, coefficient of variation is 20 %). The variability of PWV_{DN} was better in the young (0.5 m/s) than in the older subject group (0.8 m/s). The intra-subject variability of PWV_{SF} was the same for both age groups (1.1 m/s).

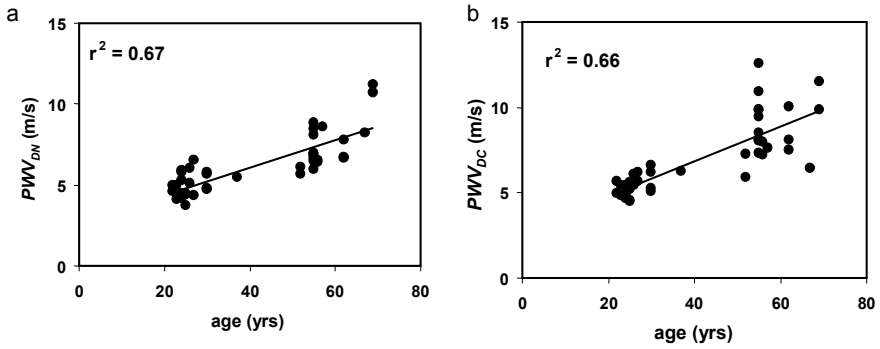

Figure 6.3 (a) Correlation between age and pulse wave velocity measured locally in the CCA, using dicrotic notch as time-reference point (PWV_{DN}). (b) Correlation between age and pulse wave velocity calculated from the distensibility coefficient (PWV_{DC}).

Accuracy

No significant difference between left and right CCA could be detected for PWV_{DN}, PWV_{SF}, PWV_{DC}, distension or diastolic diameter ($p > 0.2$, for all comparisons). Therefore, the left and right CCA measurements were pooled. Both PWV_{DN} and PWV_{DC} were significantly different between the young and old subject groups ($p < 0.0001$, Figure 6.2). PWV_{DN} was 5.0 ± 0.7 m/s in the young and 7.5 ± 1.5 m/s in the older subjects, compared to 5.4 ± 0.6 m/s and 8.7 ± 1.5 m/s for the pulse wave velocity derived from the distensibility coefficient. PWV_{SF} was similar for both age groups: 5.4 ± 1.9 versus 5.3 ± 2.0 m/s ($p = 0.4$). Figure 6.3a and b show the correlation between age and PWV_{DN} ($r^2 = 0.67$, $p < 0.0001$) and PWV_{DC} ($r^2 = 0.66$, $p < 0.0001$), respectively; the older the subject is, the higher the pulse wave velocity will be.

The agreement between PWV_{DN} and PWV_{DC} was analyzed using scatter and Bland-Altman plots (Figure 6.4). The correlation between PWV_{DN} and PWV_{DC} was significant $r^2 = 0.54$; ($p < 0.0001$). The methods showed a mean difference of 0.8 m/s with a standard deviation of the difference of 1.4 m/s. Figure 6.5

shows that PWV_{DN} correlates significantly with relative distension ($r^2 = 0.50$, $p < 0.0001$). PWV_{SF} did not correlate with PWV_{DC}, PWV_{DN}, age or relative distension (all $r^2 < 0.01$, data not shown).

6.4 Discussion

In a previous study (Hermeling et al. 2008) we have shown that local assessment of the pulse wave velocity using the systolic foot of the distension waveform as time-reference point may introduce inaccuracies, due to an early wave reflection. In the present study, we investigated whether the dicrotic notch of the distension waveform can be used as an alternative time-reference point for measuring local pulse wave velocity (PWV_{DN}). Like the systolic foot, the dicrotic notch could be easily obtained from the second derivative of the distension waveform in both age groups. It is shown that PWV_{DN} has a good intra-subject reproducibility and correlates well with age and other measures of arterial stiffness, and discriminates well between age categories. The correlation between PWV_{DN} and PWV_{DC} was less strong than the correlation of either PWV_{DN} or PWV_{DC} with age. The systolic foot is not suitable as time-reference point for local pulse wave velocity measurement as corroborated by the absence of a significant correlation of PWV_{SF} with age, PWV_{DN}, PWV_{DC} or relative distension. Moreover, PWV_{SF} could not identify differences in stiffness between young and older subjects.

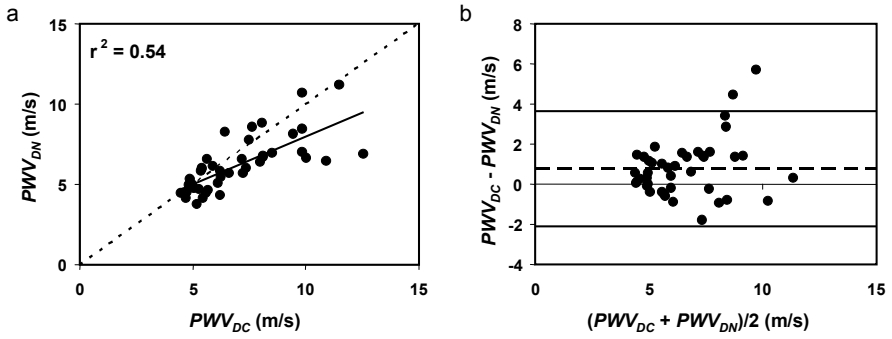

Figure 6.4 Scatter and Bland-Altman plots of PWV_{DC} (pulse wave velocity calculated from distensibility coefficient) and PWV_{DN} (pulse wave velocity measured locally in CCA using the dicrotic notch as time-reference point). The difference between the two methods is 0.8 m/s with a standard deviation of 1.4 m/s.

Comparing PWV_{DN} and PWV_{DC}

Although both PWV_{DN} and PWV_{DC} show good correlation with age, the agreement between both pulse wave velocity estimates was rather poor. A number of explanations can be given for the discrepancies between the two pulse wave velocity estimates. First, the distensibility coefficient is calculated using the change in pressure and area over the whole cardiac cycle (Equation 6.1). A non-linear pressure-area relation (Hayashi et al. 1980, Langewouters et al. 1984, Meinders and Hoeks 2004) will introduce an overestimation of the distensibility coefficient and consequently an underestimation of PWV_{DC}. Second, the adventitia-adventitia diameter is used instead of the lumen diameter in calculating the distensibility coefficient, which results in an overestimated PWV_{DC}. Third, blood pressure is measured in the brachial artery, where pulse pressure is amplified (Waddell et al. 2001), causing underestimation of the distensibility coefficient, and, hence, overestimation of PWV_{DC} in the common carotid artery. Alternatively, local pulse pressure can be obtained by extrapolation while assuming constant mean and diastolic blood pressures in the arterial tree and a linear pressure-area relation (Van Bortel et al. 2001). Preliminary analysis on our data showed that this indeed lowers the average PWV_{DC} by 1 m/s, but the correlation of this method with age and PWV_{DN} becomes worse because extrapolation algorithm introduces additional noise on the pulse pressure assessment (data not shown). Fourth, pulse pressure is calculated from the average pulse pressure of three measurements before and three measurements after ultrasound recordings; no simultaneous pressure and distension measurements were performed. Fifth, mean blood flow velocity may increase PWV_{DN} independent of arterial stiffness (Histand and Anliker 1973).

A wave reflection from the cerebral arterial tree disturbs PWV_{SF}

Reflections that occur in the arterial tree may alter the pressure and diameter waveforms. The pulse wave velocity measured at a certain time-reference point, e.g., the systolic foot or the dicrotic notch will only be influenced by reflections propagating in opposite direction. In an earlier study we have shown that in the common carotid artery of young subjects a reflected wave propagating in opposite direction arrives 40 ms after the systolic foot (Hermeling et al. 2008). This reflection affects systolic foot detection in M-lines closest to the carotid artery bifurcation most pronouncedly, resulting in underestimation of the pulse wave velocity. This phenomenon will be most pronounced in older subjects in

whom reflections arrive earlier in the cardiac cycle due to increased pulse wave velocity (Laurent et al. 2006, Schiffrin 2004).

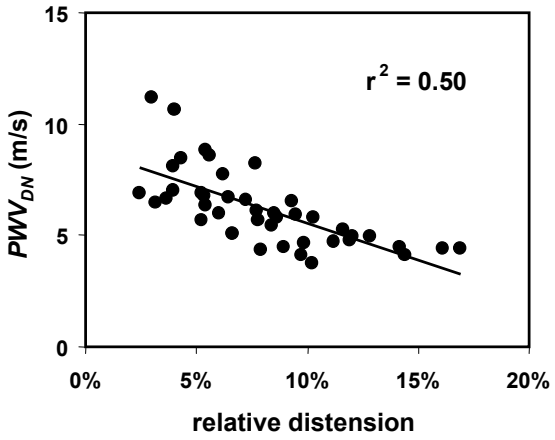

Figure 6.5 Correlation between pulse wave velocity measured locally using the dicrotic notch as time-reference point (PWV_{DN}) and relative distension (strain), i.e. distension divided by diameter.

PWV_{DN} as stiffness parameter.

It is important to understand that PWV_{DN} measured locally is different from carotid-femoral pulse wave velocity in terms of trajectory and operating pressure. First of all, carotid-femoral pulse wave velocity is measured over a long trajectory, therefore, this method provides an average measure for stiffness of the elastic and muscular arteries within this trajectory. In the present study, pulse wave velocity is measured locally in the CCA, which is an elastic artery. In principle, the PWV_{DN} method could be applied to other superficial arteries, like the femoral artery, allowing independent analysis of vessel wall stiffness of muscular and elastic segments in response to aging and disease. Second, the carotid-femoral pulse wave velocity is measured using the systolic foot at end-diastolic pressure, while PWV_{DN} is measured at the instantaneous pressure during the dicrotic notch, which is close to mean arterial pressure (Hebert et al. 1995). The pressure-area relation is in general non-linear (Hayashi et al. 1980, Langewouters et al. 1984, Meinders and Hoeks 2004), which results in a pressure dependent pulse wave velocity, exhibiting a variation of 40 % over the cardiac cycle (Langewouters et al. 1984, Meinders and Hoeks 2004). Therefore, the pulse wave velocity measured using the dicrotic notch as time-reference point differs intrinsically from that using the systolic foot as time-reference point,

which is the case in the carotid-femoral pulse wave velocity measurements. Because the carotid-femoral pulse wave velocity is measured at diastolic pressure, it may underestimate the average arterial stiffness. Therefore, PWV_{DN}, which is measured at a pressure value near mean arterial pressure (Hebert et al. 1995), may better reflect the effective arterial stiffness over the cardiac cycle, which determines the load the left ventricle is subjected to as it ejects blood.

Pulse travelling distance is dictated by ultrasound probe

In a study by Portaluppi et al., the dicrotic notch was used as time-reference point to measure the transit time over the suprasternal notch to right CCA trajectory (Portaluppi et al. 1983). The results of their study were disappointing, probably because the distance between the measurements points was unknown. In the present study, the distance between the distension waveforms is dictated by the echo-line interspacing, which is a known equipment property. Therefore, our method is devoid of uncertainties due to distance measurements.

Improvement of local pulse wave velocity measurement technique

In our study only 80 % of all CCAs and 65 % of all measurements were accepted for further analysis, mainly because real-time feedback about the quality of the distension waveforms was not available yet. When real-time feedback is incorporated, a more reliable estimate and a higher acceptance rate will be achieved. Moreover, real-time assessment of the regression coefficient, a measure of the quality of the PWV_{DN} estimate, could assist the operator in optimizing the quality of the PWV_{DN} measurements. Increasing temporal resolution may further improve the intra-subject variability of the PWV_{DN} method: the transit time over the 16.4 mm long arterial segment is just 2.2 ms (for waves travelling at 7.5 m/s), which is currently less than twice the sample time (1.3 ms). If the error made in determining the time-reference point (dicrotic notch) is independent of the location, i.e., no interference of reflections, an increase in spacing between the M-lines will further decrease the intra-subject variability of the PWV_{DN} estimate.

6.5 Conclusion

We showed that local pulse wave velocity can be measured with relatively good intra-subject reproducibility (coefficient of variation is 10 %), by means of multiple M-line ultrasound using the dicrotic notch as time-reference point. The method correlates well with age and relative distension (strain). The method discriminates differences in arterial stiffness between young and older subjects well. The proposed method circumvents two major problems of current measures of arterial stiffness, i.e. inaccurate distance measurement as occurs for the carotid-femoral pulse wave velocity, and inaccurate local pulse pressure measurement in calculating distensibility coefficients.

References

Bland JM and Altman DG. Statistical methods for assessing agreement between two methods of clinical measurement. The Lancet I: 307-310, 1986.

Bramwell J and Hill A. The velocity of the pulse wave in man. Proc Roy Soc London Ser B 93: 298-306, 1922.

Brands PJ, Hoeks APG, Ledoux LAF, and Reneman RS. A radio frequency domain complex cross-correlation model to estimate blood flow velocity and tissue motion by means of ultrasound. Ultrasound Med Biol 23: 911-920, 1997.

Brands PJ, Willigers JM, Ledoux LA, Reneman RS, and Hoeks AP. A noninvasive method to estimate pulse wave velocity in arteries locally by means of ultrasound. Ultrasound Med Biol 24: 1325-1335, 1998.

Eriksson A, Greiff E, Loupas T, Persson M, and Pesque P. Arterial pulse wave velocity with tissue Doppler imaging. Ultrasound Med Biol 28: 571-580, 2002.

Hayashi K, Handa H, Nagasawa S, Okumura A, and Moritake K. Stiffness and elastic behavior of human intracranial and extracranial arteries. J Biomechanics 13: 175-184, 1980.

Hebert JL, Lecarpentier Y, Zamani K, Coirault C, Daccache G, and Chemla D. Relation between aortic dicrotic notch pressure and mean aortic pressure in adults. Am J Cardiol 76: 301-306, 1995.

Hermeling E, Reesink KD, Reneman RS, and Hoeks AP. Measurement of local pulse wave velocity: effects of signal processing on precision. Ultrasound Med Biol 33: 774-781, 2007.

Hermeling E, Reesink KD, Reneman RS, and Hoeks APG. Confluence of incident and reflected waves interferes with systolic foot detection of the carotid artery diameter waveform. J Hypertens: in press, 2008.

Histand MB and Anliker M. Influence of flow and pressure on wave propagation in the canine aorta. Circ Res 32: 524-529, 1973.

Hoeks APG, Brands PJ, Willigers JM, and Reneman RS. Non-invasive assessment of mechanical properties of arteries in health and disease. Proc Insttn Mech Engrs 213: 195-202, 1999.

Khir AW, O'Brien A, Gibbs JS, and Parker KH. Determination of wave speed and wave separation in the arteries. J Biomech 34: 1145-1155, 2001.

Langewouters GJ, Wesseling KH, and Goedhard WJA. The static elastic properties of 45 human thoracic and 20 abdominal aortas in vitro and the parameters of a new model. J Biomech 17: 425-435, 1984.

Laurent S, Boutouyrie P, Asmar R, Gautier I, Laloux B, Guize L, Ducimetiere P, et al. Aortic stiffness is an independent predictor of all-cause and cardiovascular mortality in hypertensive patients. Hypertension 37: 1236-1241., 2001.

Laurent S, Cockcroft J, Van Bortel L, Boutouyrie P, Giannattasio C, Hayoz D, Pannier B, et al. Expert consensus document on arterial stiffness: methodological issues and clinical applications. Eur Heart J 27: 2588-2605, 2006.

Laurent S, Katsahian S, Fassot C, Tropeano AI, Gautier I, Laloux B, and Boutouyrie P. Aortic stiffness is an independent predictor of fatal stroke in essential hypertension. Stroke 34: 1203-1206, 2003.

Mattace-Raso FU, van der Cammen TJ, Hofman A, van Popele NM, Bos ML, Schalekamp MA, Asmar R, et al. Arterial stiffness and risk of coronary heart disease and stroke: the Rotterdam Study. Circulation 113: 657-663, 2006.

McEniery CM, Wilkinson IB, and Avolio AP. Age, hypertension and arterial function. Clin Exp Pharmacol Physiol 34: 665-671, 2007.

McVeigh GE, Hamilton PK, and Morgan DR. Evaluation of mechanical arterial properties: clinical, experimental and therapeutic aspects. Clin Sci (Lond) 102: 51-67, 2002.

Meinders JM and Hoeks AP. Simultaneous assessment of diameter and pressure waveforms in the carotid artery. Ultrasound Med Biol 30: 147-154, 2004.

Meinders JM, Kornet L, Brands PJ, and Hoeks AP. Assessment of local pulse wave velocity in arteries using 2D distension waveforms. Ultrason Imaging 23: 199-215, 2001.

Millasseau SC, Stewart AD, Patel SJ, Redwood SR, and Chowienczyk PJ. Evaluation of carotid-femoral pulse wave velocity: influence of timing algorithm and heart rate. Hypertension 45: 222-226, 2005.

Nichols WW and O'Rourke MF. Properties of the arterial wall: theory. In: McDonald's blood flow in arteries (5th edition ed.). London: Edward Arnold, 2005, p. 59.

Portaluppi F, Knighten V, and Luisada AA. Transmission delays of different portions of the arterial pulse. A comparison between the indirect aortic and carotid pulse tracings. Acta Cardiol 38: 49-59, 1983.

Rabben SI, Stergiopulos N, Hellevik LR, Smiseth OA, Slordahl S, Urheim S, and Angelsen B. An ultrasound-based method for determining pulse wave velocity in superficial arteries. J Biomech 37: 1615-1622, 2004.

Reneman RS, Meinders JM, and Hoeks AP. Non-invasive ultrasound in arterial wall dynamics in humans: what have we learned and what remains to be solved. Eur Heart J 26: 960-966, 2005.

Schiffrin EL. Vascular stiffening and arterial compliance: implications for systolic blood pressure. Am J Hypertens 17: 39S-48S, 2004.

Van Bortel LM. Is arterial stiffness ready for daily clinical practice? J Hypertens 24: 281-283, 2006.

Van Bortel LM, Balkestein EJ, van der Heijden-Spek JJ, Vanmolkot FH, Staessen JA, Kragten JA, Vredeveld JW, et al. Non-invasive assessment of local arterial pulse pressure: comparison of applanation tonometry and echo-tracking. J Hypertens 19: 1037-1044, 2001.

Van Bortel LM, Duprez D, Starmans-Kool MJ, Safar ME, Giannattasio C, Cockcroft J, Kaiser DR, et al. Clinical applications of arterial stiffness, Task Force III: recommendations for user procedures. Am J Hypertens 15: 445-452, 2002.

Waddell TK, Dart AM, Medley TL, Cameron JD, and Kingwell BA. Carotid pressure is a better predictor of coronary artery disease severity than brachial pressure. Hypertension 38: 927-931, 2001.

Chapter 7

Consequences of a non-linear pressure-area relationship for the assessment of arterial stiffness

Submitted as:

Evelien Hermeling, Arnold P.G. Hoeks, Mark Winkens, Johannes Waltenberger, Robert S Reneman, Abraham A Kroon, Koen D. Reesink. Proper non-invasive assessment of arterial compliance should include stiffness in the systolic pressure range.

Abstract

Arterial stiffening plays an important role in the development of hypertension and cardiovascular disease. The pressure dependency of arterial stiffness has serious consequences for the non-invasive assessment of arterial elastic properties, but has not been studied in detail among individual patients. The aim of this study was to determine the degree of non-linearity of the pressure-area curve and the consequences of this non-linearity for the assessment of arterial stiffness. We obtained intra-arterial pressure and common carotid artery diameter waveforms in patients undergoing coronary angiography. Single and dual exponential models were used to describe the measured pressure-area curve, and to obtain incremental pulse wave velocity. Additionally, sectional distensibility coefficients were obtained using the dicrotic notch as cut-off to derive sectional pulse wave velocity estimates at high and low pressure levels. We found that in one third of the patients a dual exponential model could accurately describe the pressure-area curve. The incremental pulse wave velocity at systolic, but not at diastolic pressure, exhibited a strong association with pulse pressure and age. Comparable results were obtained for sectional pulse wave velocities. These data suggest that, in these patients, arterial stiffness at diastolic pressure is only a minor predictor of the pulsatile load on the left ventricle. Therefore we conclude that the non-linearity of arterial stiffness indeed has serious consequences for the non-invasive assessment of arterial function especially in patients with isolated systolic hypertension.

7.1 Introduction

Decreased elasticity of the arterial wall plays an important role in the development of hypertension and related cardiovascular complications such as renal failure, heart failure, and stroke (Jankowski et al. 2008, Mitchell et al. 2007, Roman et al. 2007, Safar et al. 2006). Assessment of arterial stiffness has recently entered the ESH/ESC Guidelines for the management of hypertension (Mancia et al. 2007). Basic studies have shown that, especially in the elderly, the elastic behaviour of the arterial system is non-linear, i.e. arterial stiffness is pressure dependent (Armentano et al. 1991, Hayashi et al. 1980, Langewouters et al. 1984, Shadwick 1999, Sokolis 2007, Wolinsky and Glagov 1964). This intrinsic property of the arterial system may have serious consequences for quantitative assessment of arterial stiffness and possible changes therein, in response to physiological stress (Sokolis 2007) and possibly anti-hypertensive

treatment (Armentano et al. 2006, Bussy et al. 2000, Laurent et al. 1994, Tropeano et al. 2006).

Hayashi et al. found that, in *ex vivo* human cranial and femoral arteries, the relationship between transmural pressure and vessel radius can be described by a single exponential (Hayashi et al. 1980). Meta-analysis of studies on the relationship between pressure and cross-sectional vessel area by Powalowski confirmed this finding (Powalowski and Pensko 1988). However, Wolinsky and Glagov (rabbit aorta, *ex vivo*) and Armentano and colleagues (dog aorta, *in vivo*) observed a more marked change in elasticity as function of distending pressure related to the ultrastructural interaction of elastin and collagen fiber networks in the tunica media (Armentano et al. 1991, Wolinsky and Glagov 1964). Existing studies in humans, based on either non-invasive or invasive data, have utilized simplified mathematical models to describe the pressure-area relationship (Armentano et al. 2006, Laurent et al. 1994, Meinders and Hoeks 2004). To the best of our knowledge, the degree of non-linearity of arterial stiffness in relation to actual blood pressure in individual patients with cardiovascular disease has not been studied in detail.

The aim of the present study was to quantify the non-linearity of the arterial pressure-area relationship and to evaluate the consequences of non-linearity for the assessment of arterial elastic properties. Therefore, pressure-area relationships were obtained from carotid artery diameter and intra-arterial pressure recordings in patients undergoing coronary angiography. We employed single and dual exponential analytical models to describe the pressure-area relationship in each individual. From these models we derived both incremental and sectional stiffness indices, with our main focus on pulse wave velocity. Subsequently, we quantified possible errors in estimating local systolic pressure and carotid artery stiffness in terms of pulse wave velocity presuming a simple exponential relation. We will discuss our findings with regard to the associations with pulse pressure and age within our study population and the potential consequences for the applicability of non-invasive methods in future clinical use.

7.2 Methods

Study population

Patients referred for a diagnostic coronary angiographic procedure (either standard contrast angiography alone or combined with fractional flow reserve assessment) were recruited in the outpatient clinic. Patients included in the study were either suspected of coronary artery disease (anginal complaints) or had had previous percutaneous transluminal coronary angioplasty or coronary artery bypass grafting. All 21 included patients gave written informed consent prior to enrolment. The study was approved by the joint medical ethical committee of Maastricht University and Maastricht University Medical Centre, Maastricht, the Netherlands.

Protocol

Patients were prepared for the invasive diagnostic procedure following a standard protocol: overnight fast, refrainment from smoking, and prophylactic anticoagulation (Clopidogrel). Diabetes medication (Metformin), if any, was discontinued on the day of the examination; other medications were taken as usual. The age, weight, and height of the patients were copied from their clinical files.

During antiseptic preparations and application of ECG electrodes, patients were in supine position on the catheterization table, allowing localization of the left common carotid artery (CCA) by means of a 7 MHz linear array/high frame-rate ultrasound system (PICUS, Esaote Europe, Maastricht, the Netherlands). All echo recordings (see data acquisition) were obtained with the patients in this position. If the vessel was located too deep (due to dermal fat) for high frame-rate image acquisition, the patient was excluded from the study. Non-invasive blood pressure was recorded intermittently by an automatic brachial-cuff oscillometric device (I-Connect, Fysicon Medical Technology, Oss, the Netherlands).

After percutaneous access was established by the interventional cardiologist, an angiographic guiding catheter (6 Fr or 7 Fr, Wiseguide, Boston Scientific, Natick, MA) was advanced over a guide wire and placed with the tip in the ostium of the targeted coronary artery. After initial coronary angiograms were obtained, the catheter was flushed with saline to wash out radiopaque contrast fluid and the

connection to the contrast pump was blocked to achieve the highest possible bandwidth for and minimal ringing in the aortic pressure signal. Subsequently, in less than four minutes at least three and maximally five repeated echo recordings of the left CCA were obtained simultaneously with a continuous registration of aortic pressure. The recording session took less than four minutes to perform. After the last recording the angiographic procedure was continued by the intervention cardiologist.

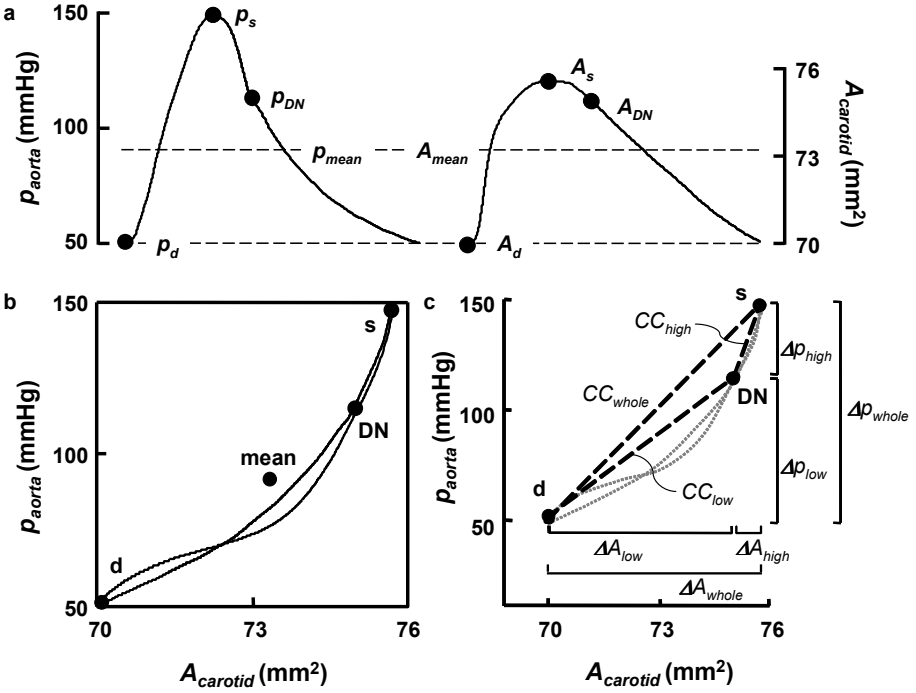

Figure 7.1 a) Illustration of measured pressure (p) and cross-sectional area (A) waveforms. The waveforms are scaled such that diastolic and mean values of pressure and area are aligned. b) Corresponding pressure-area curve from this patient shows clear non-linearity (left panel). c) The change in cross-sectional area (ΔA) and pressure (Δp) over different sections of the pressure-area curve (low, whole and high) as used to determine sectional arterial stiffness indices. d, diastolic minimum; DN, dicrotic notch level; s, systolic maximum.

Data acquisition

During the echo recordings a crude B-mode image based on fourteen M-lines was depicted on screen and an on-line echo-tracking algorithm showed real-time anterior and posterior wall displacements. The radiofrequency signal of the PICUS ultrasound scanner was fed to a dedicated PC-based acquisition system

(ART.LAB, Esaote Europe, Maastricht, the Netherlands), with a sampling frequency of 33 MHz, for off-line processing. Aortic pressure was recorded with a standard pressure transducer (Namic Custom angiographic kit, Namic, Glens Falls, NY) connected to the diagnostic catheter. The transducer was connected to a RADI pressure measurement console (RadiAnalyzer Xpress, RADI Systems, Uppsala, Sweden), whose output was connected to a cardiac-floating data acquisition system (MPAQ, IDEE Instruments, Maastricht, the Netherlands). Lead II of the patient ECG was relayed from the catheterization lab system (Fysicon I-Connect) to both the MPAQ system and the PICUS ultrasound scanner to provide a synchronous time-reference.

Signal processing

The radiofrequency data acquisition and processing have been described in detail before (Brands et al. 1997, Hoeks et al. 1990). Pulse repetition frequency for each M-line was 800 Hz (frame rate). Spatial and temporal estimation windows for wall echo-tracking were 800 μm and 5 ms, corresponding to 34 and 4 sample points, respectively. Temporal estimation windows were 3 points overlapping, resulting in an effective sample rate of 800 samples/s. We used one of the fourteen M-lines to obtain the distension waveforms. Apart from the echo-tracking, all data processing was performed in Matlab (version 7.5, The Mathworks, Natick, MA). Diameter and pressure waveforms were filtered by a zero-phase low-pass filter with a cut-off frequency of 40 Hz. The second time-derivatives of both signals were calculated over the recording length (six seconds) by passing the signals through a zero-phase second order high-pass filter (i.e. a differentiator; cut-off at 100 Hz). Signals were then segmented into separate beats with diameter and pressure beat pairs. Because misalignment in time of pressure and diameter waveforms distorts the pressure-area curve (Hoeks et al. 2000), the waveforms were aligned on the dicrotic notch, which is identified as a local maximum in the second time-derivative (Hermeling et al. 2008, Reesink et al. 2007). Diameter waveforms were converted to cross-sectional area waveforms, assuming circular cross-section: $A(t) = \pi d^2(t) / 4$, in mm^2. Subsequently, the pressure and diameter waveforms, and the pressure-area plot, were visually checked per beat for proper alignment and signal quality. All beats showing baseline shift over the beat (e.g. due to tracking problems or arrhythmias) or excessive ringing (due to pressure catheter resonance or mechanical artefact) were excluded. To further smooth the pressure-area curve, both signals were additionally filtered by a second order zero-phase low-pass filter with a cut-off frequency of 10 Hz. Both the upslope and downslope in the

pressure-area plot were resampled into 100 pressure-area pairs, with the area samples rather than the time samples equidistantly spaced. The total of 200 pressure-area pairs was used to fit two mathematical models to describe the pressure-area relationship.

Model definitions and fitting procedure

The following single-exponential (1-exponential) model (Meinders and Hoeks 2004, Powalowski and Pensko 1988) was fitted to the pressure and area data for each beat:

$$p(A) = p_d e^{\alpha\left(\frac{A}{A_d}-1\right)} \qquad 7.1$$

With: $p(A)$, pressure as a function of cross-sectional area (A); p_d, diastolic pressure; A_d, diastolic area; α, vascular stiffness index. To estimate the value for p_d and α, linear regression was applied to the logarithmic transformed pressure and relative area (A / A_d) data:

$$\ln(p) = \beta_1 \frac{A}{A_d} + \beta_0 \qquad 7.2$$

The vascular stiffness index (α) and diastolic pressure (p_d; Equation 7.1) were calculated from the regression parameters β_0, β_1 and A_d. Subsequently, an error minimization procedure (function fmincon, Matlab, MathWorks, Natick, MA, USA) was used to fit a higher order non-linear model based on two summed exponential functions (2-exponential):

$$p(A) = p_d e^{\alpha'\left(\frac{A}{A_d}-1\right)} + \varepsilon e^{\gamma\left(\frac{A}{A_{thr}}-1\right)} \qquad 7.3$$

With: $p(A)$, A, p_d, A_d, as defined above; α', stiffness index; γ, stiffness index; A_{thr}, cross-sectional area at which the 2-exponential model starts to deviate ε from the first term in Equation 7.3, with ε, threshold level, preset to 2 mmHg.

In the fitting procedure for the 2-exponential model the following constraints were forced: $\alpha' < \alpha$ and $A_{thr} < A_s$ (systolic area). To enable comparison between individual patients, given any difference in A_d, the relative A_{thr} was calculated as: 100 % ($A_{thr} - A_d$) / ($A_s - A_d$). In some patients, the 2-exponential fitting procedure

lead to values of γ and relative A_{thr} close to zero, indicating that the second component did not improve the fit, and thus the pressure-area curve could be accurately described by the 1-exponential model. In these cases the stiffness index α' was set equal to α, and γ and A_{thr} were considered to be non-existent.

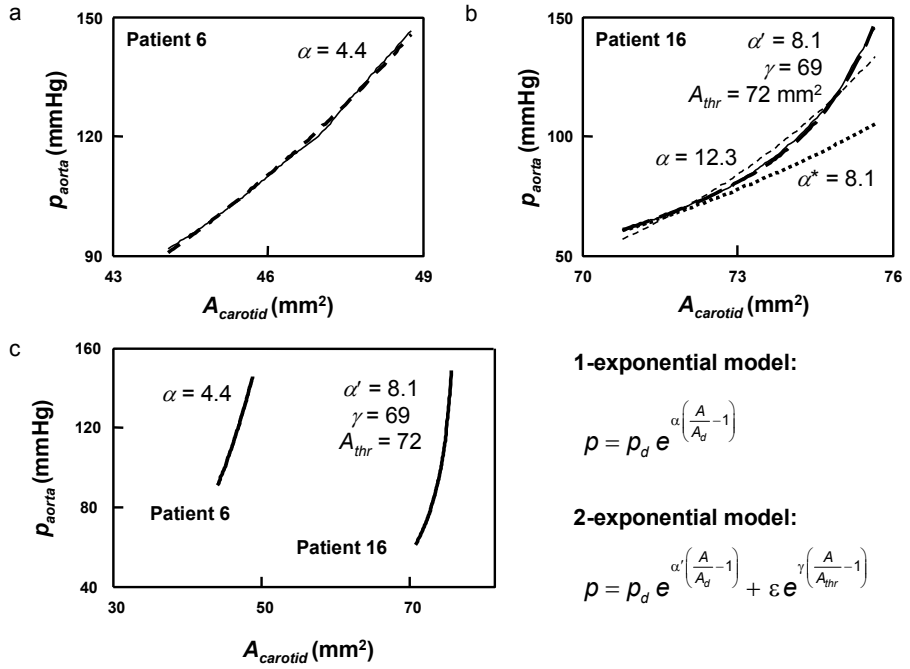

Figure 7.2. a) Example of a pressure-area relationship (thin line) that is accurately described by the 1-exponential model (thick dashed line, patient 6). b) Example of a pressure-area relation (thin line) that requires the 2-exponential model to accurately describe the curve (thick dashed line, patient 16), because the 1-exponential model poorly describes this relation (thin dashed line). The dotted line is the contribution of the first term in the 2exponential model. c) Both cases depicted in one pressure-area plane.

To analyze the quality of the fit for both exponential models, root mean square errors (RMSE) and the errors in estimated systolic blood pressure (ΔSBP) were calculated per individual.

Incremental arterial stiffness

To obtain incremental stiffness indices at the different pressure levels over the cardiac cycle, pulse wave velocity (*iPWV*) was derived from both models using the Bramwell-Hill equation (Bramwell and Hill 1922, Meinders and Hoeks 2004).

$$iPWV(A) = \sqrt{\frac{A\,\partial p}{\rho\,\partial A}} \qquad 7.4$$

From the incremental pulse wave velocity (*iPWV*) the average ($iPWV_{mean}$), maximum ($iPWV_{max}$, at systolic pressure), and minimum pulse wave velocity ($iPWV_{min}$, at diastolic pressure) were obtained (Figure 7.3a).

Sectional arterial stiffness

The dicrotic notch, signalling the closure of the aortic valve, can be detected in the second derivative of both the distension and the pressure waveform (Hermeling et al. 2008, Reesink et al. 2007). Diastolic, systolic and dicrotic notch data points enable evaluation of the pressure-area curve in a piecewise linear manner. We obtained distensibility and compliance coefficients over the whole cardiac cycle (DC_{whole}, CC_{whole}), and for the sections of the pressure-area curve below ($DC_{low,}$ CC_{low}) and above the dicrotic notch ($DC_{high,}$ CC_{high}), as indicated in Figure 7.1c:

$$DC = \frac{\Delta A}{A^{*}\,\Delta p}$$
$$CC = \frac{\Delta A}{\Delta p} \qquad 7.5$$

With: ΔA and Δp, the change in area and pressure over the section of interest (either the whole, lower or higher section), and A^{*}, the minimal cross-sectional area in that section, which is A_d for the whole and lower sections, and A_{DN} (dicrotic notch area) for the higher section. To enable direct comparison to the incremental pulse wave velocity, the Bramwell-Hill equation was used to convert sectional distensibility coefficients to sectional pulse wave velocity estimates (Bramwell and Hill 1922), indicated as *sPWV*.

Statistical analysis

For the blood pressure variables and model parameters, we determined the precision by calculating the intra-subject inter-measurement standard deviation, averaged over all patients. We divided our study population into high and low pulse pressure groups based on a cut-off value of 60 mmHg (Franklin et al. 1999) and compared them using Student's two-sample t-test. Statistical

differences in variables within the groups were tested by paired Student t-test. A p-value below 0.05 was considered statistically significant.

Table 7.1. Patient characteristics

	mean ± SD	**range**
age (years)	64 ± 12	(37 – 81)
sex (m / f)	15 / 6	
heart rate (1/min)	72 ± 20	(48 – 127)
SBP (mmHg)	145 ± 26	(98 – 194)
PP (mmHg)	69 ± 24	(25-117)
MBP (mmHg)	105 ± 16	(74 – 132)
DBP (mmHg)	76 ± 13	(52 – 101)
d_d (mm)	7.8 ± 0.9	(6.3 – 9.5)
Δd (mm)	0.4 ± 0.2	(0.1 – 1.1)
$\Delta d/d_d$ (%)	4.8 ± 3.2	(1.8 – 16.5)

Number of patients is 21. SBP, systolic blood pressure; DBP, diastolic blood pressure; MBP, mean blood pressure; d_d, diastolic carotid artery diameter; Δd, diameter change, SD standard deviation.

7.3 Results

Patient characteristics are given in Table 7.1, showing considerable inter-individual variability. Figure 7.2 shows two examples of pressure-area curves. The curve of patient 6 is approximated well by the 1-exponential function (Equation 7.1), while for patient 16 only the 2-exponential model (Equation 7.3) provided an accurate description of the pressure-area relationship (Figure 7.2).

Table 7.2 lists the blood pressures and estimated model parameters for each patient. The precision of the estimated model parameters (bottom rows, Table 7.2) was below the inter-subject variability, indicating that discrimination of individual differences and differences between (sub) groups is possible.

Eight out of 21 patients had a higher order non-linearity of the pressure-area relationship, and consequently an underestimation of systolic blood pressure (SBP) of more than 5 mmHg with the 1-exponential model. With the 2-exponential model the error in SBP estimation was below 5 mmHg for all patients (ΔSBP = 2.0 ± 1.7 mmHg) and was not significantly dependent on pulse

pressure ($r = 0.41$, $p = 0.06$), whereas for the 1-exponential model the error in estimating SBP was roughly double ($\Delta SBP = -4.0 \pm 4.6$ mmHg) and pulse pressure dependent ($r = -0.60$, $p < 0.01$). The position within the curve at which the 2-exponential model starts to deviate from a 1-exponential relation (relative A_{thr}) varied from just above the diastolic area (~10 %) to above the average area (~50-75 %). Compared to the 1-exponential model, the 2-exponential model also better described the pressure-area relation as a whole: root mean square error (RMSE) 3.2 ± 1.3 mmHg against 4.0 ± 1.7 mmHg.

An example of the change in pulse wave velocity over the cardiac cycle is displayed in Figure 7.3a. Incremental pulse wave velocity obtained from the 2-exponential model gave a better approximation of the pulse wave velocity calculated directly from the pressure and area waveforms. In contrast, the 1-exponential model showed a blunted profile.

Because the pulse wave velocity directly calculated from the pressure-area curve is rather noisy, it was not used to derive *iPWV* continuously over the cardiac cycle.

Figure 7.3b shows the associations of pulse pressure with maximum, mean and minimum pulse wave velocity derived from the 2-exponential model. $iPWV_{max}$ showed a significantly stronger correlation with pulse pressure than $iPWV_{min}$ (Figure 7.3b). A similar pattern was observed for the 1-exponential model, although $iPWV_{min}$ correlated slightly better with pulse pressure and $iPWV_{max}$ slightly worse than for the 2-exponential model (data not shown). Interestingly, sectional estimates ($sPWV_{whole}$, $sPWV_{low,}$ and $sPWV_{high}$) showed a similar pattern of higher sensitivity to pulse pressure of pulse wave velocity at higher pressure levels (Figure 7.3d).

The model-derived $iPWV_{mean}$ and the corresponding $sPWV_{whole}$ were not significantly different, but significant differences were observed between $iPWV_{min}$ and $sPWV_{low}$ ($p < 0.005$), and similarly between $iPWV_{max}$ and $sPWV_{high}$ estimates ($p < 0.05$; Figure 7.3c).

Table 7.2. Exponential model parameters per individual

pts.	DBP mmHg	PP mmHg	α	RMSE mmHg	ΔSBP mmHg	α′	γ	rel. A_{thr} %	RMSE mmHg	ΔSBP mmHg
1	58	41	5.4	1.7	-4.4	3.6	47	50	1.3	0.2
2	87	106	9.3	3.5	-2.7	7.3	38	15	3.1	4.2
3	73	26	3.1	1.9	-1.5	2.1	34	54	1.9	0.5
4	61	50	7.5	2.0	-2.0	7.5	—	—	—	—
5	75	39	5.3	2.2	-0.4	4.7	27	79	1.9	-0.3
6	82	64	3.7	5.6	4.0	3.7	—	—	—	—
7	85	66	10.6	3.7	-1.5	9.1	57	33	2.5	2.8
8	80	90	6.2	5.2	-0.7	3.2	36	33	4.2	3.6
9	83	55	4.0	5.3	-3.0	3.0	28	49	4.6	1.1
10	87	90	4.3	6.8	-6.9	2.5	20	–4	6.2	3.9
11	73	66	9.9	4.0	-6.1	6.9	59	17	3.1	-1.0
12	83	66	13.0	4.3	-7.2	7.7	91	20	2.9	3.0
13	52	74	9.3	3.7	-5.8	7.6	43	19	3.2	0.3
14	66	83	11.7	3.3	-7.4	7.2	55	16	1.8	3.2
15	86	62	4.1	4.3	-4.6	3.0	29	26	4.0	0.3
16	53	96	14.2	7.6	-15.7	8.4	62	25	4.0	1.8
17	77	117	12.0	6.2	-11.9	7.7	54	12	5.1	2.2
18	72	77	7.5	3.5	-5.9	4.9	32	16	2.5	2.6
19	101	34	3.9	2.1	4.8	3.9	—	—	—	—
20	90	75	1.7	2.8	-1.9	1.2	13	33	1.8	4.8
21	78	61	14.5	3.8	-2.7	10.7	82	21	3.8	1.9
mean	76	68	7.7	4.0	-4.0	5.9	46	29	3.2	2.0
SD	13	24	3.9	1.7	4.6	2.7	20	19	1.3	1.7
prec.	2.2	3.0	1.06	0.90	2.82	1.32	15.0	10.8	1.16	1.58

Diastolic and systolic blood pressure (DBP and SBP) and pulse pressure (PP), and parameters of the 1-exponential (α) and 2-exponential (α', γ and rel. A_{thr}) models are shown. Relative A_{thr}, position within the diastolic-to-systolic area range at which the 2-exponential model deviates from the 1-exponential curve. Quality of the fit: Root mean square error (RMSE) and systolic blood pressure error (ΔSBP). In patients 4, 6 and 19 the 2-exponential model did not improve the fit, so α' was set equal to α. The group standard deviation (SD) exceeds the intra-subject precision (bottom rows). pts: patients, prec: precision.

Pulse pressure correlated only weakly with stiffness index α of the 1-exponential ($r = 0.47$, $p = 0.05$) and no correlation was found with the α' or γ parameters of the 2-exponential model. A clear association, however, was observed between the relative A_{thr} and pulse pressure ($r = 0.74$, $p < 0.001$, data not shown)

Table 7.3. High pulse pressure is associated with reduced arterial compliance above dicrotic notch pressure level.

	PP < 60 mmHg	PP > 60 mmHg	p-value
number	6	15	-
relative A_{thr} (%)	58	20	<0.0001
ΔA_{high} (mm^2)	0.99	1.02	0.93
ΔA_{low} (mm^2)	3.27	3.57	0.75
ΔA_{low} / ΔA_{whole} (%)	74	78	0.44
Δp_{high} (mmHg)	10	30	0.002
Δp_{low} (mmHg)	30	45	0.01`
Δp_{low} / Δp_{whole} (%)	26	38	0.02
CC_{high} (mm^2/kPa)	0.82	0.27*	0.0002
CC_{low} (mm^2/kPa)	0.87	0.64	0.26
CC_{high} / CC_{whole} (%)	48	31	0.002

PP, pulse pressure. Relative A_{thr}, position within the diastolic-to-systolic area range at which the 2-exponential model deviates from the 1-exponential curve. ΔA_{high}, change in area from dicrotic notch to systolic maximum. ΔA_{low}, change in area from diastolic minimum to dicrotic notch; Δp_{high} and Δp_{low}, respective changes in pressure. CC_{high} and CC_{low}, linearly approximated compliance coefficients. *$p < 0.0001$, CC_{high} compared to CC_{low} in the high pulse pressure group.

Differences in sectional pressure- and area-changes, and compliance between low and high pulse pressure groups are given in Table 7.3. The relative increase in area over the lower section (ΔA_{low} / ΔA_{whole}) was not different between the two groups. Δp_{low} was higher in the high pulse pressure group ($p = 0.01$), but the main contribution to elevated pulse pressure is reflected by Δp_{high} (30 mmHg in the high versus 10 mmHg in the low pulse pressure group, $p = 0.002$), and is likely to be attributable to the three-fold lower CC_{high}: 0.27 versus 0.82 mm^2/kPa, respectively ($p = 0.0004$). Interestingly, within the high pulse pressure group sectional compliance coefficients were significantly different (CC_{high} is about CC_{low} / 3, $p < 0.0001$), but not so in the patients with a pulse pressure < 60 mmHg ($p = 0.8$). Lower section compliance was not different between the groups (0.87 and 0.64 mm^2/kPa, $p = 0.26$). The relative position of

the threshold (relative A_{thr}) for the 2-exponential model was closer to the diastolic area in patients with high compared to those with low pulse pressure (20 % versus 58 %, $p < 0.0001$).

In our study population, model-derived *iPWV* was significantly associated with age (Figure 7.4). The average increase per year of $iPWV_{min}$ was 0.08 m/s ($r = 0.51$, $p = 0.03$) while $iPWV_{max}$ increased 0.28 m/s per year ($r = 0.71$, $p < 0.001$).

7.4 Discussion

Our findings show that carotid artery stiffness is significantly non-linear among patients with present cardiovascular disease. Therefore, the pressure-area curve can be described best by the 2-exponential model rather than the 1-exponential model. Pulse wave velocity at systolic blood pressure levels ($iPWV_{max}$) exhibits a much stronger association with the actual pulse pressure and age than pulse wave velocity at diastolic pressures. Lastly, the sectional stiffness estimates ($sPWV_{high}$ and $sPWV_{low}$), as obtained by segmentation of the pressure-area curve, show a comparable pattern as the incremental *PWV* estimates, suggesting that DC_{high} or $sPWV_{high}$ are better and more selective indices of arterial stiffness than those based on diastolic properties.

Pressure dependence of arterial stiffness

Our findings show that the non-linear elastic properties of the arterial system have consequences for the quantitative assessment of arterial stiffness. To illustrate this, let us consider patients 5 and 18 who exhibit comparable diastolic pressures (~75 mmHg) and $iPWV_{min}$ (~7 m/s), but different pulse pressures (39 versus 77 mmHg) and $iPWV_{max}$ (9.5 versus 15.6 m/s). Indeed, in our whole study population the difference in $iPWV_{min}$ between patients with high and low pulse pressure is modest as compared to the differences observed in $iPWV_{max}$ (Figure 7.3b). Currently, aortic pulse wave velocity (carotid-femoral pulse wave velocity) is considered the gold standard for measuring arterial stiffness as it correlates well with other cardiovascular risk factors and mortality (Laurent et al. 2001, Laurent et al. 2003, Mattace-Raso et al. 2006). This method is based on the foot-to-foot technique and hence measures arterial stiffness at diastolic blood pressure levels. Consequently, in this approach it is not possible to discriminate between patients who do have a comparable diastolic but a different systolic

arterial stiffness. Therefore, as we showed previously the dicrotic notch should be used as time-reference point to measure local pulse wave velocity (Hermeling et al. 2008), which is closely related to $iPWV_{max}$ and $sPWV_{high}$ in the present study. This approach seems promising since local pulse wave velocity derived at the dicrotic notch level has a stronger association with pulse pressure and age than local pulse wave velocity measured at the diastolic level (Hermeling et al. 2008).

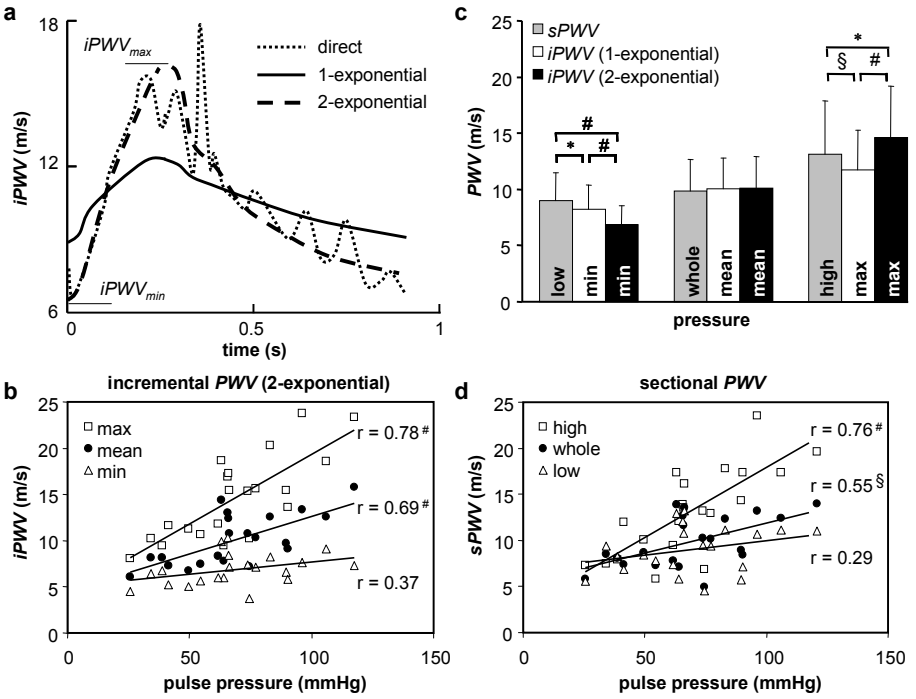

Figure 7.3. a) Change over the cardiac cycle in carotid artery incremental pulse wave velocity (*iPWV*), calculated from measured and modeled pressure-area curves. Maximum and minimum *iPWV* are indicated for 2-exponential fit. b) Associations with pulse pressure of maximal, mean and minimal incremental pulse wave velocity (from 2-exponential modeled curve). c) Comparison of the incremental and sectional pulse wave velocity estimates. d) Associations of pulse wave velocity based on the sectional distensibility coefficients (*sPWV*) with pulse pressure. # $p < 0.001$, * $p < 0.005$, § $p < 0.05$.

Clinical epidemiological relevance

In our patients, $iPWV_{min}$ is significantly associated with age (0.08 m/s per year), which corresponds well with previously reported increase rates of aortic pulse wave velocity (Khoshdel et al. 2006, Paini et al. 2006). Interestingly, the

correlation of *iPWV* measured at higher pressure values is stronger with age (0.28 m/s per year, r = 0.71, Figure 7.4) and pulse pressure (r = 0.78, Figure 7.3b). The correlation of pulse pressure and $iPWV_{min}$ is not significant, suggesting that diastolic stiffness, compared to $iPWV_{max}$ (systolic stiffness) is a minor predictor of the pulsatile load on the left ventricle. Systolic stiffness might be a more suitable candidate to quantify effective arterial stiffness, especially in patients with isolated systolic hypertension when diastolic blood pressure is normal or even decreased. This observation is of clinical/epidemiological importance, but to make the approach applicable in patients the assessment of the pressure-area curve should ideally be entirely non-invasive. However, the non-invasive measurement of central (pulse) pressure is still problematic (Reneman et al. 2005), limiting accurate assessment of stiffness as a function of pressure.

Impact of non-linearity on non-invasive assessment of stiffness

Recently, in a large population it was shown that the 1-exponential model improves pulse pressure estimation, as compared to a linear model (Vermeersch et al. 2008). The method used in that study provides a non-invasive estimate of the vascular stiffness index (α) based on brachial diastolic and mean blood pressure (Meinders and Hoeks 2004). Our data show that the 1-exponential model may substantially underestimate the non-linearity of the pressure-area relationship in patients with elevated pulse pressure. Due to the presumed validity of a single exponential pressure-area relationship, arterial stiffness may be underestimated, especially if the vascular stiffness index (α) is obtained from diastolic and mean blood pressures (Meinders and Hoeks 2004, Vermeersch et al. 2008).

An alternative to quantify non-invasively arterial stiffness of superficial arteries at a blood pressure level other than diastolic may be the combined use of applanation tonometry and ultrasound diameter waveforms. Qualitative assessment of the degree of non-linearity present in the pressure-area curve may be possible by quantifying sectional compliances, based on diastolic, systolic and dicrotic notch levels in the diameter and (uncalibrated) tonometry waveforms. Such an approach might be less sensitive to tonometry transduction and cushioning artefacts and calibration, while it utilizes relative rather than absolute pressure differences.

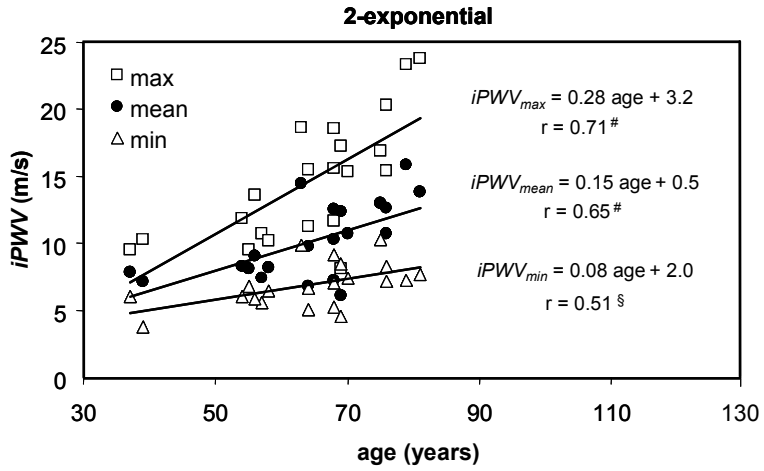

Figure 7.4. Association with age of maximum, mean and minimum incremental pulse wave velocity obtained from the 2-exponential modeled curve. # $p < 0.001$, § $p < 0.05$.

Ultrastructural basis of observed non-linearity

The arterial wall is composed of a complex network of elastin and collagen fibers (Armentano et al. 1991, Sokolis 2007, Wolinsky and Glagov 1964), surrounding the smooth muscle cells in the media which modulate the stiffness of the ultrastructure. The pressure dependent bearing of mechanical forces exhibits a gradual transition from elastin at lower pressures towards collagen at higher pressures with low and high stiffness, respectively, as has been demonstrated in *ex vivo* and *in vivo* experiments (Armentano et al. 1991, Wolinsky and Glagov 1964). With the employed 2-exponential model we were able to describe properly the pressure-area relation at both lower (α') and higher (γ) pressure levels within the actual diastolic-to-systolic pressure range (Table 7.2). In contrast to Armentano et al. (Armentano et al. 1991), we are hesitant to directly link α', or γ to fiber content because it implies direct (quantitative) extrapolation towards fiber elastic moduli, which disregards the dynamic orientation of the ultrastructure under varying stress (Wolinsky and Glagov 1964). Nonetheless, our mathematical description of the pressure-area relationship does enable quantitative analysis of non-linear arterial stiffness in relation to hemodynamic load on the left ventricle and of the effect of blood pressure lowering treatment (Westerhof and O'Rourke 1995).

The relative position within the curve at which the pressure-area relationship starts to deviate from a 1-exponential function varied considerably among

individuals (inter-subject standard deviation of A_{thr} is 19 % at a mean of 29 %, Table 7.2) and was significantly correlated with pulse pressure. This suggests that arterial wall fiber content, composition and ultrastructure do play a role in the creation of elevated pulse pressure and systolic hypertension. The transition from diastolic stiffness to systolic stiffness occurs at lower values in patients with a pulse pressure in excess of 60 mmHg (relative A_{thr} 20% versus 58 % for PP < 60 mmHg; Table 7.3). This may be indicative of either a different working range on the pressure-area curve or a more advanced remodelling process within the arterial wall in patients with relatively elevated pulse pressure.

Relevance to cardiovascular interaction

Our data allow discrimination of the contribution of sectional compliance to pulse pressure between the low and high pulse pressure group (Table 7.3). Both groups exhibit a similar compliance for pressures below the dicrotic notch (CC_{low}), but above this pressure level the compliance (CC_{high}) is significantly lower in the high pulse pressure group. This indicates that in the latter group volume storage capacity is impaired at higher pressure. To be able to extrapolate this observation to the ascending aorta, it is of interest to note that Studinger et al. observed similar overall distensibility in the carotid artery and aorta in humans (Studinger et al. 2000). This prompts the conclusion that the left ventricle delivers the last 25 % of its stroke volume against a less compliant load in the high pulse pressure group. Consequently, the fraction of the pulse pressure generated by the last 25 % of the stroke volume is increased in the high versus the low pulse pressure group (38 % versus 26 %, p = 0.02). In other words, the pressure-dependence of arterial stiffness in these patients may actually contribute to elevated pulse pressure, and hence, to increased cardiac afterload.

Study limitations

In the present study, pressure and diameter waveforms were not obtained from the same location, which may potentially distort the pressure-area curve. Because we aligned the pressure and diameter waveforms (on the dicrotic notch) and manually checked misalignment for each beat, we are confident that these distortions of the pressure-area curve had a negligible effect on our results.

We studied pressure-area relationships in patients undergoing coronary angiography. Furthermore, some of these patients may have experienced considerable psychological stress that can affect central hemodynamics. Therefore, our findings cannot be extrapolated directly to the normal population.

7.5 Conclusion

Our findings indicate that more than one-third of the patients with manifest cardiovascular disease exhibit a non-linear carotid artery pressure-area relationship of a higher order than the currently accepted simple exponential. The pressure-dependence of arterial stiffness in these patients may actually contribute to an elevated pulse pressure. This has serious consequences for the non-invasive quantification of arterial stiffness in individual patients, and stresses the need for new, high-resolution methods.

Acknowledgements

The authors thank Mr. Erik Brands for testing and certifying electrical safety of the equipment set-up. Thanks to Mr. Bert Hoenjet and all cathlab personnel for their full cooperation. Thanks to Dr. Mark Winkens for introducing the researchers to intervention cardiology practice.

References

Armentano RL, Barra JG, Santana DB, Pessana FM, Graf S, Craiem D, Brandani LM, et al. Smart damping modulation of carotid wall energetics in human hypertension: effects of angiotensin-converting enzyme inhibition. Hypertension 47: 384-390, 2006.

Armentano RL, Levenson J, Barra JG, Fischer EI, Breitbart GJ, Pichel RH, and Simon A. Assessment of elastin and collagen contribution to aortic elasticity in conscious dogs. Am J Physiol 260: H1870-1877, 1991.

Bramwell J and Hill A. The velocity of the pulse wave in man. Proc Roy Soc London Ser B 93: 298-306, 1922.

Brands PJ, Hoeks APG, Ledoux LAF, and Reneman RS. A radio frequency domain complex cross-correlation model to estimate blood flow velocity and tissue motion by means of ultrasound. Ultrasound Med Biol 23: 911-920, 1997.

Bussy C, Boutouyrie P, Lacolley P, Challande P, and Laurent S. Intrinsic stiffness of the carotid arterial wall material in essential hypertensives. Hypertension 35: 1049-1054, 2000.

Franklin SS, Khan SA, Wong ND, Larson MG, and Levy D. Is pulse pressure useful in predicting risk for coronary heart Disease? The Framingham heart study. Circulation 100: 354-360, 1999.

Hayashi K, Handa H, Nagasawa S, Okumura A, and Moritake K. Stiffness and elastic behavior of human intracranial and extracranial arteries. J Biomechanics 13: 175-184, 1980.

Hermeling E, Reesink KD, Reneman RS, and Hoeks AP. Local pulse wave velocity as alternative to reliably measure carotid artery stiffness in humans. Submitted, 2008.

Hoeks AP, Brands PJ, Smeets FA, and Reneman RS. Assessment of the distensibility of superficial arteries. Ultrasound Med Biol 16: 121-128, 1990.

Hoeks AP, Willigers JM, and Reneman RS. Effects of assessment and processing techniques on the shape of arterial pressure-distension loops. J Vasc Res 37: 494-500, 2000.

Jankowski P, Kawecka-Jaszcz K, Czarnecka D, Brzozowska-Kiszka M, Styczkiewicz K, Loster M, Kloch-Badelek M, et al. Pulsatile but not steady component of blood pressure predicts cardiovascular events in coronary patients. Hypertension 51: 848-855, 2008.

Khoshdel AR, Thakkinstian A, Carney SL, and Attia J. Estimation of an age-specific reference interval for pulse wave velocity: a meta-analysis. J Hypertens 24: 1231-1237, 2006.

Langewouters GJ, Wesseling KH, and Goedhard WJA. The static elastic properties of 45 human thoracic and 20 abdominal aortas in vitro and the parameters of a new model. J Biomech 17: 425-435, 1984.

Laurent S, Boutouyrie P, Asmar R, Gautier I, Laloux B, Guize L, Ducimetiere P, et al. Aortic stiffness is an independent predictor of all-cause and cardiovascular mortality in hypertensive patients. Hypertension 37: 1236-1241., 2001.

Laurent S, Caviezel B, Beck L, Girerd X, Billaud E, Boutouyrie P, Hoeks A, et al. Carotid artery distensibility and distending pressure in hypertensive humans. Hypertension 23: 878-883, 1994.

Laurent S, Katsahian S, Fassot C, Tropeano AI, Gautier I, Laloux B, and Boutouyrie P. Aortic stiffness is an independent predictor of fatal stroke in essential hypertension. Stroke 34: 1203-1206, 2003.

Mancia G, De Backer G, Dominiczak A, Cifkova R, Fagard R, Germano G, Grassi G, et al. 2007 Guidelines for the Management of Arterial Hypertension: The Task Force for the Management of Arterial Hypertension of the European Society of Hypertension (ESH) and of the European Society of Cardiology (ESC). J Hypertens 25: 1105-1187, 2007.

Mattace-Raso FU, van der Cammen TJ, Hofman A, van Popele NM, Bos ML, Schalekamp MA, Asmar R, et al. Arterial stiffness and risk of coronary heart disease and stroke: the Rotterdam Study. Circulation 113: 657-663, 2006.

Meinders JM and Hoeks AP. Simultaneous assessment of diameter and pressure waveforms in the carotid artery. Ultrasound Med Biol 30: 147-154, 2004.

Mitchell GF, Guo CY, Benjamin EJ, Larson MG, Keyes MJ, Vita JA, Vasan RS, et al. Cross-sectional correlates of increased aortic stiffness in the community: the Framingham Heart Study. Circulation 115: 2628-2636, 2007.

Paini A, Boutouyrie P, Calvet D, Tropeano AI, Laloux B, and Laurent S. Carotid and aortic stiffness: determinants of discrepancies. Hypertension 47: 371-376, 2006.

Powalowski T and Pensko B. A noninvasive ultrasonic method for the elasticity evaluation of the carotid arteries and its application in the diagnosis of the cerebro-vascular system. Arch Acoustics 13: 109-126, 1988.

Reesink KD, Hermeling E, Hoeberigs MC, Reneman RS, and Hoeks AP. Carotid artery pulse wave time characteristics to quantify ventriculoarterial responses to orthostatic challenge. J Appl Physiol 102: 2128-2134, 2007.

Reneman RS, Meinders JM, and Hoeks AP. Non-invasive ultrasound in arterial wall dynamics in humans: what have we learned and what remains to be solved. Eur Heart J 26: 960-966, 2005.

Roman MJ, Devereux RB, Kizer JR, Lee ET, Galloway JM, Ali T, Umans JG, et al. Central pressure more strongly relates to vascular disease and outcome than does brachial pressure: the Strong Heart Study. Hypertension 50: 197-203, 2007.

Safar ME, Thomas F, Blacher J, Nzietchueng R, Bureau JM, Pannier B, and Benetos A. Metabolic syndrome and age-related progression of aortic stiffness. J Am Coll Cardiol 47: 72-75, 2006.

Shadwick RE. Mechanical design in arteries. J Exp Biol 202: 3305-3313, 1999.

Sokolis DP. Passive mechanical properties and structure of the aorta: segmental analysis. Acta Physiol (Oxf) 190: 277-289, 2007.

Studinger P, Lenard Z, Reneman R, and Kollai M. Measurement of aortic arch distension wave with the echo-track technique. Ultrasound Med Biol 26: 1285-1291, 2000.

Tropeano AI, Boutouyrie P, Pannier B, Joannides R, Balkestein E, Katsahian S, Laloux B, et al. Brachial pressure-independent reduction in carotid stiffness after long-term angiotensin-converting enzyme inhibition in diabetic hypertensives. Hypertension 48: 80-86, 2006.

Vermeersch SJ, Rietzschel ER, De Buyzere ML, De Bacquer D, De Backer G, Van Bortel LM, Gillebert TC, et al. Determining carotid artery pressure from scaled diameter waveforms: comparison and validation of calibration techniques in 2026 subjects. Physiol Meas 29: 1267-1280, 2008.

Westerhof N and O'Rourke MF. Haemodynamic basis for the development of left ventricular failure in systolic hypertension and for its logical therapy. J Hypertens 13: 943-952, 1995.

Wolinsky H and Glagov S. Structural Basis for the Static Mechanical Properties of the Aortic Media. Circ Res 14: 400-413, 1964.

Chapter 8

General Discussion

8.1 Introduction

In this thesis we provided a short overview of different parameters to characterize the mechanical properties of the arterial wall and their interrelationship (Chapter 2). We developed a new technique to determine arterial wall stiffness based on locally measured pulse wave velocity by means of multiple M-line ultrasound and tested this method in a phantom set-up (Chapter 3). Pulse wave velocity was determined from the transit time of the arterial distension waveform over a fixed arterial segment of 16.4 mm. Furthermore, we investigated the reliability of different time-reference points in the distension waveform, i.e., the systolic foot, an inflection point in the systolic upstroke and the dicrotic notch, in assessing of local pulse wave velocity, *in vivo* (Chapter 4 and 6). The influence of reflected waves on pulse wave velocity measurements were studied in Chapter 4. In Chapter 5 we discuss an article that describes a technique to obtain aortic pulse wave velocity, using an inflection point in the pressure waveform (Qasem and Avolio 2008). In the last part we studied the pressure dependency of pulse wave velocity in subjects undergoing coronary angiography (Chapter 7). In the next sections a short overview of the technical and physiological aspects of the pulse wave velocity measurements is given. Moreover we will give an integrated interpretation of the work described in the previous Chapters. We will analyze whether local pulse wave velocity can be used to determine intrinsic arterial stiffness and local pulse pressure. An attempt is made to quantify the effect of reflected wave interference in identifying both the systolic foot and the dicrotic notch time-reference points used in the measurement of local pulse wave velocity. At the end of this chapter, the dicrotic notch is used as time-reference point in the assessment of carotid-femoral pulse wave velocity.

8.2 Technical aspects influencing the pulse wave velocity estimate

Throughout the studies, multiple M-mode ultrasound is used to obtain local pulse wave velocity. A multiple M-mode provides a crude B-mode picture containing fourteen M-lines spaced over 16.4 mm. The low number of lines boosts the maximal frame-rate of the system from about 30 Hz in normal B-mode to 800 Hz in multiple M-mode. Pulse wave velocity in arteries is typically 5 to 10 m/s.

Consequently, the transit time over the 16.4 mm segment will be 1.5 to 3 ms, which is about 1 to 2 times the temporal resolution of the ultrasound system. For each M-line the diameter waveform is obtained using a wall track algorithm, based on a complex cross-correlation method with a relatively large spatial window and a small temporal window.

Linear regression is performed on the time-reference points and their corresponding positions in each diameter waveform, the reciprocal of the regression slope being a measure for the pulse wave velocity. In Chapter 3, we showed in a phantom set-up that local pulse wave velocity can be obtained with good precision (coefficient of variation is 0.5 %) and accuracy (relative error is 3 %), where a 1 % error converts to a time precision of 0.03 ms for a pulse wave velocity of 5 m/s.

Temporal resolution

We also showed in the phantom set-up that the method is sensitive to the characteristics of the filter applied to the distension waveforms. If small wave perturbations in the distension waveform are not filtered out, because the cut-off frequency of the low pass filter is too high, the precision of the pulse wave velocity estimate degrades strongly (coefficient of variation went up from 0.5 % to 10.5 %). These small wave perturbations could be induced by arterial wave reflections. In Chapter 4 it is shown that the systolic foot, a time-reference point for pulse wave velocity assessment, is followed by an inflection point indicative of the onset of a superimposed reflection wave. Lowering the cut-off frequency of the low pass filter will increase the effect of reflected waves on the incident waves and the accuracy of the pulse wave velocity estimate will deteriorate (see Table 8.1). For *in vivo* measurements, the cut-off frequency of the low-pass filter needs to be at least 60 Hz to reduce this smearing effect on reflections.

Spatial resolution

To reduce the effect of changes in speckle pattern in the ultrasound signal, a large spatial window (0.8 mm) is used in the wall tracking algorithm. Assuming a constant wall volume, wall thickness will decrease inversely to an increase in diameter. Consequently, a large spatial window will cover wall parts exhibiting gradually decreasing displacements (Chapter 2), resulting in a lower distension estimate. Since in multiple M-line system this phenomenon will occur for all lines

similarly, it will probably hardly affect the precision and accuracy of pulse wave velocity estimates.

Distance dictated by the ultrasound probe

A major advantage of the proposed local pulse wave velocity measurement is that it does not require distance measurements, as the propagation distance is determined by the spacing between the piezo-electrical elements of the ultrasound probe. In Chapter 3, it was shown that the residual of the pulse wave velocity estimate shows a peculiarly regular pattern, likely caused by not exactly aligned piezo-electrical elements. Misalignment of the piezo-electrical elements causes a slight variation in ultrasound beam alignment and, hence, a bias in the pulse wave velocity estimate. Although this bias increases with increasing pulse wave velocity, the error (bias divided by true pulse wave velocity) is independent of the pulse wave velocity, but will be larger for arteries located further away from the ultrasound probe.

Table 8.1. The general effects of changes in data acquisition and processing parameters on precision and accuracy of pulse wave velocity estimate.

variable	precision	accuracy
⬇ low pass cut-off frequency	⬆	⬇
⬆ spatial window (WTS)	⬘	=
⬆ active array size	⬘	=
⬇ distance interspacing	⬆	⬇

The increase (⬆) or decrease (⬇) of a system parameter leads to an increased (⬆), decreased (⬇) or unchanged (=) precision and accuracy of the pulse wave velocity. Precision is a measure for the degree of repeatability and accuracy is the difference between the true value and its measured value. WTS, wall track system.

Active array of ultrasound probe

In the multiple M-mode used throughout this study less than half of the ultrasound probe is used: active array of 16.4 mm of a total of 40 mm. Increasing the active array range will increase the wave transit time and, hence, the pulse wave velocity estimate will become less sensitive to random noise. However, for a larger array size, some M-lines will be closer to a reflection site and will encounter greater interference of reflections (Chapter 4), biasing the pulse wave velocity estimate.

Number of M-lines

By reducing the interspacing between the M-lines, a larger number of M-lines is obtained without increasing the active array size. The originally selected distance between the M-lines in multiple M-mode matches the focal width of the ultrasound beam. A decrease of the interspacing, however, makes the M-lines dependent on each other. Consequently, decreased interspacing will have only minor effects on the precision of the pulse wave velocity estimate.

Online feedback

The quality of the pulse wave velocity estimate, i.e. its standard error, is indicated by the regression coefficient. Although non-random noise, like reflective interference, might decrease the quality of the pulse wave velocity estimate, it does not necessarily deteriorate the regression coefficient. The ultrasound system used in this study does neither provide real-time feedback about the distension waveforms or its derivatives nor standard error readings. Online presentation of the distension waveform may reveal possible reflective interference, while online display of the regression coefficient may assist the operator in optimizing the quality of the pulse wave velocity estimate.

8.3 Physiological aspects influencing the pulse wave velocity estimate

Pulse wave velocity, the speed at which the pressure wave propagates through the arterial system, is a measure of arterial stiffness. The stiffness of an arterial wall depends among other factors on the type of artery (elastic or muscular) and the pressure working range.

Pulse wave velocity in stiff arteries

The quality of the pulse wave velocity estimate may be sensitive to the degree of arterial stiffness itself. Increased arterial stiffness is associated with decreased distension and, therefore, noise on the distension waveform will be more pronounced, affecting the accuracy of identifying time-reference points in the distension waveform. Moreover, higher pulse wave velocities are associated with lower transit times, and the influence of random noise on transit time

measurements is more dominant. In addition, increased pulse wave velocity makes reflections to arrive earlier in the cardiac cycle and consequently may increase the interference of reflected waves.

Wave reflections in the arterial system

In Chapter 4 it is shown, that an inflection point in the upstroke of the carotid artery distension waveform is propagating backwards and consequently signals a reflected wave. It is possible to calculate the distance from the measurement site to the reflection site, by using the locally measured pulse wave velocity and the round trip time, i.e. the time difference between the incident wave, signalled by the systolic foot, and the reflected wave, signalled by the inflection point. In this way the distance to the reflected site was estimated to be at about 13 cm distal to the measurement site in the common carotid artery (see Chapter 4). The reverse process, i.e. to use of the round trip time to calculate the pulse wave velocity as proposed by (Qasem and Avolio 2008), however, is not possible for several reasons (Chapter 5). Firstly, there are many reflection sites in the arterial tree (O'Rourke and Taylor 1967). Secondly, due to arterial tapering continuous wave reflection can be observed (Segers and Verdonck 2000). Even in case of a single reflection site, inter-individual differences in time appearance of the inflection point in the distension waveform have to be appreciated, due to variations in anatomy and/or artery wall properties. The latter was confirmed experimentally by Westerhof et al., demonstrating that a fixed reflection site is elusive (Westerhof et al. 2008).

Frequency dependency of wave velocity

The acceleration waveform, from which the pulse wave velocity is obtained using either the systolic foot or the dicrotic notch as time-reference point (Chapter 6), has a dominant frequency of about 30 Hz (Chapter 4). The phase velocity is a frequency dependent variable (Li et al. 1981) and, hence, the observed pulse wave velocity corresponds to the phase velocity at about 30 Hz. The phase velocity at higher frequencies (> 5 Hz) is very close to the Moens-Korteweg wave speed in an artery with a purely elastic wall with in-viscid fluid (Chapter 2).

Alternative measures of arterial stiffness

Local elastic properties of a blood vessel are usually derived from a locally measured diameter waveform and blood pressure values obtained from another artery, e.g. the radial or brachial artery. Blood pressure is a major predictor of cardiovascular outcome (Franklin 2004, Laurent et al. 2006), but central blood pressure may differ substantially from peripheral blood pressure in shape and in value. Towards the periphery pulse pressure is amplified, because of tapering (Belardinelli and Cavalcanti 1992), wave reflections and progressive increasing arterial stiffness, due to an increase of smooth muscle content in the artery wall (Nichols 2005). Arterial stiffness, as well as reflection site and amplitude, may change due to aging and disease (Mitchell et al. 2004, Nichols 2005, Westerhof et al. 2008). Pulse pressure amplification decreases in older subjects or patients with cardiovascular disease (Waddell et al. 2001), and brachial pulse pressure better matches central pulse pressure. As a consequence of these disease and age related differences the pulse pressure obtained from the brachial artery has less prediction of central blood pressure and, hence, of cardiovascular risk (Jankowski et al. 2008, Roman et al. 2007, Waddell et al. 2001)

8.4 Isobaric stiffness and local pulse pressure obtained from local pulse wave velocity

In Chapter 6, we showed that local pulse wave velocity allows determination of local elastic properties without requiring any local (pulse) pressure measurement. The locally measured pulse wave velocity is associated with aging and other measures of arterial stiffness, like distensibility, and is a pressure dependent parameter (Chapter 7). For vascular risk assessment and treatment of vascular disorders, it is important to make a distinction between wall material-related (intrinsic) and pressure-related (effective) arterial stiffness (Chapter 7).

Estimation of isobaric stiffness index

Intrinsic arterial stiffness can be estimated from locally measured pulse wave velocity by assuming an exponential pressure-area relation:

$$p(A) = p_d e^{\alpha\left(\frac{A}{A_d}-1\right)} \qquad 8.1$$

with $p(A)$, arterial pressure as a function of cross-sectional area (A); p_d, diastolic pressure; A_d, diastolic area. The vascular stiffness index, α, is a pressure-independent parameter (Hayashi et al. 1980, Meinders and Hoeks 2004, Powalowski and Pensko 1988) and can be derived from local pulse wave velocity and one pressure recording (diastolic blood pressure), using the Bramwell-Hill equation (Bramwell and Hill 1922).

$$PWV = \sqrt{\frac{1}{\rho D}} \qquad 8.2$$

with PWV, pulse wave velocity, ρ the density of the blood (assumed to be 1060 kg/m^3) and D, the incremental distensibility, which is defined by:

$$D = \frac{\partial A}{A \partial p} \qquad 8.3$$

Assuming an exponential pressure-area relation (Equation 8.1), the derivative of the pressure is:

$$\frac{\partial p}{\partial A} = \frac{\alpha p_d}{A_d} e^{\alpha\left(\frac{A}{A_d}-1\right)} \qquad 8.4$$

Combining Equation 8.2, 8.3 and 8.4 results in:

$$PWV = \sqrt{\frac{A \partial p}{\rho \partial A}} = \sqrt{\frac{A}{A_d}\frac{\alpha p_d}{\rho} e^{\alpha\left(\frac{A}{A_d}-1\right)}} \qquad 8.5$$

If a pulse wave velocity is obtained in diastole ($A = A_d$), like PWV_{SF} (pulse wave velocity obtained using the systolic foot as time-reference point, see Chapters 4 and 6), this equation reduces to:

$$PWV_{SF} = \sqrt{\frac{\alpha p_d}{\rho}} \qquad 8.6$$

$$\alpha = \frac{\rho PWV_{SF}^2}{p_d} \qquad 8.7$$

The poor quality of PWV_{SF} (Chapter 6) prompted a switch to estimating the pulse wave velocity at the dicrotic notch (PWV_{DN}). Unfortunately at this time-reference point the instantaneous pressure (non-invasively determined) is unknown:

$$PWV_{DN} = \sqrt{\frac{A_{DN}}{A_d}\frac{\alpha p_{DN}}{\rho}} = \sqrt{\frac{A_{DN}}{A_d}\frac{\alpha p_d}{\rho} e^{\alpha\left(\frac{A_{DN}}{A_d}-1\right)}} \qquad 8.8$$

$$\alpha e^{\alpha\left(\frac{A_{DN}}{Ad}-1\right)} = \frac{\rho PWV_{DN}^2}{p_d}\frac{A_{DN}}{A_d} \qquad 8.9$$

With A_{DN}, the cross-sectional area at the dicrotic notch, p_{DN}, instantaneous pressure at the dicrotic notch. This Equation 8.9 can be solved using the Lambert-W function in, for example, MATLAB. The intrinsic stiffness index obtained, using PWV_{DN} shows good agreement with the stiffness index obtained iteratively with the *MAP* method as proposed by Meinders et al. ((Meinders and Hoeks 2004), Chapter 2). The *MAP* method assumes a constant *MAP* along the arterial tree, calculated as diastolic blood pressure plus 0.4 times pulse pressure (Bos et al. 2007, Chemla et al. 2005). Using data from Chapter 6, the observed difference between the stiffness indices is 0.6 ± 0.9 (Figure 8.1) with a correlation $r^2 = 0.74$.

Local pulse pressure estimation

Central pulse pressure is a better predictor of cardiovascular risk than peripheral pulse pressure (Jankowski et al. 2008, Roman et al. 2007, Waddell et al. 2001), but is difficult to obtain accurately and non-invasively (Reneman et al. 2005). As an alternative to the use of peripheral pulse pressure it is possible to estimate local (central) pulse pressure from the stiffness index, using the vascular stiffness index calculated using either the *MAP* or PWV_{DN} method in Equation 8.1, substituting of $A = A_s$ and subtracting the diastolic blood pressure. The pulse pressure obtained from the PWV_{DN} *method* does not correlate well and shows considerable bias with either brachial pulse pressure or pulse pressure obtained with the *MAP* method (Figure 8.2), although both models are

based on an exponential pressure-area relationship established for a large population (Vermeersch et al. 2008).

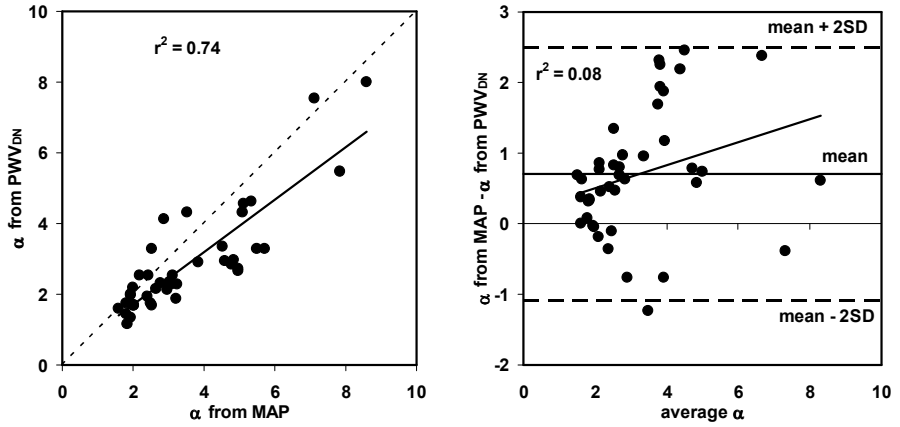

Figure 8.1. Scatter (a) and Bland-Altman (b) plots of the stiffness indices (α) based on either the *MAP* method or the PWV_{DN} method.

In Chapter 7 we demonstrated that the pressure-area relation may exhibit higher order non-linearity. The effect of a slight deviation from the exponential relationship on pulse pressure estimation based on the PWV_{DN} method is easily demonstrated by considering three theoretical pressure-area relations (Figure 8.3a). All three pressure-area relations have the same systolic and diastolic blood pressures *SBP* / *DBP* = 120 / 78 mmHg, hence the assumed pulse pressure is 42 mmHg. The first pressure-area curve is exponential (Hayashi et al. 1980, Meinders and Hoeks 2004, Powalowski and Pensko 1988, Vermeersch et al. 2008), the second has a linear relation (Sugawara et al. 2000), while the third has a 2-exponential relation (Chapter 7). The latter two deviate only slightly from the exponential model (root mean square error < 1.5 mmHg).

From Figure 8.3b it is evident that even a small deviation from the exponential model leads to a relatively large error for the systolic pulse wave velocity of 0.8 m/s (14 %) and -0.6 m/s (-10 %) for the 2-exponential and linear model, respectively. Subsequently, the PWV_{DN} observed at A_{DN} = 34 mm^2 for the linear and 2-exponential models is substituted in the exponential model, using Equation 8.9 to estimate the stiffness index (α). The calculated pulse pressure (Equation 8.1) deviates from the expected 42 mmHg +4.4 mmHg (11 %) and -4.7 mmHg (-11 %) for the 2-exponential and linear model, respectively (Figure 8.3). This illustration shows that the pulse pressure obtained from the PWV_{DN}

method might deviate substantially from the true pulse pressure if the actual pressure-area relation is not exactly exponential.

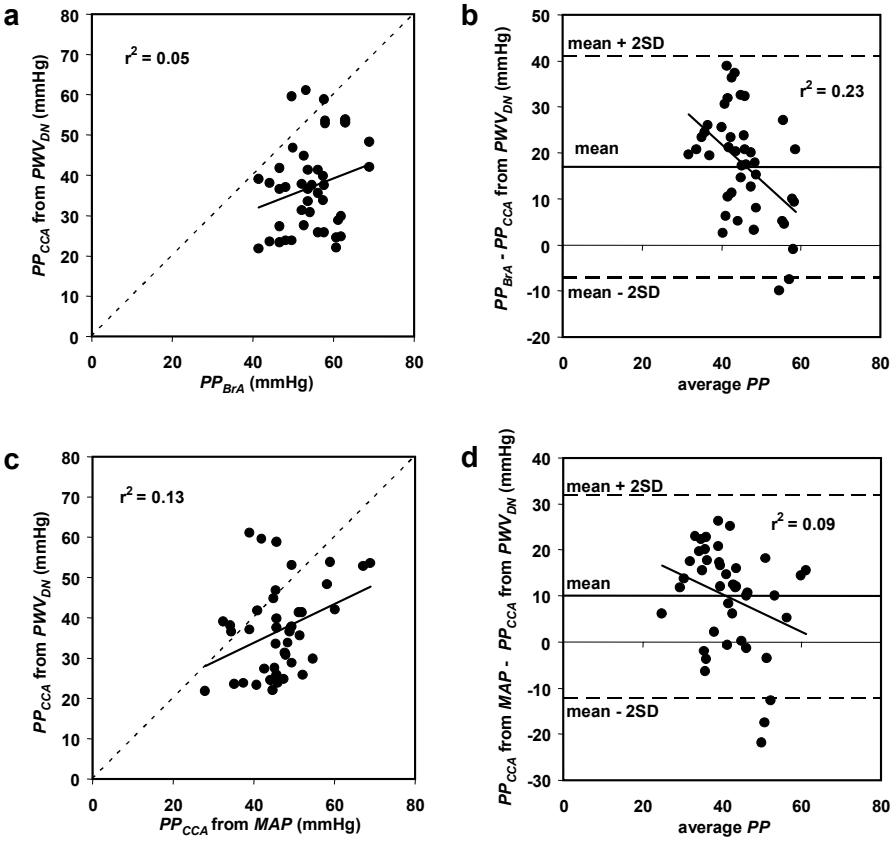

Figure 8.2. Scatter and Bland-Altman plots of the pulse pressure in the common carotid artery (CCA) obtained from the PWV_{DN} and pulse pressure measured in the brachial artery (BrA) (a and b) or calculated from the *MAP* method (c and d).

Another disadvantage of the PWV_{DN} method to estimate pulse pressure is that the method is rather sensitive to noise because the square of the pulse wave velocity is used (see Equation 8.7 and 8.9): any relative error in the pulse wave velocity estimate will appear twice as large in the estimates of stiffness index and pulse pressure.

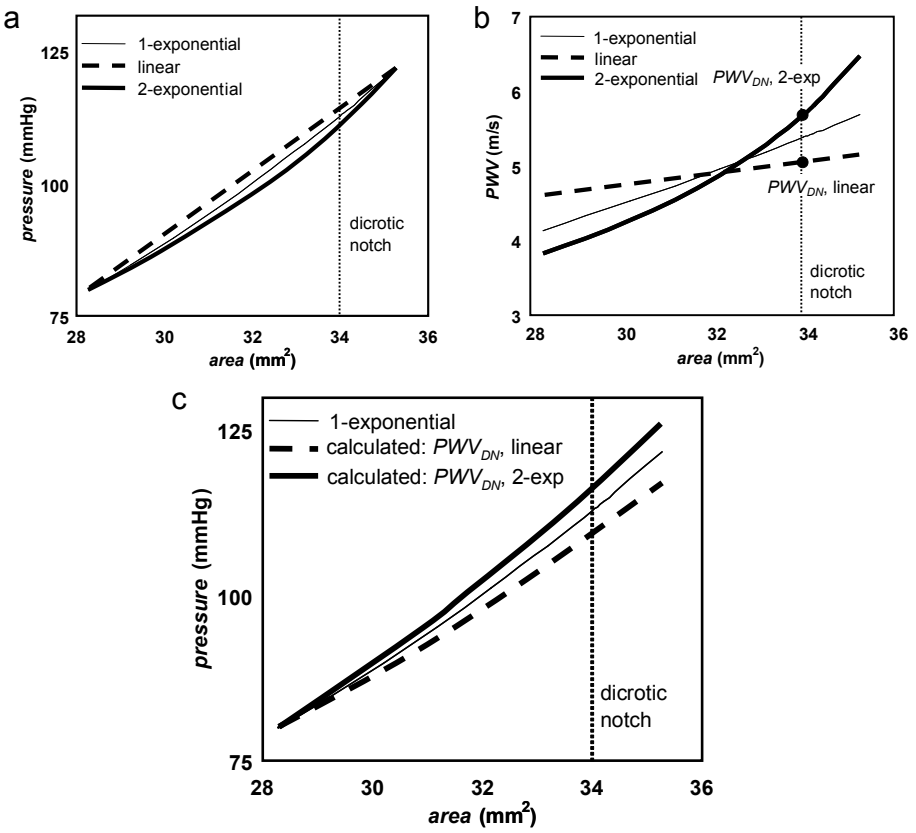

Figure 8.3. a) Illustration of different pressure-area curves, with a single exponential (thin black line), linear (gray line) and dual exponential (thick black line) pressure-area relation. b) Differences in pressure-area relation lead to differences in pulse wave velocity, despite equal systolic and diastolic blood pressure. c) The pressure-area relation obtained from PWV_{DN} for the linear or dual exponential model.

8.5 Impact of reflected waves on identification of the dicrotic notch

In Chapter 4 (Hermeling et al. 2008b) it is shown that the systolic foot is affected by reflections, rendering this wave segment less suitable to derive a time-reference point for local pulse wave velocity measurements (Hermeling et al. 2008a). In Chapter 6 it is shown that the dicrotic notch is a viable alternative time-reference point and that PWV_{DN} is associated with other measures of arterial stiffness and with aging. In the previous paragraph 8.3 we described also

a relatively good association between the stiffness indices obtained from PWV_{DN} and with those obtained using the method proposed by Meinders and Hoeks 2004 (Meinders and Hoeks 2004). However, the local pulse pressure estimated from the exponential model and PWV_{DN} exhibit a large variation (Figure 8.2). Like PWV_{SF}, PWV_{DN} might be sensitive to reflective interference, because the dicrotic notch is also followed by an inflection point (IP_{DN}), as illustrated in Figure 8.4, which propagates in opposite direction (Figure 8.5)

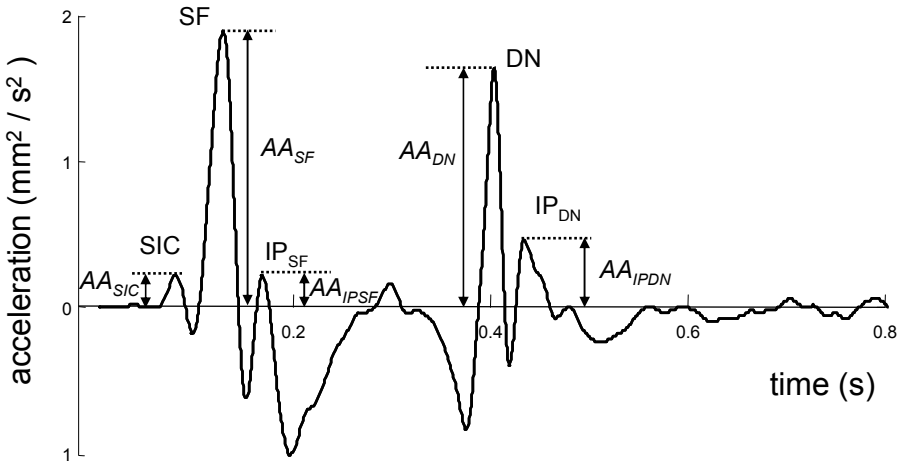

Figure 8.4. An example of an acceleration waveform, i.e., the second derivative of the distension waveform. Both the systolic foot (SF) and the dicrotic notch (DN) are followed by an inflection point (IP_{SF} and IP_{DN}). The amplitudes (*AA*) of these characteristic time-points are obtained from the acceleration waveform. Just before SF a small hump is noticeable (SIC), which signals the start of the isovolumic contraction phase of the left ventricle.

To demonstrate dicrotic notch reflective interference the data from Chapter 4 is reanalyzed. The systolic foot and dicrotic notch are defined as the maximum of the acceleration waveform before and after systolic peak distension, respectively. The inflection points of the systolic foot and dicrotic notch are defined as the local maximum of the acceleration waveforms trailing the systolic foot and the dicrotic notch, respectively (Figure 8.4). Table 8.2 shows the comparison of transit time, calculated as the time delay between the first and last M-line, of the incident waves, signalled by either the systolic foot (TT_{SF}) or the dicrotic notch (TT_{DN}) and reflected waves inflection points of either the systolic foot (TT_{IPSF}) or the dicrotic notch (TT_{IPDN}). The transit times of the incident waves (TT_{SF} = 3.2 ms and TT_{DN} = 3.1 ms,) are comparable, whereas the transit time of the reflected wave of the systolic foot (TT_{IPSF} = -3.5 ms) is higher than that of the dicrotic notch (TT_{IPDN} = -1.8 ms, p = 0.002). The time to reflection (ΔT_{SF_IP},

ΔT_{DN_IP}), defined as the time delay between the incident waves either the systolic foot or the dicrotic notch and their corresponding inflection points in the first M-line, is significantly higher for the systolic foot (ΔT_{SF_IP} = 44 ms) than for the dicrotic notch (ΔT_{DN_IP} = 34 ms, $p < 0.00001$). This can be explained by the higher blood pressure, and associated increased pulse wave velocity, at the dicrotic notch.

Table 8.2. Difference in transit time and acceleration waveform amplitude between the systolic foot and the dicrotic notch and their corresponding inflection points.

		Systolic foot	Dicrotic notch	P-value
transit time (ms)	incident	3.2 ±1.0	3.1 ± 0.8	0.80
	reflected	-3.5 ± 2.6	-1.8 ± 2.2	0.002
acceleration amplitude (mm^2/s^2)	incident	2.2 ± 0.5	1.8 ± 0.5	0.0002
	reflected	0.7 ± 0.5	0.6 ± 0.3	0.63
time to reflection (ms)		44 ± 8	34 ± 8	<0.00001
acceleration amplitude ratio (-)		0.28 ± 0.17	0.37 ± 0.10	0.01

Difference in transit time, the time difference between the first and last M-line, and amplitude of the acceleration waveform the systolic foot and the dicrotic notch (as incident wave) and their corresponding inflection points (reflected wave) expressed as mean ± standard deviation. Differences in time to reflection, i.e. time delay between incident and reflected wave. The acceleration amplitude ratios, i.e. the acceleration amplitude of the incident divided by the reflected wave, are also shown.

The acceleration waveform amplitudes (*AA*) at the time-reference points (AA_{SF}, AA_{DN}, AA_{IPSF} and AA_{IPDN}, Figure 8.4) are significantly different for the incident (AA_{SF} = 2.2 mm^2/s^2 and A_{DN} = 1.8 mm^2/s^2, p = 0.0002), but not for the reflected wave (AA_{IPSF} = 0.7 mm^2/s^2, and AA_{IPDN} = 0.6 mm^2/s^2, p = 0.6). Hence, the acceleration amplitude ratio, i.e. the acceleration amplitude of the reflected wave (either AA_{IPSF} or AA_{IPDN}) divided by the acceleration amplitude of the incident wave (AA_{SF} or AA_{DN}, respectively), is significantly higher for the dicrotic notch (0.37, p = 0.01) compared to the systolic foot (0.28). This might be explained by a pressure dependent reflection coefficient, i.e. the impedance mismatch causing the reflection to be higher for higher pressure levels augmenting the amplitude of the reflected wave (and that of the acceleration waveform).

Alternatively the frequency content of the systolic foot and the dicrotic notch may differ and the frequency dependent attenuation causes the difference in acceleration amplitude ratio between the systolic foot and the dicrotic notch.

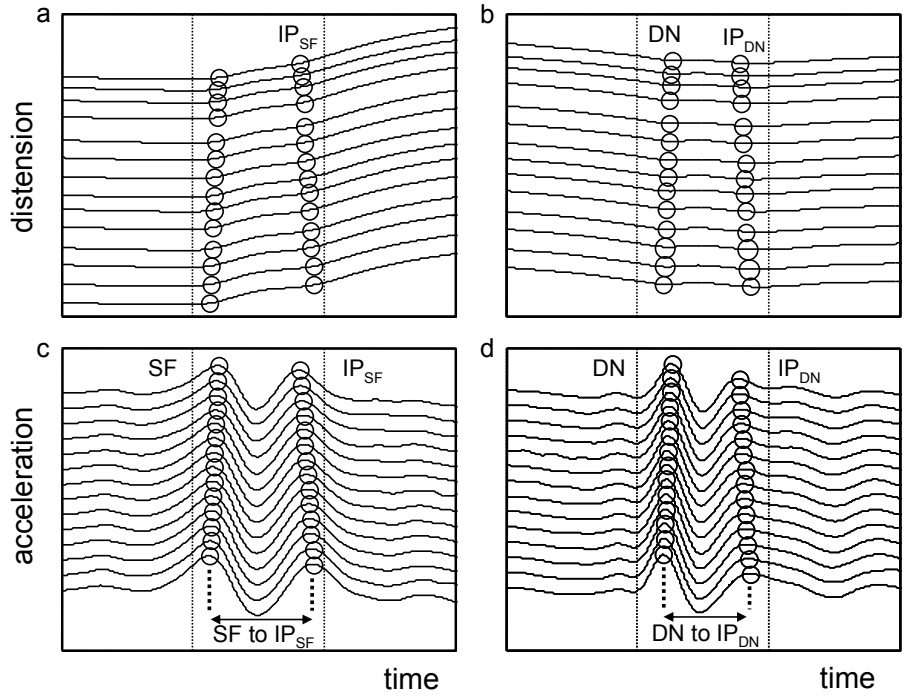

Figure 8.5. a) Fourteen simultaneously recorded distension waveforms, displayed with an offset (bottom trace proximal registration) focused on the foot of the wave. The circles indicate the characteristic time-points of either systolic foot (SF) or the inflection point associated with the systolic foot (IP_{SF}). b) Same as in a) but here for the dicrotic notch. The circles indicate the dicrotic notch (DN) and the corresponding inflection point (IP_{DN}). c) The acceleration waveform of (a) and d) the acceleration waveforms of b). Times to reflection are indicated by the arrows of SF to IP_{SF} and DN to IP_{DN}.

In both cases the interference of reflected waves on dicrotic notch detection will probably be higher than on systolic foot detection. An alternative explanation for the difference in acceleration amplitude ratio is that other waves contribute selectively to the amplitude of either the systolic foot, the dicrotic notch or their corresponding inflection points, e.g. the wave referred to as start of isovolumic contraction (Figure 8.4) prior to the systolic foot (Reesink et al. 2007, van Houwelingen et al. 2007). This point is probably associated with coronary artery compression caused by the contraction of the left ventricle (Davies et al. 2006). It is possible that the start of the isovolumic contraction wave enhances the

acceleration amplitude of the systolic foot, causing the observed difference in amplitude ratio between the systolic foot and the dicrotic notch.

From the above analysis it cannot be concluded that the influence of reflections on systolic foot detection is larger than that on dicrotic notch detection. The question therefore remains why PWV_{SF} in contrast to PWV_{DN} did not correlate with aging nor other measures for arterial stiffness.

8.6 Why is the dicrotic notch a better time-reference point than the systolic foot?

Lack of difference in diastolic pressure or diastolic arterial stiffness?

In Chapter 7, it is shown that pulse wave velocity at diastolic pressure is less associated with age than pulse wave velocity measured at either mean or systolic pressure. The difference between arterial stiffness of both age categories (Chapter 6) might, therefore, be less pronounced for PWV_{SF}, which is measured at diastolic pressure. However, the two age categories as discussed in Chapter 6 exhibit quite a significant difference in diastolic blood pressure: 74 ± 8 mmHg in the young and 90 ± 9 mmHg ($p < 0.0001$) in the older subjects. The range of diastolic pressures is relatively large (60-111 mmHg), but this is not associated with PWV_{SF} ($r^2 = 0.001$, see Figure 8.6). PWV_{DN} is measured at the instantaneous pressure at the dicrotic notch, which can be estimated by assuming an exponential relation (Equation 8.1), using the stiffness index obtained with the PWV_{DN} method (paragraph 8.3), and the cross-sectional area at the dicrotic notch. A significant difference in instantaneous pressure at the dicrotic notch is observed between the young (96 ± 9 mmHg) and older subjects (123 ± 11 mmHg, $p < 0.0001$). The instantaneous dicrotic notch pressure (78-141 mmHg) has a wider distribution than diastolic pressure, and does significantly correlate with PWV_{DN} ($r^2 = 0.42$, $p < 0.001$, Figure 8.6).

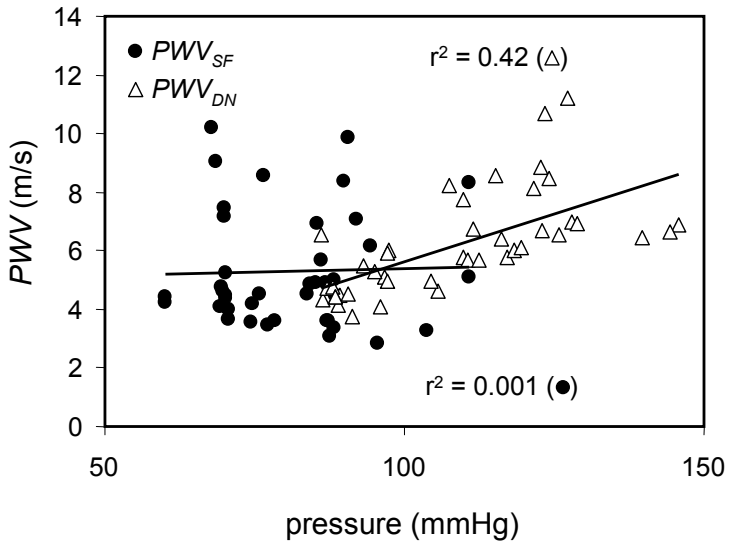

Figure 8.6. The relation between instantaneous pressure at the systolic foot (black dots) and the dicrotic notch (white triangles) and the pulse wave velocity obtained using the systolic foot and dicrotic notch, respectively.

To further demonstrate the pressure effect, we calculated the pulse wave velocity at diastolic pressure (PWV_d) from PWV_{DN} by assuming an exponential model, according to:

$$PWV_d^2 = PWV_{DN}^2 \frac{p_d}{p_{DN}} \frac{A_d}{A_{DN}} \qquad 8.10$$

with p_d, p_{DN} blood pressure in diastole and at the dicrotic notch, respectively and A_d, A_{DN} the cross-sectional area at diastole and at the dicrotic notch, respectively. The pulse wave velocity at diastolic pressure extrapolated from PWV_{DN} was significantly different for both age categories ($p < 0.0001$, Figure 8.7). Hence the lack of differentiation between the age categories by PWV_{SF} cannot be explained by the small difference in blood pressure or arterial stiffness in diastole.

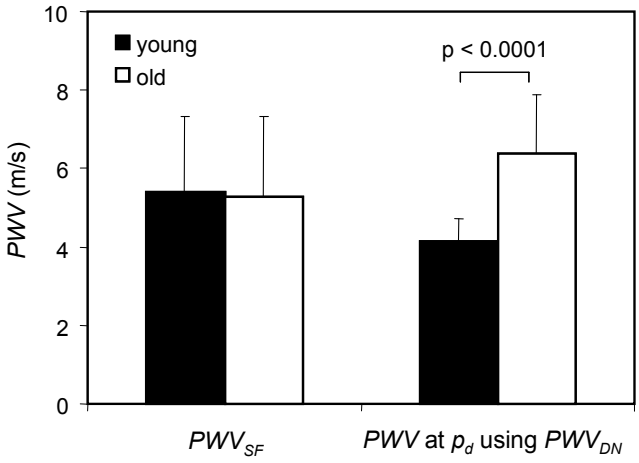

Figure 8.7 the pulse wave velocity obtained using the SF as time-reference point (PWV_{SF}) and pulse wave velocity obtained using DN as time-reference point (PWV_{DN}) corrected for diastolic pressure (P_d).

Interference of an other reflected wave on PWV_{SF}

An alternative explanation may be that another wave is interfering with the systolic foot detection. In the previous section (8.4) the start of the isovolumic contraction is suggested as an additional noise source for the systolic foot detection. To explore this, we obtained the amplitude and transit time of the wave signalling the start of the isovolumic contraction for the young subjects described in Chapter 4. The start of the isovolumic contraction is defined as the local maximum in the acceleration waveform prior to the systolic foot (Figure 8.4). The transit time between the last and first M-line (TT_{SIC} = 3.3 ± 1.1 ms) is comparable to the transit time of the systolic foot and the dicrotic notch, confirming that the start of the isovolumic contraction wave is indeed propagating in the same direction (forward) as the dicrotic notch and the systolic foot. In a segment without branches or tapering only backward propagating waves may differentially affect the first and the last M-line distension waveforms and interfere with pulse wave velocity estimation (Chapter 4), but the acceleration waveform does not show a backward propagating wave prior to the systolic foot. Both the systolic foot and the point signalling the start of the isovolumic contraction travel at diastolic pressure with probably a similar time to reflection (44 ms). Since the time delay between start of the isovolumic contraction and the systolic foot is 39 ± 6 ms, the reflected wave of the start of the isovolumic

contraction wave will probably arrive at about the systolic foot, but will be largely obscured by the wave of the systolic foot. The acceleration amplitude of the start of the isovolumic contraction wave (Figure 8.4) is associated with PWV_{SF} (Figure 8.8), corroborating that the start of the isovolumic contraction wave reflections may indeed influence the systolic foot pulse wave velocity estimate. No association was found between the amplitude of start of the isovolumic contraction and PWV_{DN}.

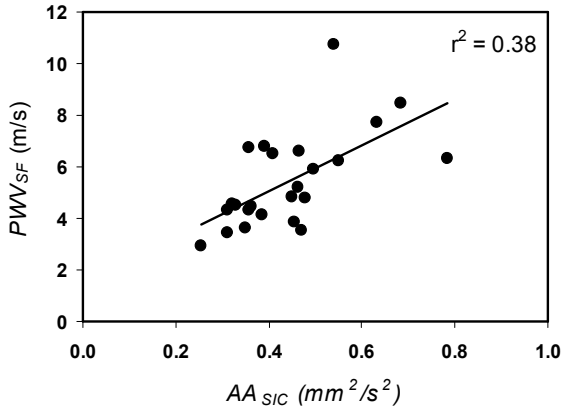

Figure 8.8. Relation between the amplitude of the acceleration waveform at the start of isovolumic contraction (AA_{SIC}) and pulse wave velocity obtained using the systolic foot as time-reference point (PWV_{SF}).

Conclusion

The poor association of PWV_{SF} with age cannot be explained by the lack of difference in diastolic pressure or arterial stiffness. In addition to the trailing systolic foot reflection, the start of the isovolumic contraction wave reflection might interfere with the detection of systolic foot and deteriorate PWV_{SF}.

8.7 Carotid-femoral pulse wave velocity based on the dicrotic notch

In Chapter 6, we described a method to determine local pulse wave velocity based on the dicrotic notch of distension waveforms obtained by multiple M-mode ultrasound. The benefit of this method is that it determines arterial stiffness

at the dicrotic notch blood pressure level which corresponds to the effective average arterial stiffness in the cardiac cycle the left ventricle is exposed to (Chapter 7). On the other hand, the proposed method requires a very high precision of the measurements (see paragraph 8.1). Alternatively, carotid-femoral pulse wave velocity can be used, having the benefit of a long trajectory (approximately 0.75 m), and hence will put less demand on the precision of the transit time measurements. This method based on the systolic foot as time-reference point (*cfPWV$_{SF}$*) is an independent predictor of cardiovascular disease and mortality (Laurent et al. 2001, Laurent et al. 2003, Mattace-Raso et al. 2006).

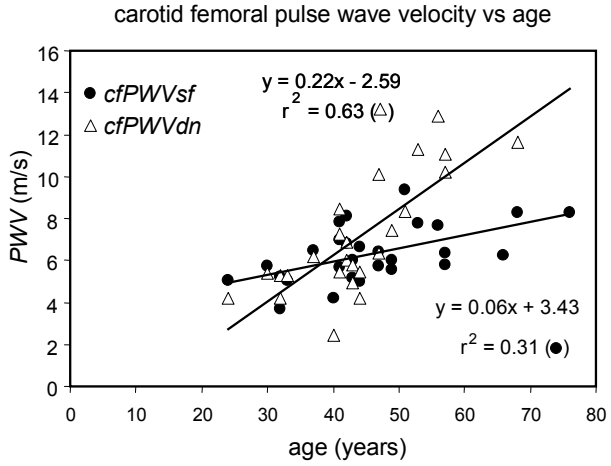

Figure 8.9. Relation between carotid-femoral pulse wave velocity obtained using systolic foot (*cfPWV$_{SF}$* dots) or dicrotic notch (*cfPWV$_{DN}$*, triangles) and age.

In a data-set obtained from 28 presumed healthy (12 male) volunteers, aged 24-76 yrs, the carotid-femoral pulse wave velocity based on the dicrotic notch (*cfPWV$_{DN}$*) has a stronger association with age (r^2 = 0.63) than that based on the systolic foot (*cfPWV$_{SF}$*) (r^2 = 0.31, Figure 8.9). The data set was obtained by tonometry measurements subsequently applied on the right common carotid and the right common femoral artery. After low pass filtering, using a second order Savitzky-Golay filter with a window length of 0.2 s, the second derivative was obtained using a derivative filter with a cut-off frequency of 30 Hz. The systolic foot and the dicrotic notch, defined as the maximum of the second derivative before and after systolic pressure, respectively (Figure 8.10), were used to calculate transit time and pulse wave velocity. The increase in pulse wave velocity per year of *cfPWV$_{SF}$* (0.06 m/s per year) is close to the values of *cfPWV$_{SF}$* of 0.08 m/s per year reported by Paini et al. and of 0.06 m/s per year by

reported by Khosdel et al. (Khoshdel et al. 2006, Paini et al. 2006), and the $iPWV_{min}$ of Chapter 7 (0.08 m/s per year, Figure 7.4). However, the $cfPWV_{DN}$ increased 0.22 m/s per year which is closer to the values of $iPWV_{max}$ and $iPWV_{mean}$ from Chapter 7.

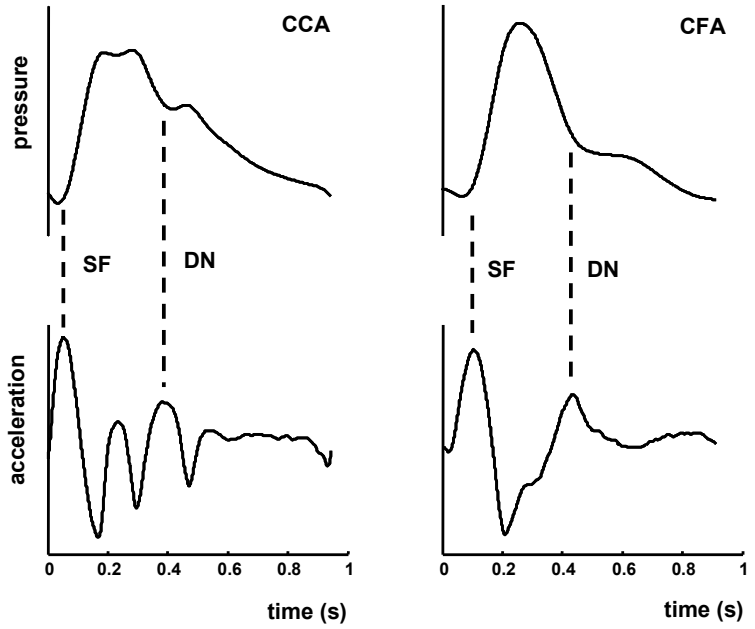

Figure 8.10. a) Tonometeric pressure and acceleration waveforms in the common carotid artery (CCA), the systolic foot (SF) and dicrotic notch (DN) being obtained from the acceleration before and after systolic peak. b) Like a) but here for the common femoral artery (CFA).

The $cfPWV_{DN}$, as measure of arterial stiffness, however is sensitive to changes in hemodynamic conditions during the measurement, because the position of the dicrotic notch, signalling the closure of the aortic valve (Reesink et al. 2007), may be modulated by changes in ejection period and heart rate. The precision and accuracy of the method will improve if both carotid and femoral waveforms are measured simultaneously rather than sequentially. However, reflections may still affect dicrotic notch detection and this may deteriorate the precision and accuracy of $cfPWV_{DN}$. Despite these limitations, the results show that $cfPWV_{DN}$ can be of additional clinical value to determine arterial stiffness, especially for the assessment of effective arterial stiffness. Moreover, $cfPWV_{DN}$ and $cfPWV_{SF}$ can be combined to obtain the degree of pressure dependency of arterial stiffness in individual subjects.

8.8 General Conclusion

In this thesis we developed a method to measure local pulse wave velocity in the common carotid artery based on multiple M-line ultrasound providing a measure of arterial stiffness without the necessity of measuring (pulse) pressure. The method is based on the dicrotic notch as time-reference point in the carotid artery distension waveform, and consequently gives a measure of arterial stiffness at a higher pressure level, which is closely associated with age and pulse pressure. However, the precision of this local pulse wave velocity method in patients with cardiovascular disease is as yet unknown and requires further investigation. In these patients the recorded common carotid artery distension waveform may be of less quality due to increased arterial stiffness. Moreover pulse wave velocity measurements in these patients may be subjected to potentially increased interference of reflected waves due to reduced transit times.

References

Belardinelli E and Cavalcanti S. Theoretical analysis of pressure pulse propagation in arterial vessels. J Biomech 25: 1337-1349, 1992.

Bos WJ, Verrij E, Vincent HH, Westerhof BE, Parati G, and van Montfrans GA. How to assess mean blood pressure properly at the brachial artery level. J Hypertens 25: 751-755, 2007.

Bramwell J and Hill A. The velocity of the pulse wave in man. Proc Roy Soc London Ser B 93: 298-306, 1922.

Chemla D, Antony I, Zamani K, and Nitenberg A. Mean aortic pressure is the geometric mean of systolic and diastolic aortic pressure in resting humans. J Appl Physiol 99: 2278-2284, 2005.

Davies JE, Whinnett ZI, Francis DP, Manisty CH, Aguado-Sierra J, Willson K, Foale RA, et al. Evidence of a dominant backward-propagating "suction" wave responsible for diastolic coronary filling in humans, attenuated in left ventricular hypertrophy. Circulation 113: 1768-1778, 2006.

Franklin SS. Systolic blood pressure: it's time to take control. Am J Hypertens 17: 49S-54S, 2004.

Hayashi K, Handa H, Nagasawa S, Okumura A, and Moritake K. Stiffness and elastic behavior of human intracranial and extracranial arteries. J Biomechanics 13: 175-184, 1980.

Hermeling E, Reesink KD, Reneman RS, and Hoeks AP. Local pulse wave velocity as alternative to reliably measure carotid artery stiffness in humans. Submitted, 2008a.

Hermeling E, Reesink KD, Reneman RS, and Hoeks APG. Confluence of incident and reflected waves interferes with systolic foot detection of the carotid artery diameter waveform. J Hypertens: accepted, 2008b.

Jankowski P, Kawecka-Jaszcz K, Czarnecka D, Brzozowska-Kiszka M, Styczkiewicz K, Loster M, Kloch-Badelek M, et al. Pulsatile but not steady component of blood pressure predicts cardiovascular events in coronary patients. Hypertension 51: 848-855, 2008.

Khoshdel AR, Thakkinstian A, Carney SL, and Attia J. Estimation of an age-specific reference interval for pulse wave velocity: a meta-analysis. J Hypertens 24: 1231-1237, 2006.

Laurent S, Boutouyrie P, Asmar R, Gautier I, Laloux B, Guize L, Ducimetiere P, et al. Aortic stiffness is an independent predictor of all-cause and cardiovascular mortality in hypertensive patients. Hypertension 37: 1236-1241., 2001.

Laurent S, Katsahian S, Fassot C, Tropeano AI, Gautier I, Laloux B, and Boutouyrie P. Aortic stiffness is an independent predictor of fatal stroke in essential hypertension. Stroke 34: 1203-1206, 2003.

Laurent S, Tropeano AI, and Boutouyrie P. Pulse pressure reduction and cardiovascular protection. J Hypertens Suppl 24: S13-18, 2006.

Li JK, Melbin J, Riffle RA, and Noordergraaf A. Pulse wave propagation. Circ Res 49: 442-452, 1981.

Mattace-Raso FU, van der Cammen TJ, Hofman A, van Popele NM, Bos ML, Schalekamp MA, Asmar R, et al. Arterial stiffness and risk of coronary heart disease and stroke: the Rotterdam Study. Circulation 113: 657-663, 2006.

Meinders JM and Hoeks AP. Simultaneous assessment of diameter and pressure waveforms in the carotid artery. Ultrasound Med Biol 30: 147-154, 2004.

Mitchell GF, Parise H, Benjamin EJ, Larson MG, Keyes MJ, Vita JA, Vasan RS, et al. Changes in arterial stiffness and wave reflection with advancing age in healthy men and women: the Framingham Heart Study. Hypertension 43: 1239-1245, 2004.

Nichols WW. Clinical measurement of arterial stiffness obtained from noninvasive pressure waveforms. Am J Hypertens 18: 3S-10S, 2005.

O'Rourke MF and Taylor MG. Input impedance of the systemic circulation. Circ Res 20: 365-380, 1967.

Paini A, Boutouyrie P, Calvet D, Tropeano AI, Laloux B, and Laurent S. Carotid and aortic stiffness: determinants of discrepancies. Hypertension 47: 371-376, 2006.

Powalowski T and Pensko B. A noninvasive ultrasonic method for the elasticity evaluation of the carotid arteries and its application in the diagnosis of the cerebro-vascular system. Arch Acoustics 13: 109-126, 1988.

Qasem A and Avolio A. Determination of aortic pulse wave velocity from waveform decomposition of the central aortic pressure pulse. Hypertension 51: 188-195, 2008.

Reesink KD, Hermeling E, Hoeberigs MC, Reneman RS, and Hoeks AP. Carotid artery pulse wave time characteristics to quantify ventriculoarterial responses to orthostatic challenge. J Appl Physiol 102: 2128-2134, 2007.

Reneman RS, Meinders JM, and Hoeks AP. Non-invasive ultrasound in arterial wall dynamics in humans: what have we learned and what remains to be solved. Eur Heart J 26: 960-966, 2005.

Roman MJ, Devereux RB, Kizer JR, Lee ET, Galloway JM, Ali T, Umans JG, et al. Central pressure more strongly relates to vascular disease and outcome than does brachial pressure: the Strong Heart Study. Hypertension 50: 197-203, 2007.

Segers P and Verdonck P. Role of tapering in aortic wave reflection: hydraulic and mathematical model study. J Biomech 33: 299-306, 2000.

Sugawara M, Niki K, Furuhata H, Ohnishi S, and Suzuki S. Relationship between the pressure and diameter of the carotid artery in humans. Heart Vessels 15: 49-51, 2000.

Van Bortel LM, Duprez D, Starmans-Kool MJ, Safar ME, Giannattasio C, Cockcroft J, Kaiser DR, et al. Clinical applications of arterial stiffness, Task Force III: recommendations for user procedures. Am J Hypertens 15: 445-452, 2002.

van Houwelingen MJ, Barenbrug PJ, Hoeberigs MC, Reneman RS, and Hoeks AP. The onset of ventricular isovolumic contraction as reflected in the carotid artery distension waveform. Ultrasound Med Biol 33: 371-378, 2007.

Vermeersch SJ, Rietzschel ER, De Buyzere ML, De Bacquer D, De Backer G, Van Bortel LM, Gillebert TC, et al. Determining carotid artery pressure from scaled diameter waveforms: comparison and validation of calibration techniques in 2026 subjects. Physiol Meas 29: 1267-1280, 2008.

Waddell TK, Dart AM, Medley TL, Cameron JD, and Kingwell BA. Carotid pressure is a better predictor of coronary artery disease severity than brachial pressure. Hypertension 38: 927-931, 2001.

Westerhof BE, van den Wijngaard JP, Murgo JP, and Westerhof N. Location of a reflection site is elusive: consequences for the calculation of aortic pulse wave velocity. Hypertension 52: 478-483, 2008.

Appendix

Determination of aortic pulse wave velocity from waveform decomposition of the central aortic pressure pulse

This section contains the abstract and Figures published by Qasem A and Avolio A. as Determination of aortic pulse wave velocity from waveform decomposition of the central aortic pressure pulse. Hypertension 51: 188-195, 2008. To help understand the letter to the editor in Chapter 5

Abstract

Aortic pulse wave velocity, calculated from pulse transit time using two separate pulse recordings over a known distance, is a significant biomarker of cardiovascular risk. This study evaluates a novel method of determining pulse transit time from waveform decomposition of central aortic pressure using a single pulse measurement. Aortic pressure was estimated from a transformed radial pulse and decomposed into forward and backward waves using a triangular flow wave. Pulse transit time was determined from cross-correlation of forward and backward waves. Pulse transit time, representing twice the pulse transit time between two specific sites, was compared with independent measurements of carotid-femoral pulse transit time in a cohort of 46 subjects (23 females; age 57 ± 14 years). Linear regression between measured pulse transit time (y; milliseconds) and calculated pulse transit time (eTR2/2, x; milliseconds) was $y = 1.05x - 2.1$ ($r = 0.67$; $P < 0.001$). This model was tested in a separate group of 44 subjects (21 females; age 55 ± 14 years) by comparing measured carotid-femoral pulse wave velocity (y; meters per second) and pulse wave velocity calculated using the estimated value of pulse transit time (eTR2/2) and carotid-femoral distance (x; meters per second; $y = 1.21 x-2.5$; $r = 0.82$; $p < 0.001$). Findings indicate that the time lag between the forward and backward waves obtained from the decomposition of aortic pressure wave can be used to determine pulse wave velocity along the aortic trunk and shows good agreement with carotid-femoral pulse wave velocity. This technique can be used as a non-invasive and no intrusive method for measurement of aortic pulse wave velocity using a single pressure recording. (Hypertension. 2008;51:188-195.)

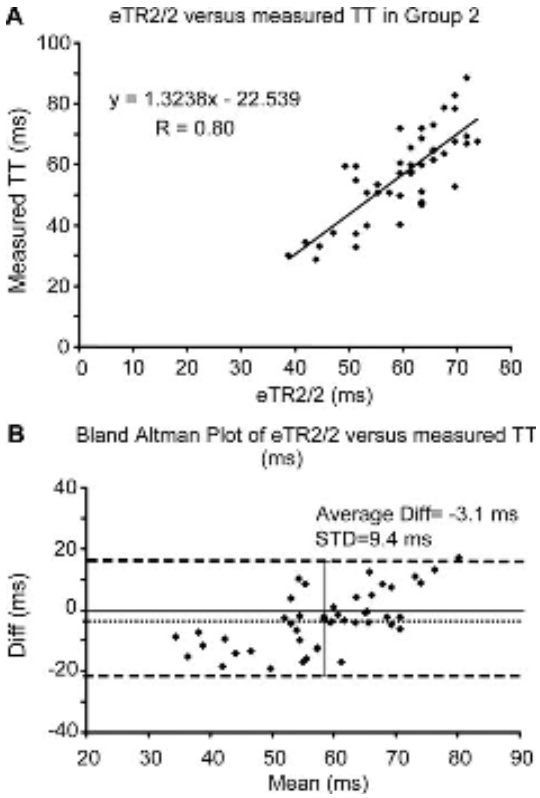

Figure 6. A, Scatter plot of estimated pulse transit time (eTR2 / 2) versus measured pulse transit time with regression line in group 2. B, Bland-Altman plot of calculated versus measured pulse transit time in group 2. Solid line is the mean difference, and the dashed lines are ± 2 standard deviation (STD) of the difference.

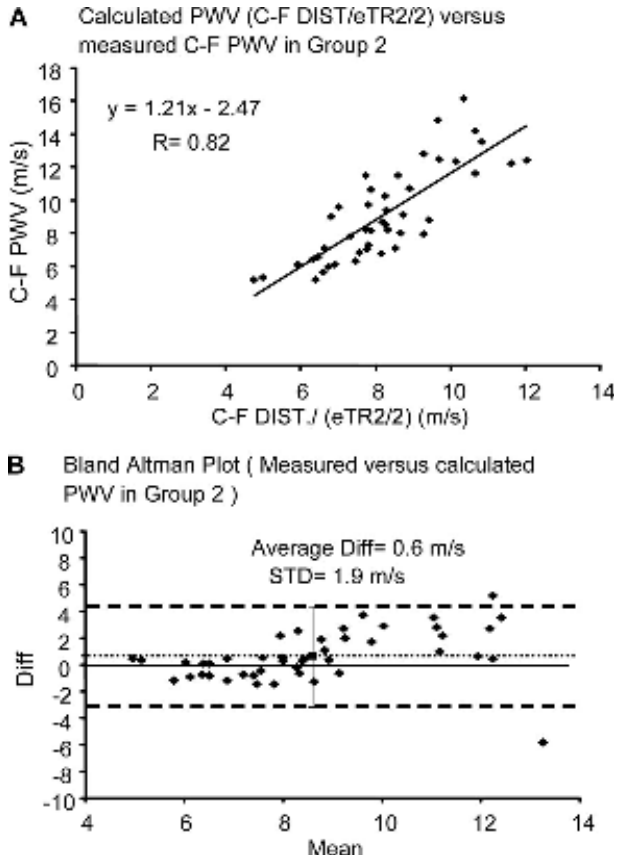

Figure 7. A, Scatter plot of pulse wave velocity calculated by dividing carotid-femoral distance (C-F DIST) by estimated PTT (eTR2/2) versus measured carotid-femoral pulse wave velocity (C-F PWV) with regression line in group 2. B, Bland-Altman plot of calculated versus measured pulse wave velocity in group 2. Solid line is the mean difference, and the dashed lines are ±2 standard deviation (STD) of the difference.

Summary

Cardiovascular disease is the number one cause of death in western society. Although patients with cardiovascular events can be free of symptoms prior to the event, the arterial tree may already exhibit structural and/or functional changes at an early stage of the disease process. For example, arteries may stiffen, which is associated with increased (systolic) blood pressure and, consequently, an increased load on the heart, or thicken their wall, especially in the intima-media layers. Both stiffening of the arteries and increased intima-media thickness have shown to be predictors of cardiac and cerebrovascular disease in epidemiological studies.

The main objective of this thesis was to develop an accurate and reliable non-invasive method to assess arterial stiffness locally. We have chosen for the assessment of local stiffness to be informed of changes in specific arteries rather than of changes in a global part of the arterial tree, including arteries with different dynamic properties. The latter information is obtained when assessing pulse wave velocity over the trajectory from the carotid to the femoral artery.

The methods, presently in use to determine local artery stiffening are, among others, arterial compliance coefficient (the increase in absolute cross-sectional area for a given increase in blood pressure) and distensibility coefficient (the relative increase in cross-sectional area for a given increase in blood pressure). These methods, however, do have limitations, because they assume a linear pressure-area relationship and require an accurate measure for the local pulse pressure, which is difficult to obtain non-invasively. Therefore, we have taken a different approach in the local assessment of artery stiffening. We have chosen to measure the propagation velocity of the arterial pulse wave over a short artery segment (less than 2 cm) by means of high resolution ultrasound. The higher this wave velocity is the faster the stiffer the artery will be.

This thesis focuses on the assessment of stiffness in elastic arteries, because of the abundant evidence that the mechanical properties of these arteries, in contrast to that of muscular arteries, changes strongly with aging and (cardiovascular) disease. The common carotid artery was taken as an example of an elastic artery, because of its prevalent involvement in atherosclerotic disease. An overview of other factors, that may influence pulse wave velocity measurement, independent of arterial stiffness, is given in Chapter 1.

In Chapter 2, we address the relevant non-invasive techniques currently available, mostly based on ultrasound, to acquire stiffness parameters in normal populations as well as in such patient groups as hypertensives and diabetics.

We discuss the mathematical and physical interrelationships between those parameters. It is shown that the assumptions made to derive these relationships, inherently lead to approximations. Moreover, we show that some characteristics, e.g. local pulse pressure, are difficult to measure directly, requiring a search for alternative measures of arterial stiffness.

In Chapter 3, we show that estimates of local pulse wave velocity can be measured reliably, by applying linear regression to characteristic time-points in the diameter waveforms of the common carotid artery, as recorded simultaneously by multiple M-line ultrasound. The proposed method circumvents two major problems of current measures of arterial stiffness, namely inaccurate distance measurement as occurs for the carotid-femoral pulse wave velocity, and inaccurate local pulse pressure measurement in calculating distensibility coefficients. The precision of this method is investigated in a phantom setup scaled according to realistic *in vivo* conditions. Special attention is paid to the identification of the systolic foot of the wave. We defined the systolic foot by 1) the maximum of the second derivative, 2) the intersecting tangent with the diastolic minimum and 3) the intersection at the 20% threshold of the systolic upstroke. Prior to systolic foot detection, the diameter waveforms are subjected to pre-processing with various filters. It is concluded that foot detection by a threshold of 20% or by the intersecting tangent method provide a more suitable identification point for the foot of the wave because these methods are less sensitive to (phase) noise than the maximum of the second derivative method and exhibit good precision with a coefficient of variation of less than 1%.

The accuracy and precision of the systolic foot identification *in vivo* may be disturbed by early wave reflections, which affect pulse wave transit time measurements. In Chapter 4, we show in healthy subjects the existence of early wave reflections and discuss their impact on systolic foot identification. The systolic foot and an inflection point, a discontinuity in the ascending limb of the diameter waveform, are identified using the second derivatives of the diameter waveforms. The observed pulse wave transit time shows a good intra-subject precision. The systolic foot runs forward while the inflection point runs backwards, indicating that it is associated with a reflected wave. Despite the good intra-subject reproducibility, confluence of incident and reflected waves disturbs identification and discrimination of the systolic foot and the inflection point, resulting in biased estimates. Therefore both points are unsuited for local pulse wave velocity measurements in the common carotid artery.

If the distance to the reflection site is known, reflections themselves might be used for the assessment of global pulse wave velocity, as discussed in Chapter 5. This technique is appealing because it requires access to only a single measurement site. However, an inflection point, signalling the arrival of a reflected wave, should be considered with caution if it is used to estimate pulse wave, because the actual site of reflection is generally unknown, leading to erroneous conclusions. Even if the site of reflection is known, this method is still debatable, because amplitude of the reflected wave and interaction of incident and reflected waves may alter the timing of the inflection point independent of the actual propagation time of the wave.

In Chapter 6, local pulse wave velocity is measured in young and older subjects (mean age 26 and 59 years, respectively), using either the systolic foot or the dicrotic notch as time-reference point. Dicrotic notch pulse wave velocity, at about mean arterial pressure, has a better intra-subject precision than systolic foot pulse wave velocity. The expected difference in stiffness between the two age categories only emerges for the dicrotic notch pulse wave velocity. The dicrotic notch method, in contrast to the systolic foot method, showed a significant correlation with relative diameter change and pulse wave velocity calculated from the distensibility coefficient. The dicrotic notch pulse wave velocity is measured close to mean arterial pressure, and is more accurate and has a better precision than the pulse wave velocity measured with the systolic foot as time-reference point.

The pressure dependence of arterial stiffness may have serious consequences for the non-invasive assessment of arterial elastic properties and is studied in detail in Chapter 7. The degree of pressure dependency and the consequence for the assessment of arterial stiffness is analyzed by measuring intra-arterial pressure and common carotid artery diameter waveforms simultaneously in patients undergoing coronary angiography. Exponential analytical models are used to describe the measured pressure-area curve, from these exponential models the pressure dependent pulse wave velocity can be obtained. Additionally, compliance coefficients were calculated separately over the diastolic and systolic pressure range, using the dicrotic notch as a cut-off. The incremental pulse wave velocity at systolic, but not at diastolic pressure, exhibits a strong association with pulse pressure and age. Moreover, we showed that patients with high pulse pressure had a three times lower compliance at systolic pressure range compared to patients with lower pulse pressures. This suggests that arterial stiffness at diastolic pressure is only a minor predictor of the pulsatile load on the left ventricle, especially in patients with high pulse pressure. This has

serious consequences for the non-invasive quantification of arterial stiffness in individual patients and stresses the need for methods to assess arterial stiffness non-invasively at higher (preferably systolic) pressure levels than at the diastolic pressure level as commonly in use.

In the general discussion (Chapter 8), an integrated interpretation of the work described in the previous Chapters was given. We analyzed whether local pulse wave velocity can be used to determine intrinsic arterial stiffness. In addition, we use the associated stiffness parameter to derive the local (central) pulse pressure by assuming an exponential pressure-area relationship and using only diastolic blood pressure as additional input. We show that, like the systolic foot, the dicrotic notch is followed by an inflection point. However, the interference of reflected waves on the dicrotic notch seems rather small. On the other hand, the poor correlation between age and systolic foot pulse wave velocity can not be attributed to the lack of difference in diastolic stiffness. Finally, the dicrotic notch method is also applied to the assessment of carotid-femoral pulse wave velocity, which shows that this method may provide additional information about arterial stiffness.

In this thesis we develop and evaluate a method to determine local arterial stiffness in the common carotid artery. The method is based on local pulse wave velocity measurements using the dicrotic notch in the diameter waveform as time-reference point. This parameter measured near systolic pressure level, may provide additional structional and functional information of arterial stiffness.

Samenvatting

In de westerse samenleving zijn hart- en vaatziekten doodsoorzaak nummer één. Ondanks dat sommige patiënten geen symptomen vertonen vóór het optreden van hart- en vaatziekten, laten slagaders (arteriën) vaak al in een vroeg stadium van het ziekteproces veranderingen zien. Voorbeelden hiervan zijn: 1) een toename van de stijfheid van de arteriële vaatwand, dat geassocieerd is met een hoge bloeddruk en een toename van de hartbelasting, en 2) een verdikking van de binnenste laag van de bloedvaatwand (intima). Epidemiologisch onderzoek heeft aangetoond dat zowel een toename in vaatstijfheid als een verdikking van de vaatwand een voorspellende waarde hebben voor het optreden van hart- en vaatziekten.

De voornaamste doelstelling van dit proefschrift was een nauwkeurige en betrouwbare methode te ontwikkelen, waarmee de vaatstijfheid lokaal gemeten kan worden. We hebben voor een lokale vaatstijfheidsmeting gekozen aangezien die informatie geeft over een specifieke slagader in plaats van over een globaal deel van de vaatboom met slagaders met verschillende dynamische eigenschappen. Dat laatste is bijvoorbeeld het geval bij de meting van de polsgolfsnelheid over het traject van hals- naar beenslagader. De methodes die op dit moment gebruikt worden om lokale vaatstijfheid te kunnen bepalen zijn onder andere gebaseerd op de compliantie coëfficiënt (de absolute toename in oppervlakte van de doorsnede van een slagader bij een gegeven toename in bloeddruk) of de distensibiliteitscoëfficiënt (de relatieve toename in doorsnede bij een bepaalde toename in bloeddruk). Deze methodes hebben echter beperkingen omdat ze uitgaan van een lineaire bloeddruk-doorsnede relatie en de lokale bloeddrukvariaties bekend veronderstellen. De voortplanting-snelheid van drukgolven in slagaders heeft geen last van deze beperkingen terwijl hij rechtstreeks gekoppeld is aan de stijfheid: hoe stijver de vaatwand van de slagader, des te hoger is de zogenaamde polsgolfsnelheid.

In dit proefschrift wordt voornamelijk gekeken naar de vaatstijfheid in elastische slagaders, omdat er vele aanwijzingen zijn dat de mechanische eigenschappen van deze slagaders, in tegenstelling tot die van musculaire slagaders, sterk veranderen met leeftijd en onder invloed zijn van (cardiovasculaire) ziekteprocessen. De overige factoren die de meting van de polsgolfsnelheid, onafhankelijk van de vaatstijfheid, kunnen beïnvloeden zijn beschreven in hoofdstuk 1.

In hoofdstuk 2 is een overzicht gegeven van de huidige niet invasieve technieken, het merendeel gebaseerd op ultrageluid, om de vaatstijfheid te meten in zowel normale populaties als in specifieke patiënten groepen zoals

mensen met hoge bloeddruk of diabetes. In dit hoofdstuk beschrijven we de mathematische en fysische onderlinge relaties tussen de verschillende parameters. We laten zien hoe de aannames, die ten grondslag liggen aan het bepalen van deze relaties, leiden tot benaderingen van de werkelijke vaatstijfheid. Bovendien laten we zien dat een aantal van deze parameters, bijvoorbeeld de lokale polsdruk, moeilijk op een niet invasieve en nauwkeurige manier te meten zijn. Dit illustreert de behoefte aan een alternatieve meettechniek waarmee de vaatstijfheid bepaald kan worden zonder de polsdruk te meten.

In hoofdstuk 3 laten we zien dat de lokale polsgolfsnelheid nauwkeurig bepaald kan worden met behulp van een lineaire regressie analyse toegepast op karakteristieke tijdspunten die bepaald zijn uit diameter golfvormen opgenomen met een meervoudige M-lijn ultrageluidstechniek. De voorgestelde methode vermijdt twee belangrijke problemen van de conventionele methode om vaatstijfheid te meten. Bij de regressiemethode ligt de afstand vast voor de gebruikte transducent, en is dus niet afhankelijk van de patiënt zoals dat het geval is voor de polsgolfsnelheidsmeting over het traject tussen hals- en beenslagader. Verder is de meting van de lokale polsdruk niet nodig, zoals voor distensibiliteitsmetingen het geval is. De precisie van de regressiemethode is onderzocht in een proefopstelling die geschaald is naar realistische condities in het menselijk lichaam. In dit hoofdstuk ligt de nadruk op de verschillende technieken waarmee de systolische voet, dat is het begin van de diameter curve, bepaald kan worden. We hebben gekeken naar (1) het maximum van de tweede afgeleide, (2) het snijpunt van de steilste raaklijn van de diametercurve met zijn minimale waarde en (3) het snijpunt met een drempel van 20% van de opgaande flank. Voordat de systolische voet bepaald wordt, zijn de diameter golfvormen bewerkt met verschillende filters. We hebben laten zien dat zowel de drempelwaarde- als de snijpuntmethode beter werken voor het bepalen van de systolische voet van de diameter curve, omdat deze technieken minder gevoelig zijn voor (fase) ruis dan de methode gebaseerd op de tweede afgeleide. De drempelwaarde en snijpuntmethode hebben een goede precisie en nauwkeurigheid, zoals blijkt uit een variatie coëfficiënt van minder dan 1%.

De nauwkeurigheid en precisie van de systolische voet identificatie *in vivo* kan worden verstoord door vroege golfreflecties en dit kan tevens de golf looptijd meting beïnvloeden. In hoofdstuk 4 laten we zien dat in de halsslagader van gezonde proefpersonen inderdaad golfreflecties optreden in een vroege fase van de hartcyclus die tot uiting komen in een inflectiepunt, een discontinuïteit in de opgaande flank van de diameter golfvorm. We gaan na wat de invloed is van

deze vroege golfreflecties op de bepaling van de systolische voet. Daartoe hebben we de systolische voet en het inflectiepunt geïdentificeerd met behulp van de tweede afgeleide van de diameter golfvorm. Ook *in vivo* blijkt dat met de regressiemethode de looptijd van de polsgolf, en dus ook de polsgolfsnelheid, met een goede precisie zijn te bepalen. Ondanks dat de precisie van de metingen goed is, zorgt het samenvloeien van de voorwaarts en terugkerende drukgolven voor een onnauwkeurigheid in de identificatie van de systolische voet en leidt derhalve tot een foute looptijd. We kunnen daarom concluderen dat beide karakteristieke punten van de diameter golfvorm ongeschikt zijn voor het bepalen van de polsgolfsnelheid.

Als de afstand tot het reflectiepunt bekend is, kan een inflectiepunt dat de aankomst van de gereflecteerde golf signaleert gebruikt worden om de globale polsgolfsnelheid te bepalen (hoofdstuk 5). Deze techniek lijkt attractief omdat er slechts op één plaats gemeten hoeft te worden. Zoals aangegeven in hoofdstuk 5, is het in het algemeen onmogelijk om het reflectiepunt en dus de afstand tot dit reflectiepunt in het lichaam te bepalen. Zelfs als het reflectiepunt bekend is, dan nog blijft deze techniek discutabel, omdat de mate van reflectie en onderlinge interactie van de heen- en teruggaande golf, het tijdsmoment van het inflectiepunt kunnen beïnvloeden, onafhankelijk van de looptijd.

In hoofdstuk 6 wordt de lokale polsgolfsnelheid in jonge en oudere proefpersonen (gemiddelde leeftijd respectievelijk 26 en 59 jaar) met de regressiemethode gemeten. Hierbij wordt gebruik gemaakt van de systolische voet en de dicrotic notch as tijdsreferentie punt. Het verwachte verschil in vaatstijfheid tussen de twee leeftijdsgroepen kon alleen worden vastgesteld met behulp van de dicrotic notch polsgolfsnelheid. Bovendien liet de dicrotic notch methode, in tegenstelling tot de systolische voet methode, een significante correlatie zien met relatieve distensie en de polsgolfsnelheid bepaald uit de distensibiliteitscoëfficiënt. De dicrotic notch polsgolfsnelheid, gemeten dichtbij de gemiddelde druk, heeft dus een betere nauwkeurigheid en precisie dan de systolische voet polsgolfsnelheid.

De drukafhankelijkheid van de vaatstijfheid kan ernstige consequenties hebben voor het bepalen van de arteriële elastische eigenschappen (hoofdstuk 7). De mate van de drukafhankelijkheid en de consequentie voor het bepalen van de vaatstijfheid is geanalyseerd door het simultaan meten van de aortadruk en diameter van de halsslagader in patiënten tijdens coronaireangiografie. De onderlinge druk-doorsnede relatie is met exponentiële modellen beschreven. Uit deze relatie kan de polsgolfsnelheid als functie van de bloeddruk berekend

worden. Bovendien is de compliantie berekend afzonderlijk voor het diastolische en systolische drukbereik, waarbij de dicrotic notch gebruikt werd als afsnijpunt. De polsgolfsnelheid bij systolische druk, maar niet bij diastolische druk, liet een sterke relatie zien met polsdruk en leeftijd. Bovendien lieten we zien dat patiënten met een hoge polsdruk een driemaal lagere compliantie in een systolisch drukbereik hebben in vergelijking met patiënten met een lage polsdruk. Dit suggereert dat in deze patiënten de vaatstijfheid bij diastolische druk maar in beperkte mate een maat is voor de belasting van het linker ventrikel. Bovendien toont dit aan dat de drukafhankelijke vaatstijfheid in deze patiënten een toename in polsdruk kan verklaren. Dit benadrukt de behoefte aan methodes om vaatstijfheid niet invasief en bij een hogere bloeddruk te bepalen dan de diastole bloeddruk wat op dit moment gebeurt.

In de algemene discussie (hoofdstuk 8) laten we zien dat de lokale polsgolfsnelheid gebruikt kan worden om de intrinsieke vaatstijfheid te bepalen. De daarbij gebruikte intrinsieke vaatstijfheidsparameter gebruiken we vervolgens weer om de lokale polsdruk te bepalen via een modelmatige exponentiële druk-oppervlakte relatie waarvoor alleen de polsgolfsnelheid en diastole bloeddruk nodig zijn. Verder laten we zien dat de dicrotic notch zoals de systolische voet gevolgd wordt door een inflectiepunt. De invloed van golfreflecties op de bepaling van de dicrotic notch blijkt echter klein te zijn. De slechte correlatie tussen leeftijd en systolische polsgolfsnelheid kan men niet verklaren met een verwaarloosbaar verschil in diastole vaatstijfheid maar moet toegeschreven worden aan de moeilijkheid om de systolische voet voldoende nauwkeurig te kunnen bepalen. Aan het einde van dit hoofdstuk laten we zien dat de dicrotic notch ook gebruikt kan worden voor het bepalen van de polsgolfsnelheid over het traject tussen hals- en beenslagader.

In dit proefschrift hebben we een methode ontwikkeld en geëvalueerd waarmee de lokale vaatstijfheid gemeten kan worden in de halsslagader. Deze methode werkt het beste als de dicrotic notch gebruikt wordt als tijdsreferentie punt voor de bepaling van de polsgolfsnelheid. Omdat dan de meting op een hogere bloeddruk wordt uitgevoerd verkrijgt men additionele structurele and functionele informatie over de vaatstijfheid.

Dankwoord

Op deze plek wil ik graag iedereen bedanken die me tijdens mijn promotie heeft bijgestaan. Ik wil de onderstaande mensen in het bijzonder bedanken.

Allereerst wil ik mijn promotor, Prof. A.P.G. Hoeks, bedanken. Beste Arnold, vanaf het eerste uur wist ik dat ik ontzettend veel van jou kon leren. Je schijnbaar onuitputtelijke hoeveelheid kennis over onder andere ultrageluid heeft me in de loop der jaren ontzettend veel geholpen. Maar bovenal je humor en “meta-conversaties” zullen me altijd bij blijven. De zinnetjes: “wat een ellende!” en “je hebt het zeker verbeterd!” zullen nooit meer dezelfde betekenis hebben als voordat ik je ontmoette.

Bovendien wil mijn tweede promotor Prof. R.S. Reneman bedanken. Beste Rob, ik wil je bedanken voor je kritische blik en je nauwgezette correcties, met de welbekende rode pen. Jou enthousiasme voor de wetenschap lijkt in al die jaren nog steeds niet te zijn verminderd. Je bent een enorme inspiratie bron.

Beste Koen, na het eerste jaar van mijn promotieonderzoek kwam jij ons team versterken. In het begin was je een goede postdoc, maar later werd je mijn co-promotor, een prettige collega en bovenal een goede vriend. Ik heb zoveel aan je gehad, dat kan ik hier niet opschrijven. Onze gesprekken waren zelden oppervlakkig, de onderwerpen van onze gesprekken waren gerelateerd aan het onderzoek of algemeen wetenschappelijk, maar soms ook heel persoonlijk. Je was, en hopelijk blijft, een goede sparringpartner. Koen super bedankt! Ik hoop dat we nog lang mogen samenwerken.

Verder wil ik de leden van de beoordelingscommissie, Prof. P.W. de Leeuw, Prof. J.G.R. de Mey, Prof. J.L. Waltenberger, Prof. F.N. van de Vosse, hartelijk bedanken voor het kritisch beoordelen van het manuscript. Dear Prof. P. Boutouyrie I want to thank for your critical evaluation of the manuscript.

Mijn dank gaat ook uit naar Prof. J.L. Waltenberger en de mensen van de cath-kamer, heel erg bedankt dat ik mijn metingen bij jullie kon verrichten.

Beste Liselotte, collega en carpoolmaatje, we hebben vele uren samen in de auto doorgebracht. Soms stil, dan weer drukpratend, soms over werk, maar meestal niet. Beide op hoog niveau spelend in een teamsport, begrepen we dat het balans vinden tussen sport en promoveren soms moeilijk is. Onze maandagochtend gesprekken gingen standaard over de wedstrijden van het weekend. Bedankt voor de vele leuke uren samen in de auto!

Beste Jeroen, ik wil je bedanken voor je technische ondersteuning bij de experimenten. Ik heb jou hulp, bij het zoveelste probleem met de soms niet al te stabiel draaiende ultrageluidsapparatuur, altijd zeer op prijs gesteld.

Dennis, bedankt voor de kopjes koffie die je de laatste jaren voor met hebt gezet, onze koffiegesprekken om 8 uur s'morgens zorgde voor een goede start van de dag. Ook de andere collega's van Biofysica, en het ArtMed project wil ik bedanken voor hun ondersteuning en gesprekken.

Frits Prinzen, Prof. Theo Arts, Tammo Delhaas en bovenal Nico Kuijpers, ik wil jullie bedanken dat jullie mij de mogelijkheid bieden mijn wetenschappelijke carrière bij jullie voort te zetten.

Beste paranimfen, lieve Pien en Mariek, leuk en fijn dat jullie mijn paranimfen wilden zijn. Maar ik wil jullie bovenal bedanken voor de humor en de lach die me op vele trainingen en wedstrijden begeleidde. Pien, bedankt dat je me introduceerde tot op heden nog niet zo bekende lach-basketbal, zonder dat had ik nooit zo van basketbal kunnen genieten. Tevens wil ik mijn overige teamgenootjes en coaches, van de afgelopen jaren, bedanken voor de broodnodige ontspanning.

Lieve paps en mams, bedankt voor jullie vertrouwen in mijn kunnen. Zonder jullie had ik na de zoveelste onvoldoende voor Engels, nooit het geloof gehad dat ik dit zou kunnen bereiken. Jullie hebben me altijd vrijgelaten in mijn (studie) keuzes. Ook hebben jullie mijn interesse gewekt voor de wonderlijke wereld om mij heen, en dat is altijd mijn drijfveer geweest in de lange weg die uiteindelijk leidde tot deze promotie. Verder wil ik ook mijn broers, Menno en Wouter, mijn schoonzus Lilian en mijn vrienden bedanken. Ik realiseer me dat het niet altijd makkelijk is geweest een vriendschap te onderhouden met iemand die aan het promoveren is. Bedankt dat ik "na vier jaar verwaarlozing" nog steeds op jullie kan rekenen.

Lieve Philippe, je bent altijd het rustpunt geweest in mijn leven, de rust die ik niet in mezelf vinden kan. Je hebt in de afgelopen jaren heel veel verhalen over mijn promotie moeten aanhoren en bent altijd een grote steun voor me geweest. Tevens wil ik je bedanken voor de puntjes op de i, je hebt mijn proefschrift helemaal doorgenomen.

Curriculum Vitae

Evelien Hermeling was born on December 21, 1978, in Wijk en Aalburg, the Netherlands.

From 1990 to 1996 she attended secondary school at the Frederik Hendrik College in s'-Hertogenbosch, and received VWO atheneum diploma in 1996.

She studied Biomedical Engineering at the Eindhoven University of Technology from 1996 till 2004. She did her external internship at Datex-Ohmeda in Helsinki, Finland on the topic: 'Determination of the level of anesthesia from EEG'. In her master project she focused on long term blood pressure regulation by the kidneys, and developed a computer simulation model. In 2004, she received the degree in Master of Science, Biomedical Engineering at the Eindhoven University of Technology.

In 2005, she started to work as a PhD student at the department of Biophysics at the Maastricht University. During this time, she studied local mechanical characteristic of the arterial wall and developed a method to measure propagation velocity of arterial pulse waves over a short artery segment, by means of high resolution ultrasound.

List of Publications

Articles and letters

Hermeling E, Reesink KD, Reneman RS, and Hoeks AP. Measurement of local pulse wave velocity: effects of signal processing on precision. Ultrasound Med Biol 33: 774-781, 2007.

Hermeling E, Reesink KD, Hoeks AP, and Reneman RS. Modeled decomposition of aortic pressure waveforms does not provide estimates for pulse wave velocity. Hypertension 51: e60, 2008a.

Hermeling E, Reesink KD, Reneman RS, and Hoeks AP. Confluence of incident and reflected waves interferes with systolic foot detection of the carotid artery distension waveform. J Hypertens 26: 2374-2380, 2008b.

Hermeling E, Reesink KD, Kornmann LM, Reneman RS, and Hoeks AP. The dicrotic notch as alternative time-reference point to measure local pulse wave velocity in the carotid artery by means of ultrasonography. submitted.

Hermeling E, Hoeks AP, Winkens M, Waltenberger J, Kroon AA, Reneman RS, and Reesink KD. Proper non-invasive assessment of arterial compliance should include stiffness in the systolic pressure range. submitted.

Kornmann LM, Curfs DM, **Hermeling E**, van der Made I, de Winther MP, Reneman RS, Reesink KD and Hoeks AP. Perfluorohexane-loaded macrophages as a novel ultrasound contrast agent: a feasibility study. Mol Imaging Biol 10: 264-270, 2008.

Reesink KD, **Hermeling E**, Hoeberigs MC, Reneman RS, and Hoeks AP. Carotid artery pulse wave time characteristics to quantify ventriculoarterial responses to orthostatic challenge. J Appl Physiol 102: 2128-2134, 2007.

Hoeks AP, Reesink KD, **Hermeling E**, and Reneman RS. Local blood pressure rather than shear stress should be blamed for plaque rupture. J Am Coll Cardiol 52: 1107-1108, 2008b.

Rensen SS, Niessen PM, van Deursen JM, Janssen BJ, Heijman E, **Hermeling E**, Meens M, , Lie N, Gijbels MJ, Strijkers GJ, Doevendans PA, Hofker MH, De Mey JG, and van Eys GJ. Smoothelin-B deficiency results in reduced arterial contractility, hypertension, and cardiac hypertrophy in mice. Circulation 118: 828-836, 2008.

Book chapter

Hoeks AP, **Hermeling E**, and Reneman RS. Artery wall mechanics determined by means of ultrasound. In: Vascular Hemodynamics: Bioengineering and clinical prespectives, edited by Yim PJ. New York: John Wiley and Sons. 2008a, p. 133-156.

Published proceedings and abstracts

Hermeling E, Reesink KD, and Hoeks APG. Measuring local pulse wave velocity using non-invasvie multiple M-line ultrasound. In: Artery 6. Greece, 2006, p. 026.

Hermeling E, Reesink KD, and Hoeks APG. Early reflection observed in the pulse wave in the common carotid artery originates from either the circle of Willis or the capillary bed of the facial musculature. In: Artery 7. Prague, 2007a, p. 10.13.

Hermeling E, Reesink KD, and Hoeks APG. In vivo validation of a non-invasively measured local pulse wave velocity: improved performance using aortic valve closure in stead of aortic valve opening. In: Artery 7. Prague, 2007b, p. 0.77.

Hoeks APG, **Hermeling E**, Reesink KD, and Reneman, RS. Local pulse wave propagation in the carotid artery. In: Trends in medical technology: acoustic wave propagation. Amsterdam, 2009, p.15-16.

Hermeling E, Reesink KD, Kroon AA, Segers P, and Hoeks AP. Determination of pressure independent arterial stiffness by correcting pulse wave velocity for pressure-area relationship. In: Artery 8. Ghent, 2008, p. 1.40.

Reesink KD, **Hermeling E**, Hoeberigs MC, and Hoeks APG. Non-invasive quantitative evaluation of systolic cardiovascular interaction by carotid artery ultrasonography. In: Artery 6. Greece, 2006, p. 070.

Reesink KD, **Hermeling E**, Ong KT, Boutouyrie P, and Hoeks APG. A non-invasive approach to quantify ventricular-arterial interaction: comparing the vascular type Ehlers-Danlos syndrome patients and normal individuals. In: Artery 7. Prague, 2007, p. 0.68.

Reesink KD, **Hermeling E**, Waltenberger J, and Hoeks AP. Increased pulse pressure is associated with long left ventricular ejection duration in isolated systolic hypertension. In: Artery 8. Ghent, 2008a, p. 2.44.

Reesink KD, **Hermeling E**, Waltenberger J, and Hoeks APG. Higher order non-linearity in arterial distensibility is present in one-third of the patients with cardiovascular disease. In: Artery 8. Ghent, 2008b, p. 1.16.